MASTER THESIS

Thesis submitted in partial fulfillment of the requirements for the degree of Master of Science in Engineering at the University of Applied Sciences Technikum Wien – Tissue Engineering and Regenerative Medicine

The role of salt-inducible kinases in osteoarthritis

By: Ing. Daniel Alexander Rotter, BSC
Student Number: 1710692020

Supervisor 1: Dip.Ing.Dr.techn. Andreas Teuschl
Supervisor 2: Marc N. Wein, MD, PhD

Vienna, 30. September 2019

FH University of Applied Sciences TECHNIKUM WIEN

Declaration of Authenticity

“As author and creator of this work to hand, I confirm with my signature knowledge of the relevant copyright regulations governed by higher education acts (for example see §§ 21, 42f and 57 UrhG (Austrian copyright law) as amended as well as § 14 of the Statute on Studies Act Provisions / Examination Regulations of the UAS Technikum Wien).

In particular I declare that I have made use of third-party content correctly, regardless what form it may have, and I am aware of any consequences I may face on the part of the degree program director if there should be evidence of missing autonomy and independence or evidence of any intent to fraudulently achieve a pass mark for this work (see § 14 para. 1 Statute on Studies Act Provisions / Examination Regulations of the UAS Technikum Wien).

I further declare that up to this date I have not published the work to hand nor have I presented it to another examination board in the same or similar form. I affirm that the version submitted matches the version in the upload tool.”

Place, Date	Signature

Kurzfassung

Gradueller Verlust von Knorpelgewebe in Osteoarthritis (OA) ist eher mit der Expression hypertroph-assoziierter Gene in artikularen Chondrozyten verknüpft als mit deren Zelltod. Parathormon (PTH) verwandtes Peptid (PTHrP) unterdrückt Hypertrophie und Aktivität von Salz-induzierbaren Kinasen (SIK) in Chondrozyten während der endochondralen Ossifikation. PTH kann jedoch nur limitierend als Medikament zur Anwendung kommen. Diese Arbeit stellt PTH/PTHrP nachahmende SIK-inhibierende Moleküle als potenzielles krankheitsverändertes Medikament in OA vor.

28 C57BL6 Mäuse wurden einer Destabilisierung des medialen Meniskus (DMM) Operation oder einer Schein-operation (Sham) unterzogen und mit pan-SIK-inhibitor YKL-05-099 oder Vehikel (VEH) über einen Zeitraum von 11 Wochen behandelt, um Veränderungen im OA artikularen Knorpelgewebe festzustellen. Zusätzlich wurden *in vitro* Experimente mit YKL-05-099 durchgeführt, um Protein Phosphorylierung und Genexpression zu untersuchen.

YKL-05-099 Behandlung reduziert die OA-research Society International (OARSI) Bewertung von OA im Vergleich zu VEH (Sham VEH vs. Sham YKL $p = 0.0826$; DMM VEH vs. DMM YKL $p = 0.2572$; $n = 7$/Gruppe) und reduziert Col X positive Zellen in Knorpelgewebe (Sham VEH vs. Sham YKL $p = 0.0746$; DMM VEH vs. DMM YKL $p = 0.1309$; $n = 7$/Gruppe). Phosphorylierung von cAMP-responsive element (CRE) binding protein (CREB) -regulated transcription coactivator 2 (CRTC2) und Histon Deacetylase 4 (HDAC4) waren in YKL-05-099, Forskolin und PTH behandelten primären Chondrozyten reduziert in Korrelation mit SIK Inaktivierung. YKL-05-099, PTH und Forskolin behandelte primäre Chondrozyten und klonale Zellen der Beinknospe hatten erhöhte *Prg4* und reduzierte *MMP13* mRNA-expression. *Prg4* und *MMP13 in situ* Hybridisierung hat keine Behandlungseffekte mit YKL-05-099 in artikularem Knorpelgewebe im OA Mausmodell offenbart.

Systemisch applizierte SIK-inhibitoren erhöhen die Integrität von artikularem Knorpelgewebe und ahmen PTH induzierte Signale in primären Chondrozyten des Sternums und klonalen Zellen der Beinknospe nach. SIK-inhibitoren stellen daher eine mögliche Krankheitsveränderte Behandlung von OA zum Erhalt des Kniegelenks dar.

Schlagwörter: Osteoarthritis, salz-induzierbare Kinasen, YKL-05-099, hypertrophe Chondrozyten, Destabilisierung des medialen Meniskus, Parathormon.

Abstract

Cartilage degradation in Osteoarthritis (OA) is rather associated with aberrant hypertrophic-like gene expression in articular chondrocytes then cell death. Parathyroid hormone-related protein (PTHrP) suppresses chondrocyte hypertrophy and activity of salt-inducible kinases (SIKS) during normal endochondral ossification. However, medical use of PTH is limited. This work presents a promising novel approach to mimic PTHrP signaling with a small molecule SIK-inhibitor as a new disease-modifying drug for OA.

28 12-week old C57BL6 were subjected to the destabilization of the medial meniscus (DMM) or sham-surgery as control and treated with pan-SIK inhibitor YKL-05-099 or vehicle (VEH) for 11 weeks to assess changes in the articular cartilage. Murine primary sternal chondrocytes and mouse clonal limb bud cells were treated with YKL-05-099 to identify changes in gene expression and protein phosphorylation.

YKL-05-099 treatment mice showed decreased OA Research Society International (OARSI) scoring in comparison to VEH treated mice (Sham VEH vs Sham YKL $p = 0.0826$; DMM VEH vs DMM YKL $p = 0.2572$; $n = 7$/group) and reduced Col X staining (Sham VEH vs Sham YKL $p = 0.0746$; DMM VEH vs DMM YKL $p = 0.1309$; $n = 7$/group). Phosphorylation of cAMP-responsive element (CRE) binding protein (CREB) -regulated transcription coactivator 2 (CRTC2) and histone deacetylase 4 (HDAC4) was down-regulated in primary chondrocytes in correlation with inactivation of SIK-3 when treated with YKL-05-099, PTH or Forskolin. The Relative mRNA expression of *Prg4* was increased and *MMP13* decreased in primary sternal chondrocytes and clonal limb bud cells treated with YKL-05-099, PTH or Forskolin. *Prg4* and *MMP13 in situ* hybridization did not reveal the treatment effects of YKL-05-099 in the OA mouse model.

Systemically-administered YKL-05-099 improves articular cartilage integrity and mimic PTH/PTHrP signaling in primary sternal chondrocytes and mouse limb bud cells, suggesting pan-SIK inhibitors as potential disease-modifying drugs in OA.

Keywords: Osteoarthritis, salt-inducible kinases, YKL-05-099, chondrocyte hypertrophy, destabilization of the medial meniscus, parathyroid hormone.

Acknowledgements

I would first like to thank my supervisor Marc N. Wein, MD, PhD, for hosting my stay in his lab at the Massachusetts General Hospital. His contagious enthusiasm for bone biology kept me excited throughout the whole project. Thank you for your teaching and expertise.

I also want to thank my father Christian Rotter, my sister Susanne Rotter, my aunt Karin Polovitzer and my brother-in-law Martin Prieler, for their constant support throughout my life and during my stay in Boston. All of this wouldn't have been possible without you.

Extraordinary gratitude goes out to Nevena Jankovic for cheering me up every day we spent together in Boston.

I am grateful for all my colleagues at the Massachusetts General Hospital for teaching me new techniques and sharing knowledge and drinks with me. Thanks to Janaina Da Silva Martins, Shiv Verma, Jialiang Wang, Chris Castro, Tadatoshi Sato, Christopher John Janton, Matthew Parker McKeon, Devon Lloyd Campbell and Margaret Marie Kobelski.

Finally, I want to thank my friends Nikolas Czepl, Martin Witek, Ehsan Suleiman and Daniel Schnuderl, which never let me down.

Thank you for your encouragement.

Table of Contents

1 Introduction 6
1.1 Mechanisms of bone development and Chondrogenesis 6
1.1.1 Endochondral bone formation 6
1.1.2 Molecular mechanisms controlling Chondrogenesis 8
1.1.3 Chondrocyte maturation and hypertrophy in the growth plate 8
1.2 The synovial joint and Articular Cartilage 10
1.2.1 Structure of the knee joint 10
1.2.2 Synovial joint formation 11
1.2.3 Composition of articular cartilage 13
1.3 PTH/PTHrP signaling and the role of salt-inducible kinases 15
1.3.1 PTH/PTHrP surrogate-signaling molecules 16
1.4 Osteoarthritis 16
1.4.1 Cartilage degradation 18
1.4.2 Molecular markers of osteoarthritis 18
1.4.3 Treatment of Osteoarthritis 19
1.5 Hypothesis 21
1.6 Aim 22

2 Methods 23
2.1 *In vivo* Experiments 23
2.1.1 Surgery 23
2.1.2 Mouse Treatment 23
2.1.3 Sample collection 23
2.2 Histology 24
2.2.1 Preparation of murine knee sections 24
2.2.2 Safranin O Staining 24
2.2.3 OARSI Scoring 24
2.2.4 Proteoglycan area measurement 25
2.2.5 Immunohistochemistry 25
2.2.6 Assessment of Immunohistochemistry 26
2.2.7 In Situ hybridization 26
2.2.8 *In Situ* hybridization assessment 27
2.2.9 Alcian blue staining 27

2.3 Serum Pre-Clinical CartiLaps® (CTX-II) ELISA 28
2.4 *In Vitro* Experiments 28
2.4.1 Chondrocyte isolation 28
2.4.2 Thawing and cultivation of cells 29
2.4.3 Western Blot 29
2.4.4 Real-time PCR 30
2.5 Statistical evaluation 32

3 Results 33
3.1 Histomorphometric assessment of Osteoarthritis. 33
3.2 Immunohistochemical assessment of murine knee sections 36
3.2.1 Collagen X 36
3.2.2 MMP13 39
3.3 *In Situ* hybridization for *Prg4* 41
3.4 *In situ* hybridization for *MMP13* 43
3.5 Mouse serum CTX-II levels 45
3.6 Western blot 46
3.7 Real-time PCR 49

4. Discussion 58

Bibliography 65

List of Figures 79

List of Abbreviations 82

1 Introduction

1.1 Mechanisms of bone development and Chondrogenesis

1.1.1 Endochondral bone formation

During embryonic development, mesenchymal stem cells condense to clusters and differentiate into chondrocytes in a process called chondrogenesis. Ossification of the chondrogenic lineage into the vertebrate skeleton is a process called endochondral bone formation. Direct differentiation of mesenchymal stem cells into bone-forming osteoblasts occurs in bones of the cranial vault and resembles the exception in the bone-forming process [1], [2], [3], [4]. Here we focus on the development of long bones (see **Figure 1**).

The process of endochondral bone formation is driven by transcription factor Sox9, which induces proliferation of chondrocytes and production of the cartilage mould. Round shaped chondrocytes keep proliferating at the edge of the enlarging cartilage [5], [6] while chondrocytes in the center of the cartilage undergo maturation (hypertrophy). This process leads to a change of the genetic program of chondrocytes and therefore to the withdrawal of the cell cycle and increase in cell volume [7]. The longitudinal growth of the cartilage mould is driven by the constant production of matrix by proliferating chondrocytes and the deposition of super-sized hypertrophic chondrocytes within the matrix. Hypertrophic chondrocytes start production of type X collagen, attract blood vessels and cause mineralization of their surrounding matrix [3], [4]. This process attracts cells from the perichondrium (a dense connective tissue that surrounds cartilage) which become osteoblasts and form a bone collar [4]. Ultimately, hypertrophic chondrocytes undergo apoptotic cell death while immature chondrocytes continue the formation of cartilage. Osteoblasts use the provided cartilaginous scaffold to transform it into bone by developing the primary spongiosa and eventually future trabecular bone. The initially created bone collar may become future cortical bone [4]. Chondrocyte maturation gets restricted by the alignment of an orientated column like stack of flattened chondrocytes forming the growth plate at the end of the bone (epiphysis). The formation of the growth plate leads to a more directed bone lengthening and the development of a secondary ossification center above the growth plate by attracting osteoblasts and blood vessels [3], [4]. Chondrocytes on top of the growth plate slow their active cell cycle and may serve as precursors for the flattened column-stacked chondrocytes of the growth plate. These round chondrocytes express a larger variety of transcription factors including Sox5 and Sox6. Furthermore, cells keep producing matrix proteins like type II collagen and aggrecan [3]. Chondrocytes of the growth plate undergo multiple stages of hypertrophy with altering sets of expressed genes. Prehypertrophic chondrocytes can be identified by the expression of parathyroid hormone (PTH) receptor 1 (Pth1r) and Indian hedgehog (Ihh). The next stage of maturing chondrocytes are early hypertrophic chondrocytes expressing type X collagen while the

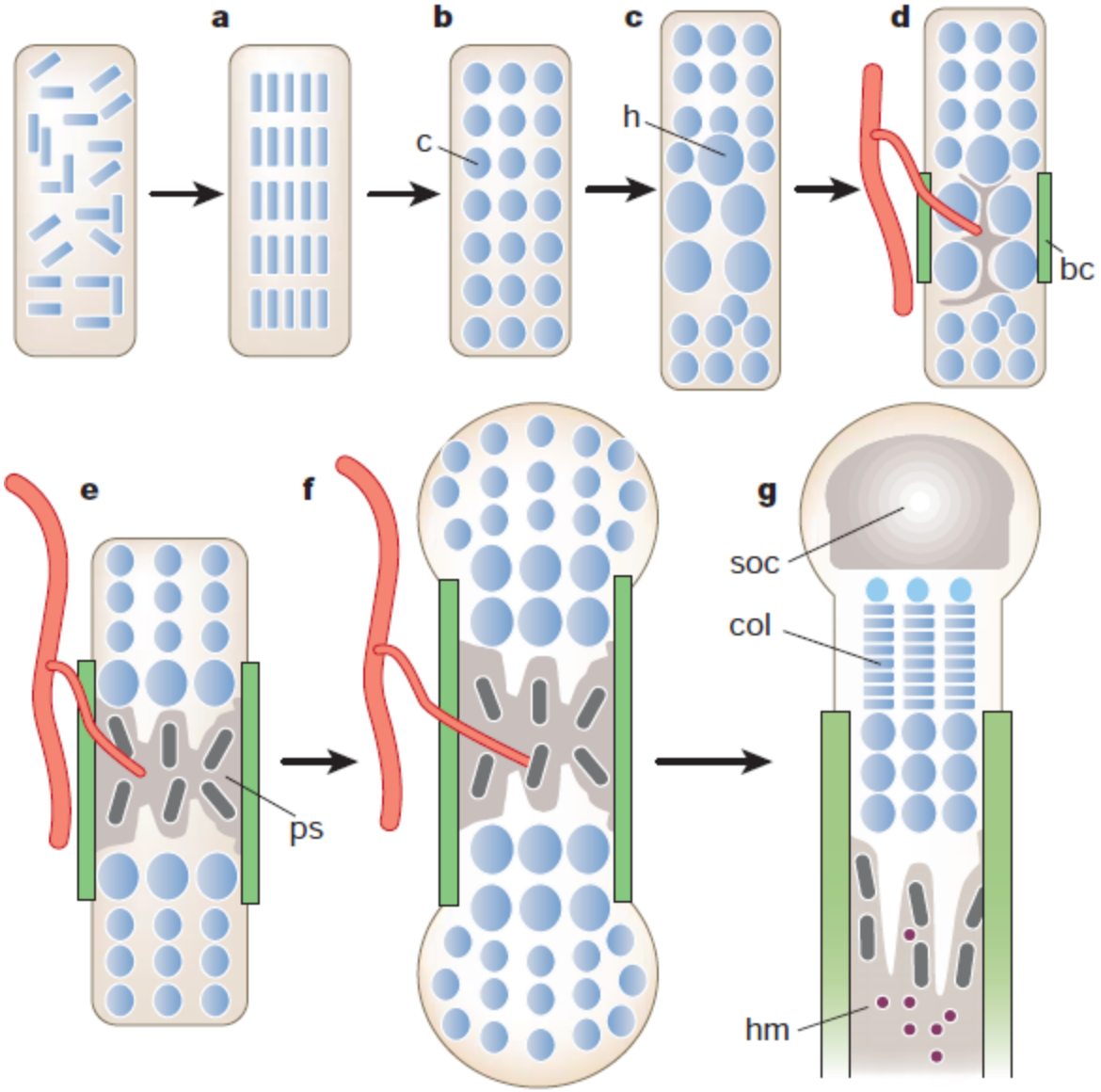

Figure 1: Endochondral bone formation [4]**. a)** Condensation of Mesenchymal stem cells. **b)** Differentiation of mesenchymal cells into chondrocytes (c). **c)** Chondrocytes become hypertrophic in the center of condensation (h). **d)** Formation of the bone collar (bc) through perichondrial cells that became osteoblasts. Hypertrophic chondrocytes direct mineralization of matrix, attract blood vessels and undergo apoptosis. **e)** Formation of primary spongiosa (ps) by osteoblasts. **f)** proliferating chondrocytes lengthen the bone, osteoblast of the bone collar become cortical bone, and Osteoblasts of the primary spongiosa may become precursors of trabecular bone. **g)** Formation of the secondary ossification center (soc), formation of the growth plate by chondrocytes stacked in columns (col). Hematopoietic marrow (hm) expands in marrow space along with stromal cells.

expression of early chondrogenic genes gets reduced.

Late hypertrophic cells stop the expression of matrix proteins and start the expression of vascular endothelial growth factor A (*VegfA*), matrix metalloproteinase 13 (*Mmp13*) and secreted phosphoprotein I (*Spp1*) [3]. The expression of the new set of genes leads to the

attraction of osteoclast and osteoblast precursors, which mature and start the transformation of the growth plate into trabecular bone [8], [9].

1.1.2 Molecular mechanisms controlling Chondrogenesis

Chondrogenesis is blocked by Wnt signaling via β-catenin/Lef1/Tcf in limb buds[10], [11]. Wnts in combination with fibroblast growth factors (FGFs) secreted by the ectoderm ensure limb bud outgrowth and the maintenance of chondrogenic precursor cells for a cartilage template [12], [13]. Once Wnt signaling is lost, *Sox9* expression is no longer blocked in mesenchymal limb bud cells [14].

As previously mentioned, endochondral bone formation is driven by transcription factor Sox9. However, activation of Sox9 is driven by sonic hedgehog (Shh) during the developmental differentiation process of the somite into the sclerotome [15], [16]. After the initial activation of sclerotome-specific markers like PaxI, Sox9 and Nkx3-2 by Shh [17], cartilage formation is initiated and Shh signaling can be dismissed [18]. Sox9 levels can be maintained in somatic cells by a self-regulating mechanism involving the activation of Nkx3-2 in combination with bone morphogenic protein (BMP) [19], [20].

While BMP signaling is important for *Sox9* expression, miss regulation in the limb bud can lead to ectopic chondrogenesis [21]. However, inhibition of BMP signaling results in inhibition of cartilage formation [21]. Yoon *et al.* have shown that BMP is mandatory for chondrocyte formation. The deletion of BMP receptor 1a (Bmpr1a) and BMP receptor 1b (Bmpr1b) leads to decreased expression of Sox-family transcription factors Sox5, Sox6 and Sox9 which regulate chondrogenesis [22], [23].

Protein kinase A (PKA) phosphorylates and activates Sox9 [24]. When PKA antagonist retinoic acid (RA) is administered to murine epiphyseal chondrocytes, expression of Wnt ligands and their receptors is increased [25]. Increased Wnt signaling leads to expression of Lef/Tcf receptors [25]. These results by Yasuhara *et al.* support the previously mentioned Sox9 inhibition via Wnt signaling through Lef/Tcf in mouse limb buds. Furthermore, it was shown that Sox9 expression and activation is increased when RA receptor-mediated signaling was blocked in primary mouse limb bud cells [26]. These results show that PKA alongside Shh, BMP and FGF play an important role in the positive regulation of Sox9 during chondrogenesis.

1.1.3 Chondrocyte maturation and hypertrophy in the growth plate

Besides the activation of the differentiation program of mesenchymal stem cells into chondrocytes, Sox9 plays an important role in chondrogenic maturation. Sox9 induces differentiation of chondrocytes directly and through induction of Sox5 and Sox6 expression, which in turn, activate the chondrogenic differentiation program [27]. Sox9 activates expression of for type II collagen [28], type IX collagen and type XI collagen [5] which can be found in immature chondrocytes. Overexpression of Sox9 slows hypertrophic maturation of chondrocytes [29] while loss of function in immature chondrocytes enhances hypertrophy

[5]. It has been shown that Sox9 degrades β-catenin and block canonical Wnt signaling [29], which promotes chondrocyte hypertrophy [11]. Sox9 is also responsible for the delay of chondrogenic hypertrophy through reduction of Runt-related transcription factor 2 (Runx2) signaling [30] and repression of type X collagen, a marker of hypertrophic chondrocytes [31]. Runx2 promotes expression of hypertrophic markers in chondrocytes [32] and gets activated by canonical Wnt signaling which is also known to enhance chondrocyte hypertrophy. Once Runx2 is activated it promotes expression of *Col10a1* [33] and *Mmp13* [34] which are typically expressed in early and late hypertrophic chondrocytes.

Myocyte enhancer factor-2 (Mef2) family transcription factors are necessary for chondrocyte hypertrophy and regulation of Runx2 expression for normal bone growth. Overexpression of Mef2 in chondrocytes leads to heavily increased ossification of the cartilaginous mould [35]. Regulators such as histone deacetylase 4 (HDAC4) influence the maturation of chondrocytes negatively and delay chondrocyte hypertrophy. HDAC4 remains in the nucleus or cytoplasm depended on their state of phosphorylation and interaction with 14-3-3 proteins [36], which mediate and regulate signaling transduction [37]. Prehypertrophic chondrocytes express HDAC4 to suppress both Runx2 [38] and Mef2 [39] activity when localized in the nucleus. Binding of 14-3-3 proteins to HDAC4 results in cytoplasmic localization [40] and uninhibited binding of Runx2 and Mef2 family members to transcriptional targets.

Chondrocyte maturation and hypertrophy is also regulated by PTH related peptide (PTHrP). Knockout of *PTHrP* in mice results in early chondrocyte maturation, increased bone formation and stops chondrocyte proliferation [41]. A similar phenotype was created when Pth1r, a G-protein coupled receptor (GCPR) was deleted in mice [42]. PTHrP is expressed in periarticular resting cells of the growth plate and early proliferating chondrocytes [41] and cause delayed differentiation when overexpressed in mice [43]. Binding of PTHrP to Pth1r activates the subunit $G_s\alpha$ and $G_q\alpha$. Stimulation of $G_s\alpha$ leads to activation of adenyl cyclase (AC) which start the production of cyclic adenosine monophosphate (cAMP) to activate PKA [44]. This process is important for the translocation of HDAC4 into the nucleus for Mef2 and Runx2 inhibition and the delay of chondrocyte hypertrophy [38], [39], [45].

PTHrP signaling is mediated by Ihh-expressing prehypertrophic and early hypertrophic chondrocytes [46]. Deletion of *Ihh* results in a similar phenotype as seen in *PTHrP* knockout mice [47]. *Ihh*-deletion can be partially rescued by constitutively active Pth1r in the growth plate to block premature chondrocyte hypertrophy [48]. However, Ihh promotes round chondrocytes into proliferating chondrocytes and proliferation of chondrocytes in general independently from PTHrP expression [48], [49].

A summary of important genes expressed by chondrocytes in different states of maturation can be seen in **Figure 2**.

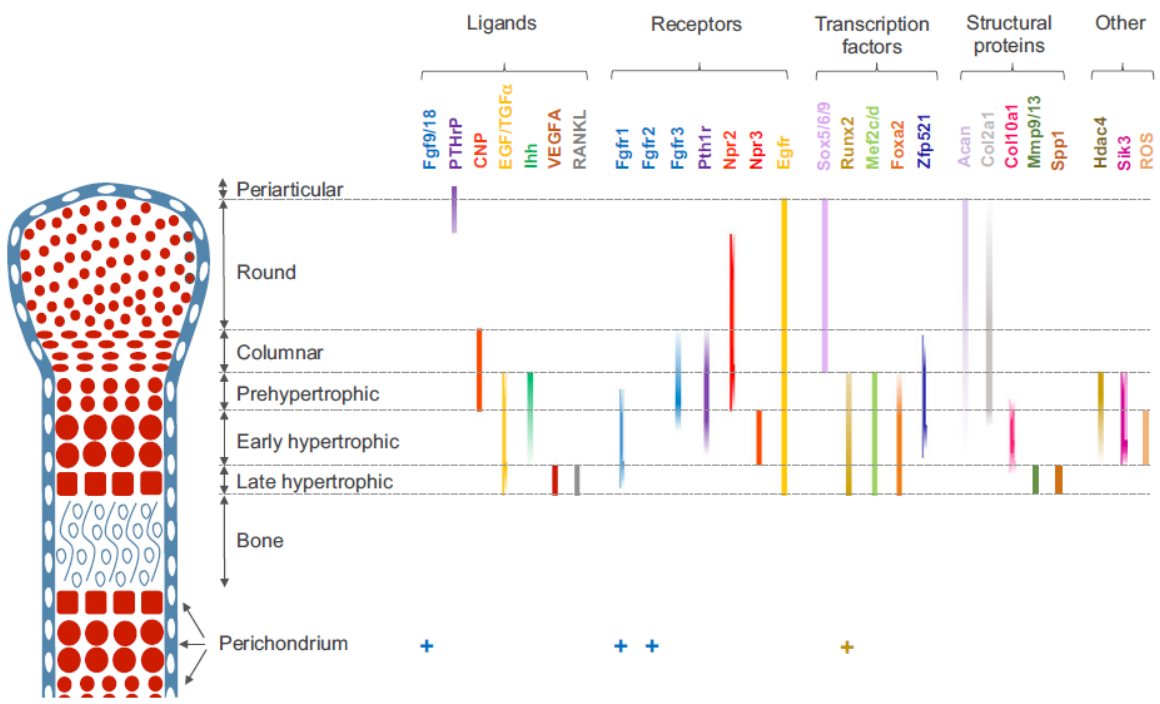

Figure 2: Regional expression of genes in chondrocytes [3]. Expression of genes is dependent on region and state of hypertrophy of chondrocytes. Immature chondrocytes express structural proteins found in cartilage such as type II collagen and aggrecan while mature chondrocytes express type X collagen and MMP13 for bone remodeling.

1.2 The synovial joint and Articular Cartilage

1.2.1 Structure of the knee joint

One of many synovial joints in the human body is the knee (see **Figure 3**). It can be divided into the tibiofemoral and a patellofemoral joint. The tibiofemoral joint connects the femur and the tibia, allowing load transmission of the body weight and motion. Load bearing surfaces are covered with articular cartilage, which has high compressive strength and provides a low friction surface for smooth joint mobility. The joint space is filled with synovial fluid that provides additional lubrication and is covered by the synovial membrane. The joint is stabilized by the medial and lateral meniscus, cartilaginous structures that distribute the load and the anterior cruciate ligament, the medial and the lateral collateral ligament [50], [51].

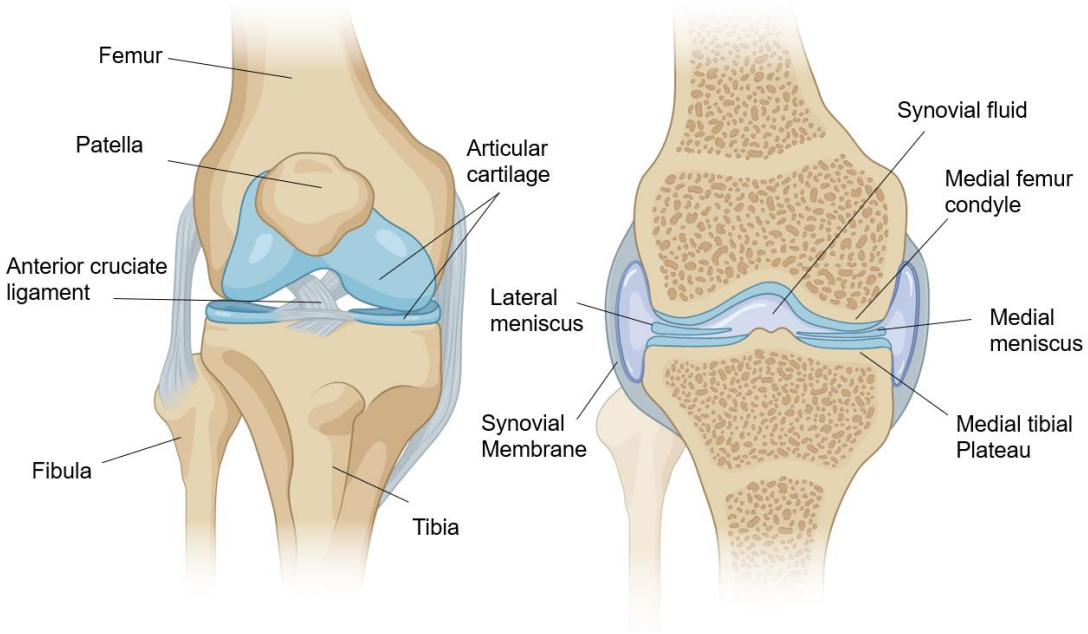

Figure 3: Anatomy of the human knee joint. The human knee joint is an assembly of the femur, the tibia, the patella, menisci and ligaments to provide stability and mobility. The distal ends of the femur and the tibia are covered with cartilage for protection from mechanical stress. The joint is covered by the synovial membrane which contains synovial fluid for joint lubrication.

1.2.2 Synovial joint formation

During the endochondral bone formation, an avascular layer of mesenchymal tissue interrupts the cartilaginous mould at prospective joint sites forming the “Interzone” [52]. The interzone consists of two outer layers of round cells separated by an inner layer of flattened cells [53]. Cells of the interzone give rise to articular cartilage, the synovial lining and intrajoint ligaments [54] while the outer layers contribute to the growing long bone epiphysis [55]. Type II collagen expressing cells within the pre-chondrogenic primordium form the articular cartilage, ligaments and the medial meniscus, while cells outside of the anlagen which do not express type II collagen contribute to the formation of the lateral meniscus [56]. Tracking experiments were able to identify early Sox9 expressing cells as precursors for chondrocytes in both, articular cartilage and growth plate cartilage, suggesting a common mesenchymal precursor population [57]. Chondrocytes of the former cartilaginous mould retire expression of their chondrocyte-specific set of genes and start expressing a new set of genes including growth and differentiation factor 5 (*GDF5*), *Wnt4*, and *Wnt9* [58], [59], [60].

GDF5 is a member of the Bone morphogenic protein (BMP) family and is expressed in the future joint site and the interzone [61]. *GDF5* expression is necessary for the formation of the epiphysis, articular cartilage, joint capsule and intra-articular cartilage ligament [62], [63], [64]. Loss of GDF5 function can be rescued by BMP-family members GDF6 and GDF7 [65]. However, loss of both GDF5 and GDF6 leads to joint fusions [66]. The expression of *GDF5*

is regulated in a very delicate manner. Decreased levels of functional GDF5 lead to malformations in cartilage and joints [67]. Overexpression of GDF5 leads to increased bone length, due to increased numbers of chondrocytes and early chondrogenesis [68], which results in joint formation disturbances [69].

In addition to GDF5, Wnt signaling via *Wnt4*, *Wnt9a* and *Wnt16* is necessary for synovial joint formation and maintenance. These signaling factors are primarily expressed in the presumptive joint and interzone. Expression of Wnt signals are complementary and overlapping but have different levels of expression depending on the zone of the forming knee joint [58], [60]. Lacking Wnt9a signaling after the formation of the interzone makes joint fusion inevitable [59]. This phenotype was also shown in knockout mice missing *β-catenin*, target of canonical Wnt signaling [58]. These studies suggest that Wnt signaling blocks chondrogenesis in the interzone to support the formation of articular cartilage.

The Interzone further differentiates into a dense “intermediate” compartment and two flanking “outer” compartments with a more disorganized arrangement [56]. Genes associated with joint formation are primarily expressed in cells found in the intermediate compartment. Cartilage maturation and hypertrophy associated genes are more likely expressed in cells of the outer compartment. Jenner *et al.* concluded that articular cartilage is formed by cells of the intermediate compartment, while cells of the outer compartment are responsible for endochondral ossification and are part of the secondary ossification center [70].

The joint formation is not only regulated by local expression of GDF5 and Wnts in the interzone but also by distal expressed signaling factors like Indian hedgehog, expressed by prehypertrophic cells of the growth plate. Indirect interaction of Ihh with PthrP regulates the length of the proliferating zone of chondrocytes of articular cartilage and the hypertrophic zone [42], [46], [48].

After these initial steps of joint formation, separation of the skeletal elements, a process called cavitation, is driven by mechanotransduction [71], [72], [73]. Movement of surrounding skeletal muscles stimulate signaling cascades which induce the production of hyaluronan. This changes the composition of extracellular matrix and leads to the loss of cell-cell integrity at the plane of cleavage and separation [74], [75]. The formed joint cavity is filled with synovial fluid to enable frictionless movement of the joint [74]. Hyaluronan production is further induced by fibroblast growth factor 2 (Fgf2) and mitogen-activated protein kinases P38 and Erk1/2 [76], [77].

Articular cartilage is growing to cover the expanding epiphysis with a thick layer of matrix. This expansion is achieved by a small layer of proliferating cells which represent the gliding surface of the joint [78], [79]. The proliferation of cells was only detected in the superficial layer of cells [78], [79] but not in deeper regions of articular cartilage [80]. Proliferating cells in the superficial layer of articular cartilage and synovial cells express *Prg4*, the main lubricant in the joint. Expression of *Prg4* starts in developing joints and continues postnatally for maintenance of normal joint function [21], [81]. *Prg4* expression is regulated by cAMP-responsive element (CRE) binding protein (CREB) and its coactivators CREB-regulated

transcription coactivator 2 (CRTCs) in a mechano-sensitive manner [82]. Ogawa *et al.* showed that epiphyseal chondrocytes subjected to fluid flow shear stress had increased CREB-dependent induction of Prg4 by PKA and Ca^{2+} signaling through secretion of extracellular prostaglandin E2 (PGE2), PTHrP and adenosine triphosphate (ATP) [82].
Another mechanical stimulator for maintaining joint integrity is load. The ion channel transient receptor potential cation channel subfamily V member 4 (TRPV4) induces cartilage-specific gene expression and matrix biosynthesis by a mechano-sensitive Ca^{2+} influx [83], [84]. Ca^{2+} can have contrary effects on chondrogenic gene expression. Articular chondrocytes express the proteoglycan lubricin, which is important for joint lubrication. Expression of *Prg4* is CREB-mediated through Ca^{2+} signaling and supports joint integrity. Pathological joint loading induces increased Ca^{2+} via ion channel via PIEZO1 and 2 that leads to cell death [85].

1.2.3 Composition of articular cartilage

Articular cartilage is formed at the end of long bones by chondrocytes. It is a highly structured tissue providing a low friction surface for joint mobility and a shock-absorbent matrix to withstand load. Even though articular cartilage is designed to bear mechanical stress, it has poor regenerative capabilities and low metabolic activity. The dense matrix of articular cartilage consists primarily of water, collagen and proteoglycans. Chondrocytes play a major role in the maintenance of the articular cartilage but are only present in a lower number [86], [87].
Articular cartilage can be divided into four distinct regions and functionalities (see **Figure 4**). The superficial zone at the distal end of the articular cartilage makes up 10 % - 20% of the total articular cartilage thickness and provides a shear resistant surface. This surface is made by collagen fibrils aligned parallel to the articular surface to facilitate smooth gliding. [86] Despite the shear resistance, the superficial zone is more likely to be deformed in comparison to the middle zone of the articular cartilage. Smooth gliding is supported by expression of proteoglycan 4 (PRG4 or lubricin) by elongated chondrocytes embedded in the matrix [88]. The protein can be found in the so-called synovial fluid film which protects moving surfaces from solid-to-solid contact. Besides lubricin, hyaluronan and surface-active phospholipids enhance boundary lubrication [89], [90].
40% to 60% of the articular cartilage volume is the middle zone. This zone has less organized collagen fibers and chondrocytes appear round shaped. The oblique alignment of thicker collagen fibrils leads to increased compressive strength in comparison to the superficial zone of the articular cartilage [86], [87], [91].
The deep zone encompasses up to 30% of the articular cartilage. This layer has the highest compressive strength due to perpendicular orientated thick collagen fibrils and a high number of proteoglycans [86], [87] [91].
The calcified cartilage region is separated from the deep zone by the tide mark. The calcified region is directly connected to the subchondral bone and contains small cells in a chondroid matrix [86], [87].

The main components of the extracellular matrix are water, type II collagen and large aggregating proteoglycans. Other types of collagen and proteins only make up a minor portion of the whole composition. Type II collagen fibrils form a three-dimensional interconnected network supported by proteoglycans. This network with interspatial voids stabilizes the matrix to resist shear and tensile stress [86].

Proteoglycans have a high affinity for water. Aggrecan is the most abundant proteoglycan in cartilage and consists of a long protein core with a high amount of chondroitin sulfate and keratan sulfate glycosaminoglycan chains. Aggrecan binds to a hyaluronate protein which interconnects with collagen fibrils. The proteoglycans are entrapped inside the interfibrillar space of the collagen network, which creates a porous-permeable matrix that determines fluid flow of water [86], [91].

The negative charge of proteoglycans creates the Donnan osmotic equilibrium by entrapment of water in the interfibrillar space of the collagen-proteoglycan matrix. This leads to high interstitial fluid pressurization and contributes to the stiffness and viscoelastic properties of the cartilage. This mechanism leads to reversible plasticity of cartilage and ultimately, protection of the solid phase by load distribution [91]–[96].

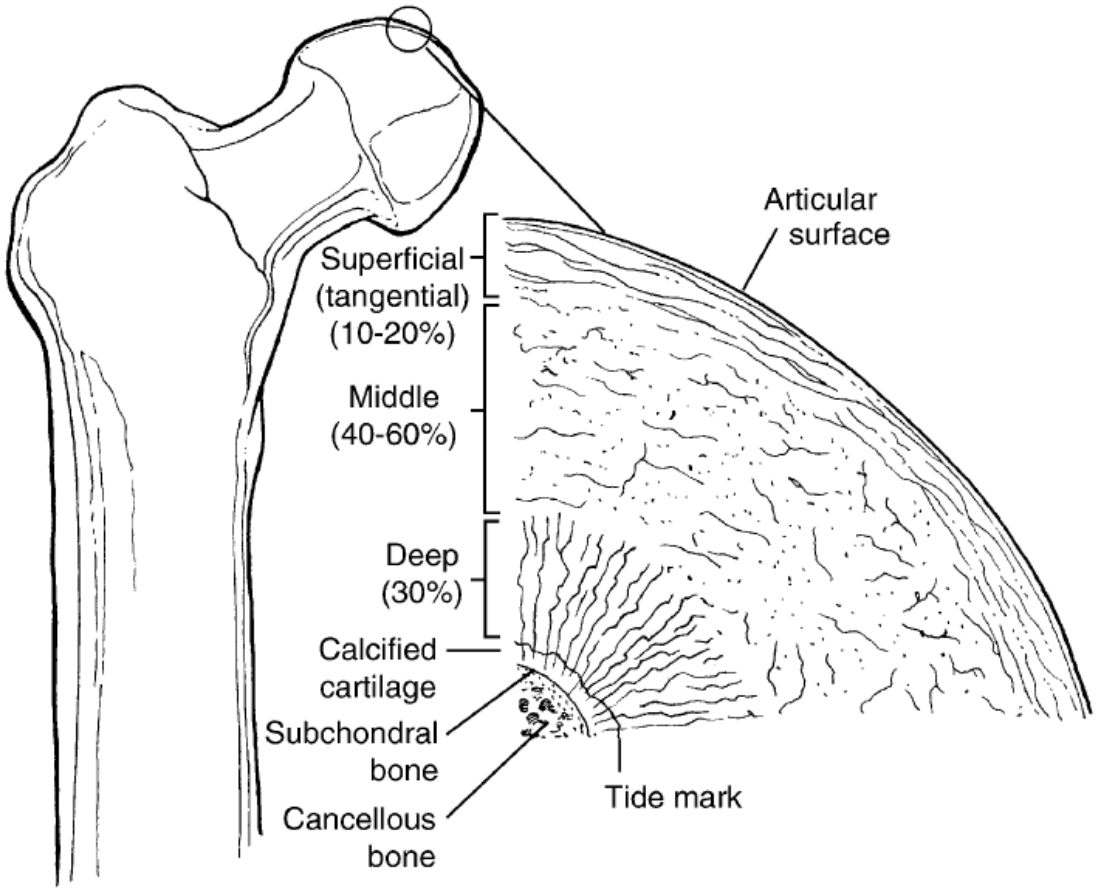

Figure 4: Zonal arrangement of articular cartilage [86]**.** Articular cartilage can be divided into the superficial, middle, deep and calcified layer of cartilage. The non-calcified region of cartilage is separated from the calcified region by the tide mark.

1.3 PTH/PTHrP signaling and the role of salt-inducible kinases

PTH is expressed in the parathyroid gland and binds to parathyroid hormone receptor 1. It regulates blood calcium and phosphate levels [97] and usually targets osteoblasts, chondrocytes, osteoclasts and tubule cells in kidney [98]. PTH signaling in bone has either catabolic effects or anabolic effects depending on the target of signaling [99]. The structurally similar PTHrP is synthesized in normal and malignant tissues, including growth plate chondrocytes and acts in many tissues as paracrine or autocrine signal during fetal development, bone development and in placental function [98], [100].

As previously discussed, chondrocyte hypertrophy is mediated by PTH/PTHrP and Pth1r. PTHrP binds to Pth1r, which is expressed in immature chondrocytes. PTH/PTHrP has a high affinity to signal through the $G_s\alpha$ subunit of the GCPR which leads to the activation of AC. AC dephosphorylates ATP to form cAMP which activates PKA [44], [100]. HDAC4 and HDAC5 is bound by protein 14-3-3 at three phosphorylation sites and retained in cytoplasm in presence of low concentrations of cAMP and activated PKA. However, increased levels of PKA leads to dephosphorylation of HDAC4 and HDAC5 and translocation into the nucelus [36]. Once HDAC4 is dephosphorylated it can translocate into the nucleus and inhibit Mef2 and Runx2 family activity [39], [45]. PKA additionally activates nuclear translocation of CRTC2 to activate CREB and Prg4 expression [82].

Wein *et al.* recently discovered the interaction of PTH/PTHrP signaling with salt-inducible kinases (SIKs) in osteocytes (terminally-differentiated osteoblasts buried within bone matrix). Activation of PKA via cAMP through PTH/PTHrP signaling leads to phosphorylation of SIK2. Inactivation of SIK2 through phosphorylation leads in turn to reduced phosphorylation of HDAC4/5 and nuclear translocation. HDAC4/5 inhibits Mef2C-driven *SOST* expression, which leads to increased bone formation. Additionally, inactivation of SIK2 leads to decreased phosphorylation of CRCT2, which allows nuclear translocation. Active CRTC2 mediates CREB mediated receptor activator of NF-κB ligand (RANKL) expression and therefore increases bone resorption [101]. But what are salt-inducible kinases and what role do these kinases play in chondrocytes?

SIKs were initially isolated from adrenocortical tissues from high salt diet-treated rats and identified as members of the AMP-activated protein kinase (AMPK) family [102]. There are three known SIKs (SIK1, SIK2, SIK3) which share a characteristic structure of a tripartite kinase containing serine-threonine domain at the N-terminal end, a sucrose non-fermenting-1 homology domain, and a long C-terminal extension containing a PKA-dependent phosphorylation site [103]. While SIK2 and SIK3 are ubiquitously expressed, SIK1 expression is regulated by high salt intake, adrenocorticotropin hormone signaling, glucagon signaling, excitable cell depolarization, and circadian rhythms [104]. The two most studied targets of SIK-signaling are class IIa histone deacetylases such as HDAC 4 and HDAC 5 [105] and CRTCs [106]. SIKs are responsible for the phosphorylation of multiple sites on

CRTCs and class II HDACs which are necessary for protein 14-3-3 binding to sequester both protein families inside the cytoplasm [107]. However, SIK family activity is blocked by PKA-mediated phosphorylation [107]. The recent finding of Nishimori *et al.* showed the deactivation of SIKs by Pth1r action and the connection of SIKs with class IIa HDACs during bone development and remodeling [108]. Additionally, SIKs regulate nuclear translocation of CRTC2 for CREB activation and the expression of *Prg4*. [82], [107]. Taken together, SIKs are important for the regulation of chondrocyte hypertrophy and maintenance of vital articular cartilage.

1.3.1 PTH/PTHrP surrogate-signaling molecules

PTH/PTHrP signaling acts through binding to G-protein coupled receptor Pth1r to activate cAMP and PKA. Molecules that activate cAMP or PKA directly can simulate downstream targets of the PTHr1 signaling cascade or other signaling pathways. Furthermore, activation of cAMP and PKA can be dismissed if downstream signals of PTH/PTHrP are directly targeted.

cAMP can be activated by Forskolin, a labdane diterpene which can be found in the root cork of *Coleus forskohlii* [109], [110]. Forskolin activates AC directly and initiates cAMP associated signaling [111]. The GPCR-independent activation of AC makes Forskolin an interesting component for studying PTH/PTHrP related signaling and other topics in biochemical research. It is also actively used as a drug for the alleviation of glaucoma [112], treatment of hypertension, heart failure [113], [114], lipolysis and body weight control [115], [110].

SIKs represent one of the downstream targets of PTH/PTHrP signaling. Small molecules like YKL-05-099 are selectively targeting SIKs over other kinases. YKL-05-099 was developed by converting the 2-aniline substituent of pan-SIK inhibitor HG-9-91-01 to a 1-methyl piperidine group. This resulted in a decreases SIK2-inhibitory effect and interleukin 10 (IL-10) enhancing activity without toxicity in doses of 10 µM or lower. Additionally, YKL-05-099 binds to SIK1, SIK2 and SIK3, which makes it a potent pan-SIK inhibitor [116]. Bone marrow-derived macrophages subjected to YKL-05-099 had decreased phosphorylation of HDAC5 at Ser259. Furthermore, increased expression of CREB target genes were seen with YKL-05-099 treatment and is also affecting the systemic inflammatory response *in vivo* by a dose-depending reduction of tumor necrosis factor α (TNFα) and induction of IL-10 levels [116].

1.4 Osteoarthritis

Osteoarthritis (OA) is one of the most common and frequent musculoskeletal diseases worldwide [117]. OA causes degradation and loss of articular cartilage and changes in the synovial fluid, synovial membrane and subchondral bone, including remodeling and osteophyte formation [86] (see **Figure 5**). These changes are associated with joint pain, stiffness, limitation of movement and chronic inflammation [118]. Symptoms have a

significant impact on daily routine activities, which may affect social integrity [118], [119], [120]. Osteoarthritis is an age-related disease [118] and can be induced by trauma in a secondary manner [119]. Pathophysiological changes are well defined to identify OA but may need to be adjusted individually depending on symptoms within different joints. The traditional opinion of OA as “wear-and-tear” destruction of articular cartilage is changing to OA as a multifactorial disease due to the finding of increased pro-inflammatory cytokine levels in the affected patients [121]. Furthermore, treatment of OA is limited to palliative drugs, physiotherapy and surgery to increase joint mobility [120] which are associated with high healthcare costs [119].

OA occurs primarily in adults over age 65, with currently 27 million people affected in the United States (US) [122]. The number of OA patients is constantly rising due to multiple risk factors such as family history, age, obesity, diabetes, synovitis, systemic inflammatory mediators, innate immunity, lower limb alignment (genu valgum and genu varum), joint shape and dysplasia, trauma, and inflammation by metabolic syndromes [121]. Knee OA has the highest prevalence in comparison to other forms of OA [122] and women tend to have a higher prevalence than man with a more severe form of OA [123]. The increased numbers of affected woman were associated with hormonal changes during menopause but haven’t been confirmed so far [122].

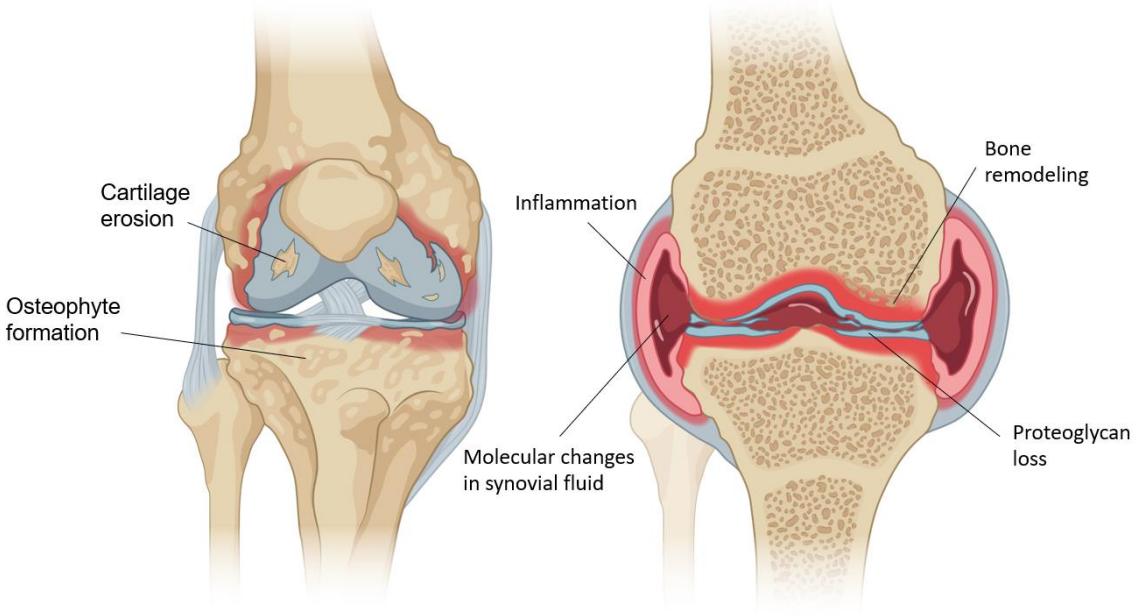

Figure 5: Changes in the osteoarthritic knee joint. OA cause degradation and loss of articular cartilage, osteophyte formation, inflammation, bone remodeling, changes of the synovial membrane and molecular changes in the synovial fluid. These changes cause pain and limitations in join mobility.

1.4.1 Cartilage degradation

Cartilage degrades progressively during OA and occurs as softening, fibrillation, and erosions [86] leading to cartilage clefts, loss of the cartilage layers, cellular necrosis, chondrocyte cloning and duplication of the tidemark [124]. The first histological changes can be seen in the superficial zone of articular cartilage. Progressing OA is associated with the loss of proteoglycans. As already discussed, proteoglycans are necessary to create an osmotic equilibrium which contributes to stiffness and viscoelastic properties of the cartilage [91]–[96]. Interestingly, more proteoglycans can be found in OA-cartilage. However, proteoglycans are degraded and unbound to the hyaluronic-backbone of collagen fibers. [125]. This leads to increased permeability of the matrix due to decreased hydraulic pressure [126], [127]. In turn the compressive strength of articular cartilage is reduced, which can be identified as softening of early chondromalacia [128], [129]. These findings suggest that repair mechanisms involving increased expression of proteoglycans [125] and increased water content in the matrix [126], [127] are insufficient to maintain matrix integrity. The internal matrix structure is also impaired by gradually increasing disorganization of the collagen interfibrillar network. Even though collagen content is maintained in early OA, structural changes lead to decreased tensile strength [130].

Progressive OA leads ultimately to the death of articular chondrocytes. However, recent studies indicate that death is not the main reason for cartilage damage but an alteration of gene expression [131]. In OA, an ectopic hypertrophic-like phenotype of articular chondrocytes expressing genes that lead to cartilage catabolism, reduced cartilage thickness, and ossification [132]. A similar gene expression program can be found in hypertrophic chondrocytes of the growth plate [4].

1.4.2 Molecular markers of osteoarthritis

OA can be characterized with radiographic methods to assess joint space width. This regularly involves measurements over a prolonged period for proper assessment. Unfortunately, radiographic methods are prone to technical difficulties [133], [134]. OA can also be determined with histological soring systems but require invasive procedures [135], [136]. Once noticeable cartilage degradation is measured, OA has already progressed [134]. Early detection of OA is necessary for timely treatment. Even though OA is considered as a mechanically driven disease, molecular mediators play an important role in the degradation of cartilage [86]. This involves soluble factors like enzymes, cytokines and chemokines, which have been implicated with OA pathogenesis [86], [137].

Metalloproteases (MMPs) are enzymes that are responsible for cartilage breakdown with its most prominent members collagenase-I (MMP-1) and collagenase-3 (MMP13) [86]. MMPs and cathepsins have a proteolytic activity in cleaving type II collagen [138]. Chondrocytes in the articular cartilage express type II collagen as the main component of the matrix but may synthesize MMPs and Cats in response to cytokines and growth factors or state of maturation [3], [138]. However, increased expression of MMPs was found in cartilage,

synovial tissue and increased concentrations in synovial fluids of OA patients [139]. Overexpression of MMPs can also be associated with mechanical loading [140]. Possible markers for detection of OA are MMPs, Cats and their associated degradation products C-telopeptide of type II collagen (CTX-II) and Helix-II. Increased levels of both fragments were detected in urine of OA patients.[141], [142], [143]. MMPs also target aggrecan. Stromelysin-1 (MMP-3) cleaves aggrecan and generates a G1 fragment which can also be used as OA biomarker [139]. Measuring the amount of sulphated glycosaminoglycans with dimethyl methylene blue gives evidence of increased aggrecan degradation [144], [145].

As mentioned above, increased expression of MMPs may be triggered by inflammatory cytokines such as TNF-α, IL-1β, IL-6, IL-37 and other interleukins which are associated with OA. Correlations between increased levels of inflammatory cytokines and cartilage degradation were found in several studies and may serve as a predictor of OA [146]–[150]. Inflammatory cytokines are released by synoviocytes, mononuclear cells in the synovial sublining layer, and by chondrocytes [86].

Increased levels of IL-1β and its receptor IL-1R1 were found in OA patients. Binding of IL-1β to its receptor triggers a cascade of signals, which leads to the expression of other cytokines, chemokines, adhesion molecules, inflammatory mediators, and enzymes [151]. It was also shown that IL-1 blocks expression of structural proteins in the extracellular matrix of cartilage by chondrocytes [152].

TNF-α is considered as key inflammatory factor in OA. TNF-α can bind either to receptor TNF-R1 or TNF-R2, which trigger signaling cascades for the expression of MMPs and cytokines [153]. Receptors can be found on synoviocytes and chondrocytes [153] Furthermore, TNF-α suppresses synthesis of proteoglycan components, protein binding proteoglycans and type II collagen [154]. Binding of TNF-α to its receptor TNF-R1 causes dramatic local effects by inducing cell death and cartilage degradation [155].

IL-6 has similar effects like IL-1β and TNF-α by inhibiting the production of cartilage matrix proteins and stimulating expression of MMPs synergistically with other cytokines and may serve as predictor for OA [148], [153].

1.4.3 Treatment of Osteoarthritis

Identification of OA is based on radiographic evidence. However, measurable radiographic change in joints may not correlate with painful OA. No cure for OA was discovered so far. Current treatment options are based on symptoms and can be summarized in three major disciplines: nonpharmacological and preventive strategies, pharmacological therapies and surgery [156].

Nonpharmacological treatment strategies focus on patient education regarding lifestyle, exercise, weight reduction and other measures [157]. Increased evidence was found that obesity plays a significant role in the development and progression of OA due to mechanical loading [158], [159]. Other studies showed that weight loss of knee OA patients increased joint mobility. However, loss of weight was not proven to slow progression of knee OA [160],

[161]. Furthermore, physical exercises show improvements in pain, function and global assessment in hip and knee OA patients [156].

Pharmacological therapies focus primarily on analgesic pain treatment. This includes paracetamol or non-steroidal anti-inflammatory drugs (NSAIDs) [162]. However, the potential of paracetamol in pain amelioration is low and has no improvements in the Western Ontario and McMaster Universities Osteoarthritis Index (WOMAC), a system to assess joint pain, stiffness and function [156]. In comparison to first-line medication paracetamol, NSAIDs including cyclo-oxygenase-2 (COX-2) selective inhibitors can reduce pain and functional disability in knee OA [162] but have more adverse events [156]. COX-2 selective inhibitors such as rofecoxib, diclofenac and indomethacin increase cardiovascular risks and should not be administered to patients with ischemic heart diseases or stroke [163]. Alternatively, topical NSAIDs can be used as short-term therapy with reduced effects and with very low systemic adverse events in comparison to oral NSAIDs [156], [157].

The use of glucosamine and chondroitin sulphate, both components of articular cartilage, show mixed results in pain relief and improvements in joint function and need further analysis to confirm the beneficial effect in OA treatment [156].

An alternative to oral drugs is intra-articular corticosteroid injections. This therapy showed improved mobility and reduced pain without serious systemic adverse events. However, there is insufficient data for long-term efficacy [164], [165].

Hyaluronic acid was also used as an intra-articular injection with inconsistent results. Further studies are necessary to confirm pain relief, range of motion and WOMAC scores [157], [166].

A new approach in OA treatment involves the inhibition of proinflammatory cytokines. Diacerein inhibits IL-1β activation by reducing the production of IL-1 converting enzyme and by inhibiting IL-receptor levels of chondrocytes. Diacerein showed similar efficacy in comparison to NSAIDs and superior efficacy in comparison to paracetamol [167].

All the described drugs are of palliative nature only and do not rescue cartilage degradation. The need for an effective diseases-modifying therapy is high but currently not available.

Recently, Sampson *et al.* performed a study on meniscal/ligamentous injured mice to test the effects of recombinant human PTH (1-34), teriparatide to elucidate the effects on chondrocytes. PTH is a Food and Drug Administration (FDA) approved treatment for osteoporosis. It was hypothesized that PTH signaling inhibits chondrocyte maturation and therefore cartilage degeneration. Teriparatide treated mice had increased bone volume within joints, increased proteoglycan content in articular cartilage and improved regeneration. However, PTH use in humans is limited by risks of hypercalcemia and osteosarcoma [168] and requires daily injections.

Surgery is the last hope for restoring joint function in the late stages of OA and should only be considered when pharmacological options are ineffective. Substantial improvements were achieved with total arthroplasty of knee and hip joints. Another option is minimally invasive arthroplasty with reduced length of hospitalization. The techniques require great expertise but achieve overall improvements in joint mobility and pain [169], [170] but younger

patients with OA (<60 years old) may not participate in joint replacement surgery as the long-term survival of prostheses is not granted. Design improvements are necessary to extend the longevity of prostheses [156] to overcome a followup surgery and age restrictions.

1.5 Hypothesis

PTHrP signaling plays a crucial role in regulating the inhibition of growth plate chondrocyte hypertrophy. The cAMP-dependent activation of PKA leads to translocation of HDAC4 and inhibition of Mef2 and Runx2 family members [39], [45]. Mef2 inhibition is necessary to block ossification of cartilage [35]. Another important cAMP-regulated signaling pathway involves CRCT2 which binds to CREB and activate *PRG4* expression, the main lubricant in joints [82].

Wein *et al.* recently discovered the interaction of PTH/PTHrP signaling with SIKs as mediators to activate HDAC4/5 and CRTC2 in osteocytes [101].

In this study, we elucidate the effects of PTH/PTHrP related signaling with pan-SIK inhibitor YKL-05-099 in a surgery-induced OA mouse model to advance our understanding in catabolic gene expression of articular chondrocytes. We observe the same regulatory mechanism of PTH/PTHrP-dependent SIK-signaling in chondrocytes to inhibit chondrocyte hypertrophy via HDAC 4/5. Additionally, we hypothesize that PTH/PTHrP dependent activation of CRTC2 in chondrocytes leads to increased *PRG*4 expression, which helps to maintain articular cartilage (see **Figure 6**).

Treatment of OA mice with teriparatide has shown reduced ectopic expression of catabolic genes in articular chondrocytes, and inhibition of articular cartilage degradation [168]. Orally-available small molecules like YKL-05-099 that mimic PTH/PTHrP action in articular cartilage may represent an alternative disease-altering agent for the treatment of osteoarthritis with improved efficacy and without the need for once daily subcutaneous injections.

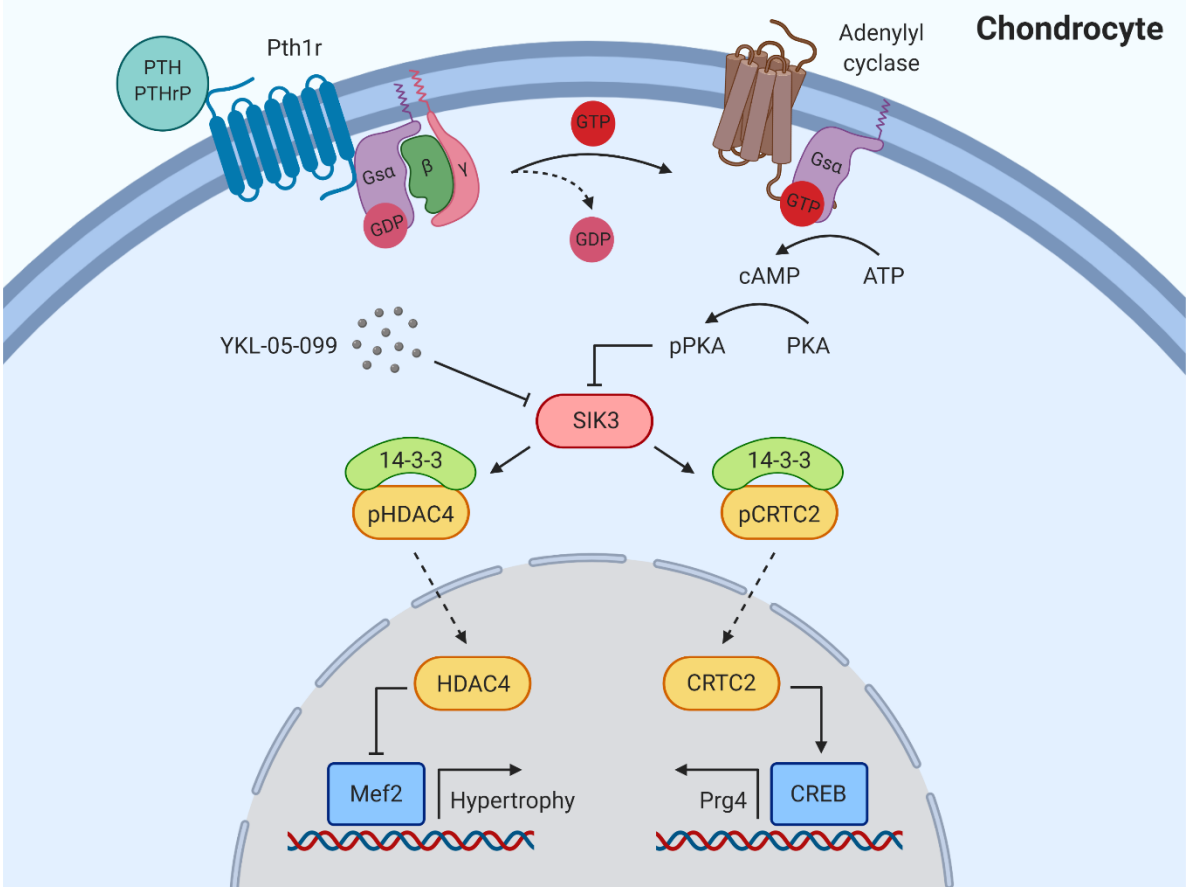

Figure 6: PTH/PTHrP dependent signaling pathway in chondrocytes. PTH/PTHrP binds to its GPCR Pth1r to activate the Gsα subunit. Activated Gsα dissociates from the βγ-subunit and stimulates adenylyl cyclase for the formation of cAMP by reducing ATP. cAMP activates PKA which in turn deactivates SIK3 by phosphorylation. Deactivation of SIK3 is also possible by direct inhibition with the small molecule YKL-05-099. HDAC4 and CRTC2 are no longer bound and sequestered in the cytosol by 14-3-3 due to lacking SIK3-dependend phosphorylation and translocate into the nucleus. HDAC4 suppress Mef2 and chondrocyte hypertrophy while CRTC2 activates CREB and stimulates *Prg4* expression.

1.6 Aim

Aim 1: Investigate the effects of systemic treatment of pan-SIK inhibitor YKL-05-099 in post-surgical OA mice. Treatment effects are elucidated on serial knee sections via histological methods, including immunohistochemistry, in situ hybridization and evaluation of OA severity via Osteoarthritis Research Society International (OARSI) scoring.

Aim 2: Elucidating the effects of YKL-05-099 treatment in primary murine sternal chondrocytes regarding gene expression and protein phosphorylation.

2 Methods

2.1 *In vivo* Experiments

2.1.1 Surgery

28 10 – 12-week-old C57BL6 mice underwent either Destabilization of the medial meniscus or Sham surgery on the right hind limb. Mice were anaesthetized with 1mg Ketamine and 0.1 mg Xylazine in 100 µl saline and treated with 1 µg Buprenex in 200 µl saline as analgesic. The surgical procedure was performed with the surgical dissecting microscope Leica MZ6. For both treatments a medial incision to the patellar tendon was done with a #15 blade to open the joint capsule. The fat pat over the intercondylar region was blunt dissected to visualize the meniscotibial ligament of the medial meniscus. Sterile cotton swabs were used to control mild hemorrhage. The procedure of Sham surgery stopped at this point. DMM surgery includes a 3 mm longitudinal incision over the distal patella to proximal tibial plateau using a # 11 or # 15 blade for destabilization of the knee joint. The subcutaneous layer was closed with 7-0 coated Vicryl and the skin was closed with 8-0 coated Vicryl (Rthion, INC, Cat#J575G and J574G)

2.1.2 Mouse Treatment

28 mice were dived into four groups (n = 7 mice per group). Mice underwent Sham surgery with vehicle treatment, DMM Surgery with vehicle treatment, Sham surgery with YKL-05-099 treatment and DMM surgery with YKL-05-099 treatment. Mice were treated for 9 – 11 weeks with either Vehicle (= 25mM HCl in PBS) or YKL-05-099 15mg/kg one week after the surgery five days per week.

2.1.3 Sample collection

Mice were sacrificed at the age of 23-weeks for sample collection. Right knees from the hind limb were isolated for histology (n = 7 per group, 28 total). Large parts of the soft tissue were dissected while keeping the knee joint intact. The femur was cut proximal to the knee joint and the tibia distal to the knee joint to prepare samples for fixation, decalcification and paraffin embedding.

We used BD Microtainer® Tubes for blood serum collection of 56 mice with Sham surgery with vehicle treatment, DMM Surgery with vehicle treatment, Sham surgery with YKL-05-099 treatment and DMM surgery with YKL-05-099 treatment (n = 14 per group). The skin was cleansed with alcohol and punctured with the lancet. The first blood drop was removed with gauze. The BD Microtainer® Tube with FloTop collector was held in an upward position to collect freely flowing blood. Whole blood was left to clot for at least 30min before mixing in a Plasma separation tube and spinning in a centrifuge for 2 min at max speed. Samples were stored at -80°C

2.2 Histology

2.2.1 Preparation of murine knee sections

Mice were sacrificed at the age of 23 weeks. Knees of the right hind limb were harvested and fixated in 4% paraformaldehyde at 4°C for 48 hours after dissection of excessive soft tissue. Samples were decalcified in a 15 ml Falcon tube filled with 20% ethylenediaminetetraacetic acid (EDTA) for two weeks. The EDTA solution was changed three times a week. Murine knees were embedded in paraffin in a flexed position for coronary sectioning. Serial sectioning of the whole knee was performed using a Leica HistoCore BIOCUT – manual rotary microtome to investigate damage on the articular cartilage. Knee sections were transferred to Fisherbrand™ Superfrost™ Plus Microscope slides (#22-037-246) and dried overnight at 37°C and stored at 4°C. We obtained 20 – 24 microscope slides per mouse knee with 4 – 8 sections per microscope slide.

2.2.2 Safranin O Staining

Every fourth slide with 4 – 8 knee sections of the respective mouse were stained according to the protocol of *Wayne et al.* [171]. Sections were incubated at 37°C overnight and incubated at 60°C for 1-hour prior staining to melt the paraffin. Deparaffinization was done with three exchanges of xylene (Fisher scientific #X3S-4) for five minutes and rehydration with two exchanges of 100% ethanol (EtOH) for 3 min, two exchanges of 95% EtOH for 2 min and distilled water (dH_2O) prior to the staining process. Sections were stained with Weigert's Iron Hematoxylin solution (Hematoxylin crystals Fisher chemicals #H345-100g) (1g in 100 ml 95% EtOH combined with 4 ml 29% aqueous iron III chloride solution in 95 ml dH_2O and 1 ml 37% hydrochloric acid (HCl)) for 10 min followed by washing under running tap water for 5 min. Each slide was rinsed in distilled water and stained in 0.1% Fast Green Working solution (Sigma-Aldrich #C.I.42053) for 10 min. Slides were placed in 1% Acetic Water for 10 -15 sec afterwards, followed by rinsing with distilled water and staining in 0.08% Safranin O working solution (Sigma-Aldrich #S2255) for 5 min. Sections were dehydrated in distilled Water, 70% EtOH, 95% EtOH and 100% EtOH followed by two exchanges of Xylene to clear slides. Slides were cover slipped with Richard-Allan Scientific™ Cytoseal™ XYL and Fisherbrand™ Microscope Cover Glass #12-544-G 22x60.

2.2.3 OARSI Scoring

The severity of osteoarthritis was assessed with the recommended semi-quantitative OARSI-scoring system by *Glasson et al.* [172] (see **Table 1**). Safranin O stained knee sections were separated in four quadrants: Lateral femur condyle (FMC), lateral tibial plateau (LTP), medial femur condyle (MFC) and medial tibial plateau (MTP). All four quadrants of 28 mouse knees (n = 7/group) were assessed separately in a randomized blinded manner with light microscope Nikon Eclipse Ni. The first round was for training purpose only. The second blinded scoring was performed one week after the initial scoring. A third unblinded round of

scoring was performed only for the medial side of knees to ensure consistency of OARSI scores among groups. Only the scoring of medial quadrants MFC and MTP were used to assess the surgery and treatment effects in murine knee joints.

Table 1: Recommended semi-quantitative OARSI scoring system for all four quadrants in mice.

Score	Osteoarthritic Damage
0	Normal Cartilage
0,5	Loss of Proteoglycan with an intact surface
1	Superficial fibrillation without loss of cartilage
2	Vertical clefts and loss of surface lamina (any % or joint surface area)
3	Vertical clefts/erosion to the calcified layer lesion for <25% of the quadrant width
4	Vertical clefts/erosion to the calcified layer lesion for 25% to 50% of the quadrant width
5	Vertical clefts/erosion to the calcified layer lesion for 50% - 75% of the quadrant width
6	Vertical clefts/erosion to the calcified layer lesion for >75% of the quadrant width

2.2.4 Proteoglycan area measurement

Knee sections were stained with Safranin O and Fast green. The proteoglycan area (Safranin O) was measured with Image J software. Images of the highest OARSI score of the MTP and MFC were used to measure the total proteoglycan area of the non-calcified region of the articular cartilage with color thresholding by adjusting hue, saturation and brightness. The selected area was controlled manually and adjusted individually for each section. Erosions or loss of proteoglycan area was measured manually via freehand drawing or polygonal selection to obtain a ratio of lost proteoglycans in the superficial layer of articular cartilage.

2.2.5 Immunohistochemistry

Sections close to the highest assessed OARSI score were baked at 37°C overnight and at 60°C for 1 h prior deparaffinization in three exchanges of Xylene for five minutes and rehydration in two exchanges of 100% EtOH and two exchanges of 95% EtOH. Slides were incubated in 3% H2O2 in MeOH for 14 min to block endogenous peroxidase activity of the tissue. Samples were washed and hydrated in phosphate-buffered saline (8g/l sodium chloride, 0.2 g/L potassium chloride, 1.44 g/l di-sodium-hydrogen-phosphate, 0.24 g/l potassium di-hydrogen-phosphate) for 3 min. Antigen retrieval of sections was done with ~100 µl 1 mg/ml trypsin at 37°C for 14 min in a humidified chamber. Sections were circled with a PAP pen for immunostaining (Sigma #Z377821) to create a hydrophobic barrier. Each section was blocked with ~100 µl TNB (5mg/ml TSA Perkin-Elmar #FP1020) for 30min at room temperature (RT). The blocking solution was removed by flicking the slide and sections

were incubated at RT for 1 hour with anti-collagen X antibody (Abcam #ab58632, 1:500 in TNB) or at 4°C overnight with anti-MMP-13 antibody (Abcam #ab84594 1:200 in TNB). Sections were washed with three exchanges of ~200µl TBST (20 µL 8M Tris, 40ml 5M NaCl, 0,4 ml Tween20 in 1 L dH_2O) per section for five minutes followed by a 30 min incubation with Goat Anti-Rabbit IgG (H+L) biotinylated secondary antibody (Vector Laboratories #BA-1000, 1:200 in TNB). Detection of antibodies was performed with Perkin Elmar TSA Biotin System (#NEL700A001KT) and Vector laboratories DAB peroxidase substrate kit (#SK-4100). After three washes with TBST, sections were incubated with SA-HRP (Vector Avidin D, Peroxidase labelled (Av-HRP), ready-to-use # A-2704) for 30min. Sections were washed three times with TBST followed by 5 min incubation with biotinyl tyramide reagent (Perkin Elmar #FP1019 1:50 in amplification diluent #FP1050) at RT. Another 30min incubation with SA-HRP after three washes with TBST was performed subsequently. Sections were washed and incubated with DAB SK-4100 (Vector Laboratories) for 1,5 – 30 min until positively stained tissue became brown. Sections were rinsed in H_2O and counterstained in 0,1% Fast Green followed by dehydration in graded alcohol solutions, clearing in xylene and cover slipping.

2.2.6 Assessment of Immunohistochemistry

Murine knee sections underwent immunohistochemical staining with anti-collagen X or anti-MMP13 antibodies to investigate protein expression of articular cartilage. Positively stained chondrocytes appear in brown to black tones and negatively stained chondrocytes in light blue to green color. Positively stained and negatively stained chondrocytes of the non-calcified region of the articular cartilage were counted with light microscope Nikon Eclipse E800 and Osteomeasure 7 v4.2.0.0. The ratio of positively stained cells vs total number of cells was used to describe effects of surgery and treatment with YKL-05-099.

2.2.7 In Situ hybridization

RNAscope® 2.5 HD Detection Reagent – Brown was used to assessing *Prg4* and *MMP13* expression in articular cartilage in paraffin-embedded knees of mice which underwent either sham or DMM surgery and were treated either with VEH or YKL-05-099. Paraffin-embedded murine brain was used as control tissue to verify the specificity of probes. Sections were dried at 37°C over-night and baked at least for 1 h at 60°C prior deparaffinization. Slides were deparaffinized in two exchanges of xylene for 5min and two exchanges of 100% EtOH for 1 min. Slides were dried at 60°C for 30 min and circled with ImmEdge Hydrophobic Barrier PAP Pen (Vector #H-400). RNAscope® Hydrogen Peroxide was added dropwise to cover the sections entirely for 10 min at RT. Sections were washed in two exchanges of dH_2O and incubated either with Pepsin Reagent Ready to Use Antigen Retriever (Sigma-Aldrich #R2283) for 10 – 30min at 40°C, 1 mg/ml Trypsin from porcine pancreas (Sigma-Aldrich #T7168) for 15 – 30 min at 40°C, proteinase K 20 µg/ml for 15 – 30 min at 40°C or RNAscope® 1x Target Retrieval Reagent in a steamer at ~95°C for 2 – 15 min. Samples

were washed in two exchanges of dH_2O after the target retrieval step. Sections treated with RNAscope® 1x Target Retrieval Reagent were incubated with 100% EtOH afterwards, dried at 60°C for 30 min, incubated with RNAscope® Protease Plus for 15min at 40°C and were washed in dH_2O. All sections were incubated either with RNAscope® Negative Control Probe, RNAscope® Positive Control Probe, RNAscope® Target Probe Prg4 diluted 1:3 in dH_2O or RNAscope® Target Probe MMP13 for 2 h at 40°C and were washed in two exchanges of RNAscope® 1x Wash Buffer for 2 min afterwards. Slides were incubated with RNAscope® 2.5 AMP 1 for 30 min at 40°C, RNAscope® 2.5 AMP 2 for 15 min at 40°C, RNAscope® 2.5 AMP 3 for 30 min at 40°C, RNAscope® 2.5 AMP 4 for 15 min at 40°C, RNAscope® 2.5 AMP 5 for 5 – 40 min at RT, RNAscope® 2.5 AMP 6 for 5 - 20 min and washed with 2 exchanges of RNAscope® 1x Wash Buffer for 2 min after each incubation step. Signal detection was performed with an equal mix of RNAscope® DAB-A and RNAscope® DAB-B solution for 2 – 10 min at RT. Sections used for evaluation of Prg4 expression were not incubated with RNAscope® 2.5 AMP 5 and RNAscope® 2.5 AMP 6 but directly exposed to DAB after the incubation with RNAscope® 2.5 AMP 4. Sections were rinsed in tap water and counterstained with 50% hematoxylin staining solution for 2 min. Slides were rinsed in tap water until they became clear and dipped into 0,02% ammonia water until the color of the sections turned blue. Slides were rinsed in tap water and dehydrated in graded EtOH solutions before clearing in xylene and cover slipping.

2.2.8 *In Situ* hybridization assessment

Murine knee sections used for in situ hybridization with RNAscope® Target Probe Prg4 were analyzed with Image J. Only the noncalcified region of the MFC and the MTP was used for the assessment. Images of the articular cartilage were split into three color channels to obtain 8-bit images. The blue channel was used for thresholding the area of positively stained chondrocytes of the non-calcified region of the articular cartilage. Additionally, positively and negatively stained chondrocytes were counted with light microscope Nikon Eclipse E800 and Osteomeasure 7 v4.2.0.0 to obtain a ratio of *Prg4* expressing cells.

2.2.9 Alcian blue staining

Alcian blue staining was used to verify immature murine primary sternal chondrocytes and differentiated mouse clonal limb bud cells (“clone 14”) [173] in *in vitro* cell culture. Alcian blue stains sulfated proteoglycans which are expressed in the extracellular matrix. Cell culture medium was aspirated, and cells were washed with PBS two times. Cells were fixed at room temperature with 4% para formaldehyde for 5 - 15 min and rinsed with 0.1 N hydrochloric acid (HCl). Cells were stained with 1% Alician blue in 0.1 N HCl for 30 -60 min. The staining solution was removed, and cells were washed twice with 0.1 N HCl. Positive staining was investigated with light microscope Nikon Eclipse Ni.

2.3 Serum Pre-Clinical CartiLaps® (CTX-II) ELISA

We used blood serum samples of each mouse to assess Carboxy-Terminal telopeptides of type II Collagen (CTX-II). Internal standards were prepared to cover the appropriate range of measurements by diluting internal standard 1 in standard 0. Internal standards were diluted by a factor of 2.5 consecutively to obtain six different concentrations for a calibration curve. The biotinylated antibody and biotinylated antibody buffer were prepared in a volumetric ratio of 1 + 100. 100 µl of this mixture was added to each well of the streptavidin-coated microtiter plate, covered with sealing tape and incubated at room temperature mixing (300 rpm) on Eppendorf Thermomixer R for 30 minutes. Each well was washed five times manually with 300 µl washing solution (Wash buffer 1 + 50). 25 µl of standards in duplicates or 25 µl of blood serum samples (n = 56 total n=14/group) were added followed by 100 µl incubation buffer. The plate was covered with sealing tape and incubated at room temperature at 300 rpm for 60 minutes. Each well was washed five times with washing buffer prior to incubation with 100 µl of 1 + 100 peroxidase-conjugated antibody in incubation buffer at room temperature and 300 rpm for 60 min. Each well was washed five times with washing buffer after the incubation. 100 µl of the substrate solution was pipetted into each well and incubated at room temperature at 300 rpm for 15 min. The reaction was stopped with 100 µl of provided sulfuric acid. Absorbance was measured at wavelength λ = 450 nm and λ = 650 nm as reference.

2.4 *In Vitro* Experiments

2.4.1 Chondrocyte isolation

27 C57BL/6 3 days-old mice were used for sternal chondrocyte isolation. Mice were sacrificed and to dissect the ventral regions of the rib cage. Rib cages were stored in iced Hank's balanced salt solution (HBSS with calcium and magnesium, without phenol red Thermofisher #140225076) until all rib cages were harvested. Muscle and connective tissue were removed under the dissecting microscope. Rib cages were digested in 0.25% Collagenase II and 2.5% Trypsin in HBSS for 1 hour 15 min at 37°C with vigorous shaking every 10 min. Digestion solution was gently aspirated, and rib cages washed with HBSS. A second digestion with 0.25% Collagenase II in HBSS for 1 hour and 20 min at 37°C with vigorous shaking every 10 min was performed. Digestion was stopped by adding an equal amount of DMEM with 10% FBS and 1% anti/anti to the digestion solution. The cell suspension was strained through 70 µm mesh and spun down before counting and plating at the desired cell density or freezing at -80°C in GC Lymphotec Inc. Bambaker Serum-free cell freezing Medium (#302-14681) medium.

2.4.2 Thawing and cultivation of cells

Primary murine sternal chondrocytes, murine clonal limb bud cells [173] and NIH3T3 cells were thawed in a water bath at 37°C. The cell suspension was transferred into a 15 ml falcon tube containing 10 ml Dulbecco's Modification of Eagle' s Medium (DMEM) with 10% fetal bovine serum (FBS), 1% antibiotic/antimycotic (Gibco Anti-Anti 100x #15240-062) and 25 µg/ml Ascorbic acid for primary murine sternal chondrocytes and NIH3T3 cell or 10 ml DMEM, high glucose, GlutaMAX™ Supplement (Thermo Fisher # 10566-016) containing 10% FBS and 1% anti/anti for murine clonal limb bud cells. The cell suspension was spun at 850x g for 5min. The cell pellet was resuspended in 1 ml fresh media. Cells were counted using a hemocytometer and trypan blue.

Primary murine sternal chondrocytes and NIH3T3 cells were plated at a cell density of 50000 cells/ml in DMEM with 10% FBS, 1% anti/anti and 25 µg/ml Ascorbic acid for all experiments. NIH3T3 cells were harvested after 6 days of cultivation. Mouse limb bud cells Isolated and immortalized from embryonic day 13 murine limb (Obtained from Vicki Rosen Lab [173]) were plated in a cell density of 70000 cell/ml in DMEM, high glucose, GlutaMAX™ Supplement with 10% FBS and 1% anti/anti. Cells were differentiated one day after seeding in DMEM, high glucose, GlutaMAX™ Supplement with 10% FBS, 1% anti/anti, 50 ug/mL Ascorbic Acid (Sigma #A5960-25G) and 1x Insulin-Transferrin-Selenium (Thermo Fisher #41400045). Mouse limb bud cells were differentiated for up to 10 days and harvested for further analysis.

Primary murine sternal chondrocytes and NIH3T3 were plated in 24-well plates for RNA isolation or in 6 well-plates for Protein isolation. Cells were treated either with 200 mM PTH for 5 min, 20 min or 60 min, 5 µg/ml Forskolin for 60 min or 10 µM YKL-05-099 for 60 min in duplicates for protein isolation. Primary murine sternal chondrocytes and mouse limb bud cells were treated with 200 nM PTH, 1 µM YKL-05-099, 10 µM YKL-05-099 or 5µg/ml Forskolin for 4 hours in triplicates or with 5 µM YKL-05-099 for 1.5 h, 3 h, 6 h and 18 h for RNA isolation.

2.4.3 Western Blot

Primary murine sternal chondrocytes or NIH3T3 were washed with PBS, scraped from the well and transferred to an Eppendorf tube. PBS was aspirated, and cells lysed in 60 - 80 µl of lysis buffer depended on the cell pellet size. Protein lysis was performed with TNT lysis Buffer (20 mM Tris pH 8.0, 200 mM NaCl, 0.5% Triton X-100 subjected with 10 µl 100x Protease inhibitors in Dimethyl sulfoxide, 1 mM dithiothreitol, 1 mM Sodium fluoride, 1 mM β-glycerophosphate and 10 µl 500x vanadate per ml TNT lysis buffer). Cells were repeatedly vortexed for 15 sec and kept on ice for 15 sec over 2 minutes. Cell fragments were spun down at 4°C with 14,000 rpm for 4 min with Eppendorf Centrifuge 5415 D. The supernatant was used to measure the protein concentration of the lysate with a Bradford reagent. Bio-Rad Protein assay dye reagent concentrate (#5000006) was diluted 1:5 with dH_2O and samples measured at λ = 595. The protein lysate was combined with 2x Laemmli sample

buffer (Bio-Rad #1610737) with 50 µl / ml ß-Mercaptoethanol in a 1:1 ratio. Samples were denatured at 95°C for 5 min and loaded immediately onto an 8% poly-acrylamide gel or stored at -80°C.
Samples were loaded with equal protein concentrations up to a volume of 30 µl per sample. Gel electrophoresis was done with 50 V for the stacking gel and 100 V for resolving gel. Bio-Rad Precision Plus Protein Standards Dual color (#161-0374) was used to identify Protein size.
Proteins were transferred in a wet transfer set up. Nitrocellulose membranes were soaked in water and placed on top of the Gel between 4 Whatman papers. The transfer was performed under constant cooling for 1 hour at 100 V.
Membranes were blocked with 5% Milk in TBST for 30 minutes. Primary antibody incubation for CRTC2 pS275 432.33 Bleed 5 0.4 mg/ml rabbit, pSIK3 yZq396 0.3 mg/ml rabbit, pHDAC4 (S246/S259/S155) rabbit (Cell Signaling #D27B5), pPKA RRXS/T rabbit (Cell Signaling #100G7E), tHDAC5 (AssayBioTech #C0225), β-tubulin (Cell Signaling #5346S) was done in a 1:1000 dilution in 5% BSA in TBST. Secondary antibody incubation was done with anti-rabbit IgG HRP (Cell Signaling 7074S) 1:2500 in TBST for 1 hour. Membranes were incubated with ECL substrate (Thermo Scientific #35050) or ECL Plus substrate (Thermo Scientific #32132) for 2 min and imaged with Azure™ Biosystems c600.

2.4.4 Real-time PCR

Primary murine sternal chondrocytes and clonal mouse limb bud cells were washed with 800 µl PBS/well and lysed in 350 µl/well RLT buffer (Thermo Scientific #79126) with 10 µl/ml ß-Mercaptoethanol. A homogenous solution was achieved by repetitive pipetting of the cell suspension. The cell solution was transferred to a QIAshredder (Qiagen #79654) and spun at 13,000x g for 3 min. An equal amount of 70% EtOH was added to the solution and mixed for homogenization. The solution was transferred to the spin cartridge (RNA isolation Pure Link RNA Minikit #12183018A) and spun at 12,000x g for 35 seconds at room temperature. The flow-through was discarded and 700 µl Wash buffer 1 was added to the spin cartridge and spun at 12,000x g for 35 seconds. The flow-through was discarded and washing of the spin cartridge with 500 µl Wash buffer 2 was performed twice. The flow-through was discarded, and the column was spun dry at 12,000x g for 35 seconds before adding 30 µl RNAse free water to elute RNA in a new collection tube after 1 min incubation at room temperature. RNA concentration was measured with Nanodrop and stored at -80°C or processed directly to cDNA.
cDNA was generated by using Takara PrimeScript™ RT reagent Kit with gDNA Eraser (Perfect Real Time) (#RR047A). Master mixes were prepared for a final volume of 10 µl cDNA. Master mix 1 contained 0.5 µl gDNA eraser and 1 µl 5x gDNA eraser Buffer per sample. Master mix 2 contains 0.5 µl Prime Script RT Enzyme Mix 1, 2 µl 5x PrimeScript RT Buffer 2 (for Real Time), 0.5 µl RT Primer mix and 2 µl RNase free dH_2O. Equal amounts of RNA per sample was added to 1.5 µl of Master Mix 1 and filled up with RNase free dH_2O to

a total volume of 5 µl. Samples were incubated at 42°C for 2 min. Afterwards 5 µl of Master Mix 2 was added to each sample and heated to 37°C for 15 min followed by a short incubation at 85°C for 5 sec. Samples were stored at -20°C or used directly for real-time polymerase chain reaction (RT-PCR or qPCR).

StepOnePlus™ Real-time PCR system was used. Each reaction mix consists of 10 µl of QuantaBio PerfeCTa® SYBR® Green FastMix®, 8 µl dH_2O, 1 µl cDNA and 1 µl of 10 µM forward and reverse primer for Prg4, MMP13 or Col10a1 (see **Table 2**). The PCR program was set up in three major stages. Holding stage consist of one step for 50°C for 2 min and a second step of 95°C for 15 min. Cycling Stage consists of four steps with 49 cycles. Step one is 95°C for 15 sec followed by step 2 at 60°C for 20 sec. Step 3 is 72°C for 20 sec and step 4 temperature is set to 79°C for 5 sec. The melt curve stage consists of 3 steps starting with step 1 at 60°C for 15 sec followed by step 2 at 95°C for 15 sec and step 3 with a temperature setting of 72°C for 6 min (see **Table 3**).

Table 2: Primer sequences for real time PCR

Primer	Sequence
MMP13 850 Forward	5′-AAGTGTGACCCAGCCCTATC-3′
MMP13 947 Reverse	5′-AAAGAGCTCAGCCTCAACCT-3′
MMP13 195 Forward	5′-AGTTGACAGGCTCCGAGAAA-3′
MMP13 281 Reverse	5′-AGGCACTCCACATCTTGGTT-3′
Prg4 280 Forward	5′-GGCAAGTGCTGTGCAGATTA-3′
Prg4 374 Reverse	5′-GCTTCCAGCTTCATCCACAG-3′
Prg4 158 Forward	5′-ACATGGAGTGCTGTCCTGAT-3′
Prg4 248 Reverse	5′-CTGGGAGTCACAGTCACACT-3′
Col10a1 Forward	5′-ACCAGGAATGCCTTGTTCTC-3′
Col10a1 Reverse	5′-CATAAAGGGCCCACTTGCTA-3′

Table 3: Real time PCR program

Stage	Step	Temperature	Duration	Cycle
Holding	1	50°C	2 min	1
	2	95°C	15 min	
Cycling	1	95°C	15 sec	49
	2	60°C	20 sec	
	3	72°C	20 sec	
	4	79°C	5 sec	
Melt curve	1	60°C	15 sec	1
	2	95°C	15sec	
	3	72°C	6 min	

2.5 Statistical evaluation

Evaluation of data was performed with GraphPad Prism 6. Each data set was tested for normality with D'Agostino-Pearson omnibus normality test, Shapiro-Wilk normality test and Kolmogorov-Smirnov test with Dallal-Wilkinson-Liliefor P-value. Differences between groups in parametric data sets were assessed with an unpaired t-test and with Mann-Whitney test for nonparametric data sets. Outliers of data sets were identified with Grubb's test for outliers and excluded if the sample size was bigger than 7.

3 Results

3.1 Histomorphometric assessment of Osteoarthritis.

Frontal right knee joint sections of 28 mice with sham or DMM surgery and YKL 05-99 or VEH treatment were stained with Safranin O to visualize proteoglycans in articular cartilage. Only the medial side of the knee joint was used for OARSI scoring and histomorphometric assessment of the proteoglycan area to evaluate morphological changes of the medial femur condyle and the medial tibial. The lateral femur condyle, the lateral tibial plateau, the lateral meniscus and the medial meniscus were not included in the assessment. 6 of 25 microscope slides with 4 – 8 sections of the knee joint were used per mouse to assess anterior, median and posterior regions.

Figure 7 shows representative images of knee joints of all four treatment groups. Safranin O stains proteoglycan rich cartilage and proteoglycan expressing chondrocytes in red seen in the articular cartilage and the growth plate. Fast green act as a counterstain for surrounding bone and soft tissue (appears in green-blue) and hematoxylin stains cell nuclei in blue-grey color. The tide mark (indicated by black arrows) allows identification of the non-calcified region of articular cartilage (distal to the secondary ossification center) and the calcified region of articular cartilage (proximal to the secondary ossification center). The total area of articular cartilage varies depending on the region of the knee joint. The area of the non-calcified region of the articular cartilage depends on the severity of induced osteoarthritis. Mild loss of proteoglycans was observed in all treatment groups. Fibrillations and minor erosions of the superficial layer of articular cartilage were observed in mice with sham surgery treated with either VEH or YKL-05-99. However, YKL-05-99 treated mice showed fewer erosions of the superficial layer of articular cartilage than VEH treated mice (see **Figure 7 B & D)**. Severe erosions of articular cartilage to the calcified region of articular cartilage was observed for 4 of 7 mice of the DMM-VEH group (**Figure 7 C**) and only 1 of 7 mice of the DMM YKL-05-99 group. Erosions of up to 50% of the non-calcified articular cartilage were seen in both treatment groups, but YKL-05-99 treated mice tend to have only erosions of the superficial layer of the articular cartilage (**Figure 7 E**). The most dramatic loss of proteoglycans and erosion of articular cartilage was observed for the medial tibial plateau in all groups. The medial femur condyle had fewer erosions and less proteoglycan loss in comparison to the medial tibial plateau in all groups.

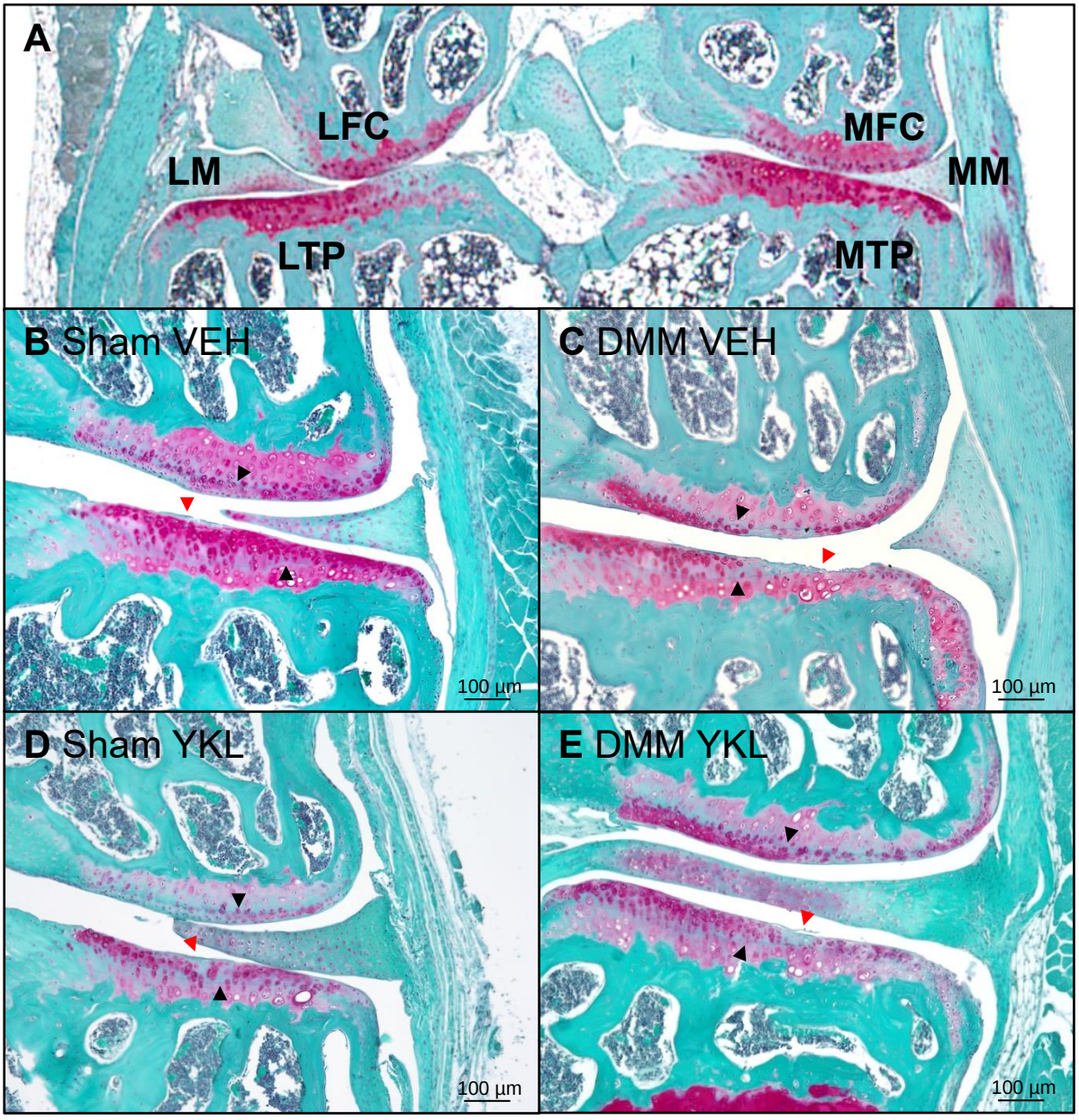

Figure 7: Histomorphometric comparison of representative right knee joints from sham / DMM operated mice with VEH / YKL-05-099 treatment. A) Division of the murine knee into structural segments: lateral femur condyle (LFC), lateral meniscus (LM), lateral tibial plateau (LTP), medial femur condyle (MFC), medial meniscus (MM), and medial tibial plateau (MTP). Representative Images of treatment groups **B)** Sham VEH, **C)** DMM VEH, **D)** Sham YKL-05-099, **E)** DMM YKL-05-099. Black arrows indicate tide mark; red arrows indicate structural changes of articular cartilage.

The severity of osteoarthritis was assessed with the recommended semi-quantitative osteoarthritis research society international (OARSI) scoring system by *Glasson et al.* [172] (see **Table 1**) to identify treatment effects of YKL-05-099 on cartilage integrity. Each set of Safranin O stained murine knee sections was assessed separately in a blinded manner two times. The third scoring was performed unblinded and included a direct comparison of knee joints to ensure consistent scoring among groups and was used as the final score for each

mouse (see **Figure 8 A**). The result of the second blinded scoring was compared with the unblinded third scoring to evaluate the bias of unblinded scoring (see **Figure 8 B & C**). There was no significant difference between blinded and unblinded scoring.
Surgical groups showed significant differences. Only mice which underwent Sham surgery treated with YKL-05-099 showed no proteoglycan loss. All other mice, including control mice with sham surgery and VEH treatment, showed loss of positive proteoglycan staining and in most cases fibrillation and small erosions of the superficial layer of the articular cartilage. The highest OARSI score was 4, which was observed for both DMM groups. Mice with DMM surgery and VEH treatment are more likely to have more severe cartilage erosions down to the calcified region in comparison to YKL-05-099 treated mice. However, the comparison of treatment groups VEH vs YKL-05-099 is not statistically significant.

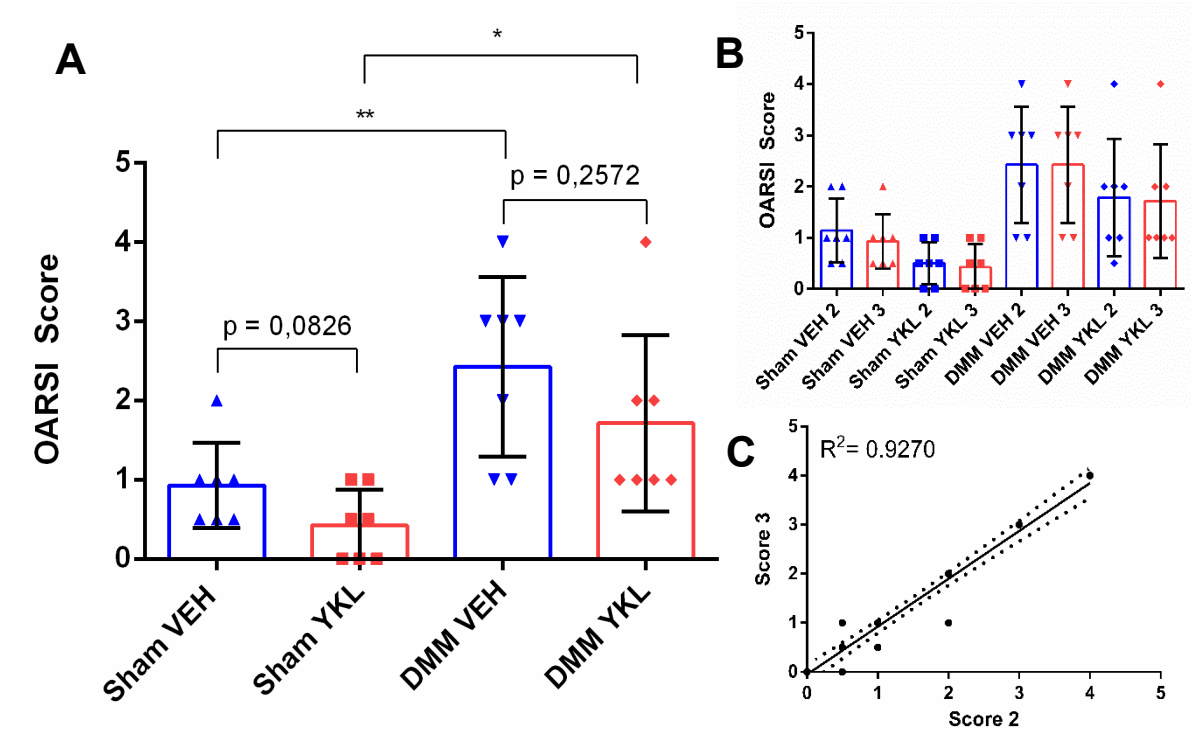

Figure 8: OARSI scores assessment murine right knee joints from sham / DMM operated mice with VEH / YKL-05-099 treatment. A) Comparison of OARSI scores of treatment groups. DMM surgery shows a significant increase in OARSI scoring in comparison to sham surgery. YKL-05-099 treatment shows a trend towards lower OARSI scores but no statistically significance (Sham VEH vs Sham VEH p = 0.0826; DMM VEH vs DMM YKL p = 0.2572). **B)** Individual group scores from OARSI scoring assessment round 2 (blinded) and 3 (unblinded). **C)** Correlation between blinded OARSI scoring (2) and unblinded scoring (3). (n = 7/group).

OA is associated with loss of proteoglycans in articular cartilage. The area of positive proteoglycan staining of murine knee sections with the highest OARSI scores was measured with ImageJ to evaluate morphological changes of the articular cartilage as an alternative method to OARSI scoring (see **Figure 9**). A ratio between the area of eroded articular cartilage to the total area of the non-calcified area of the articular cartilage was calculated for the medial femur condyle and the medial tibial plateau individually to compare differences in treatment groups and region. Loss of proteoglycans or erosion of articular cartilage was lower at the medial femur condyle in comparison to the medial tibial plateau. DMM surgery showed a dramatic decrease in positive proteoglycan area in comparison to sham surgery. However, no statistically significant difference between treatment groups was observed.

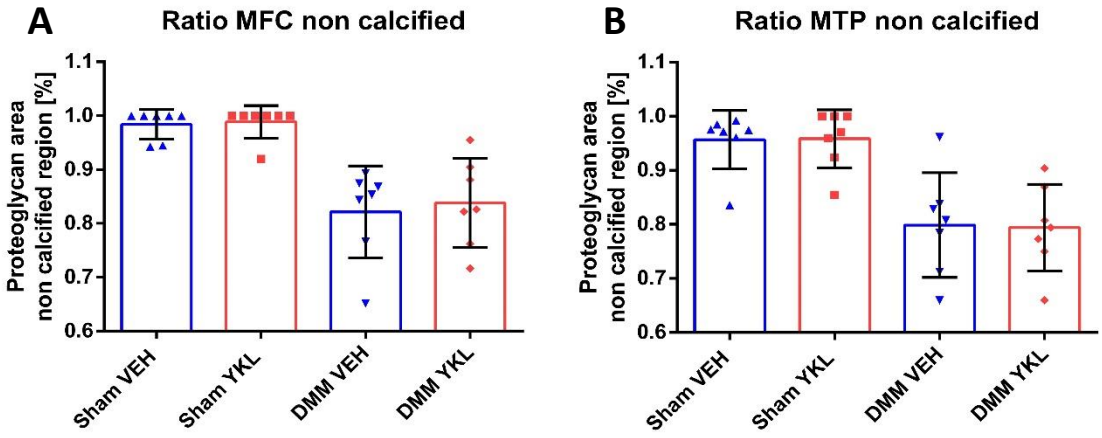

Figure 9: Proteoglycan loss of non-calcified articular cartilage. Assessment of murine right knee joints from sham / DMM operated mice with VEH / YKL-05-099 treatment. **A&B)** Proteoglycan area ratio of the medial femur condyle (MFC) and medial tibial plateau (MTP) shows no difference in YKL-05-099 treated mice in comparison to VEH treated mice. (n = 7 mice/group).

3.2 Immunohistochemical assessment of murine knee sections

It has been reported that articular chondrocytes ectopically express “hypertrophic” markers such as collagen X (Col X) and MMP13 in the setting of osteoarthritis. Therefore, immunohistochemistry was used to reveal the maturation state of articular chondrocytes in surgery-induced OA and the treatment effect of YKL-05-099.

3.2.1 Collagen X

Sections close to the highest OARSI scoring were used for immunohistochemical staining. Positive staining of Col X appears brown-black and negative staining blue-green. The total number of chondrocytes and the Col X positive stained chondrocytes of the non-calcified

region of the articular cartilage on the medial side of the knee joint were counted to assess the effects of YKL-05-099 treatment in comparison to VEH treated mice.

Figure 11 A – D shows representative images of all four treatment groups. Positive staining of Col X in the articular cartilage is visible for all groups (n = 7/group) with less positive cells in the non-calcified region when treated with YKL-05-099 (see **Figure 10**). However, no statistically significance is given. Cells in the bone were also positively stained with Col X antibody as expected. Approximately 50% of the bone marrow cells appear black due to unspecific positive staining. **Figure 11 E** depicts a representative control section incubated with Col X but not with a secondary antibody. **Figure 11 F** is a representative image of a control section incubated without Col X but with a secondary antibody. In both, **Figure 11 E & F** no positive staining of cells in the articular cartilage, bone, bone marrow or growth plate was detected.

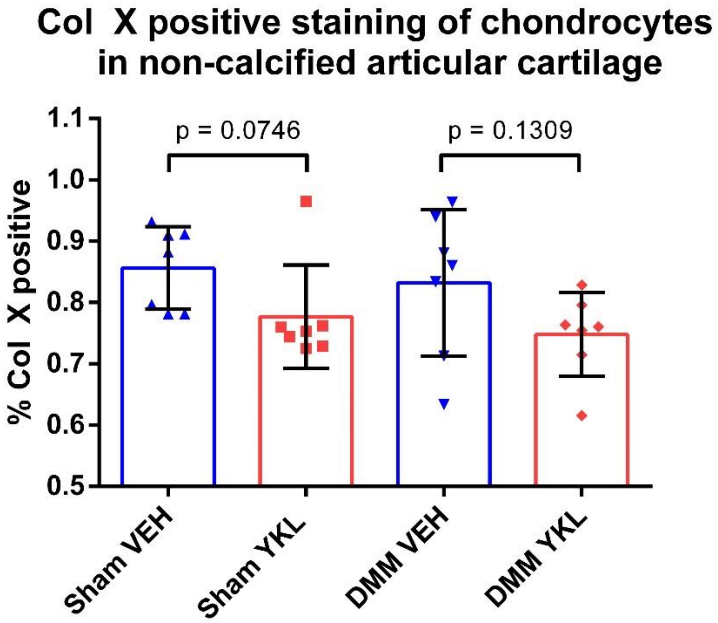

Figure 10: Ratio of Col X positive stained chondrocytes in articular cartilage. Mice with sham/DMM surgery and VEH/YKL-05-099 treatment were stained with anti-Col X antibody to assess positive staining in the non-calcified region of articular cartilage**.** Treatment with YKL-05-099 shows a decreased positive staining of Col X in comparison to VEH treated mice (Sham VEH vs Sham YKL p = 0.0746; DMM VEH vs DMM YKL p = 0.1309; n = 7 mice/group).

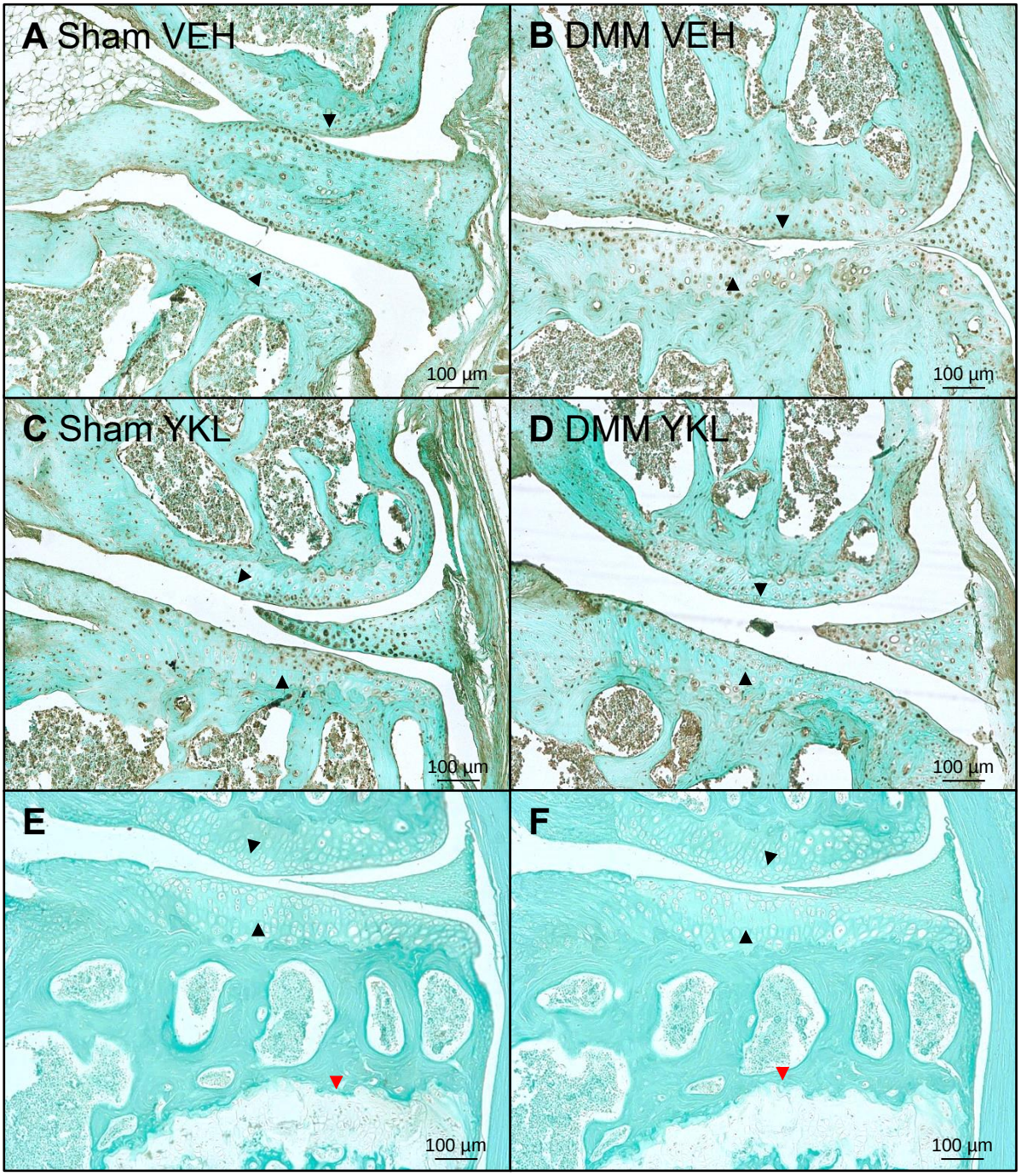

Figure 11: Type X collagen staining of murine right knees with sham/DMM surgery treated with VEH/YKL-05-099: Representative Images of treatment groups **A)** Sham VEH, **B)** DMM VEH, **C)** Sham YKL-05-099, **D)** DMM YKL-05-099. Reduced positive staining for Col X was observed in the non-calcified region of articular cartilage in YKL-05-099 treated mice. **E)** Control section incubated with anti-Col X antibody without a secondary antibody **F)** Control section incubated without anti-Col X antibody but with a secondary antibody. Black arrows indicate the tide mark, red arrows the growth plate.

3.2.2 MMP13

Paraffin-embedded knee sections from mice treated either with VEH or YKL-05-099 which underwent sham or DMM surgery were used for immunohistochemical staining of MMP13 see **Figure 12**. The tissue appears green – blue and MMP13 positive cells appear brown-black. Only cells of the medial articular cartilage from the femur condyle and the tibial plateau were used for the assessment of MMP13 staining.

Figure 12 A-D are representative images of the knees of all four treatment groups (n = 3/group) using trypsin as retrieval agent. **Figure 12 E** depicts a representative control section incubated with MMP13 but not with a secondary antibody. **Figure 12 F** is a representative image of a control section incubated without MMP13 but with a secondary antibody. Each treatment group shows weak positive staining of MMP13. Most cells in the non-calcified region proximal to the secondary ossification center (indicated by black arrows) of the articular cartilage show faint brown color. The positive staining of chondrocytes is comparable to the unspecific positive staining of bone marrow cells in both, MMP13 stained sections **(A-D)** as well as the controls **(E & F)** and is therefore considered as false-positive staining. MMP13 positive staining could also be detected below the growth plate (indicated by red arrows) in MMP13 stained sections **(A-D)**. However, no clear differences were visible between treatment groups. The same results were achieved with Proteinase K as an alternative retrieval agent (results not shown). Target retrieval with Pepsin increased positive signal but increased unspecific staining in the same proportion (results not shown).

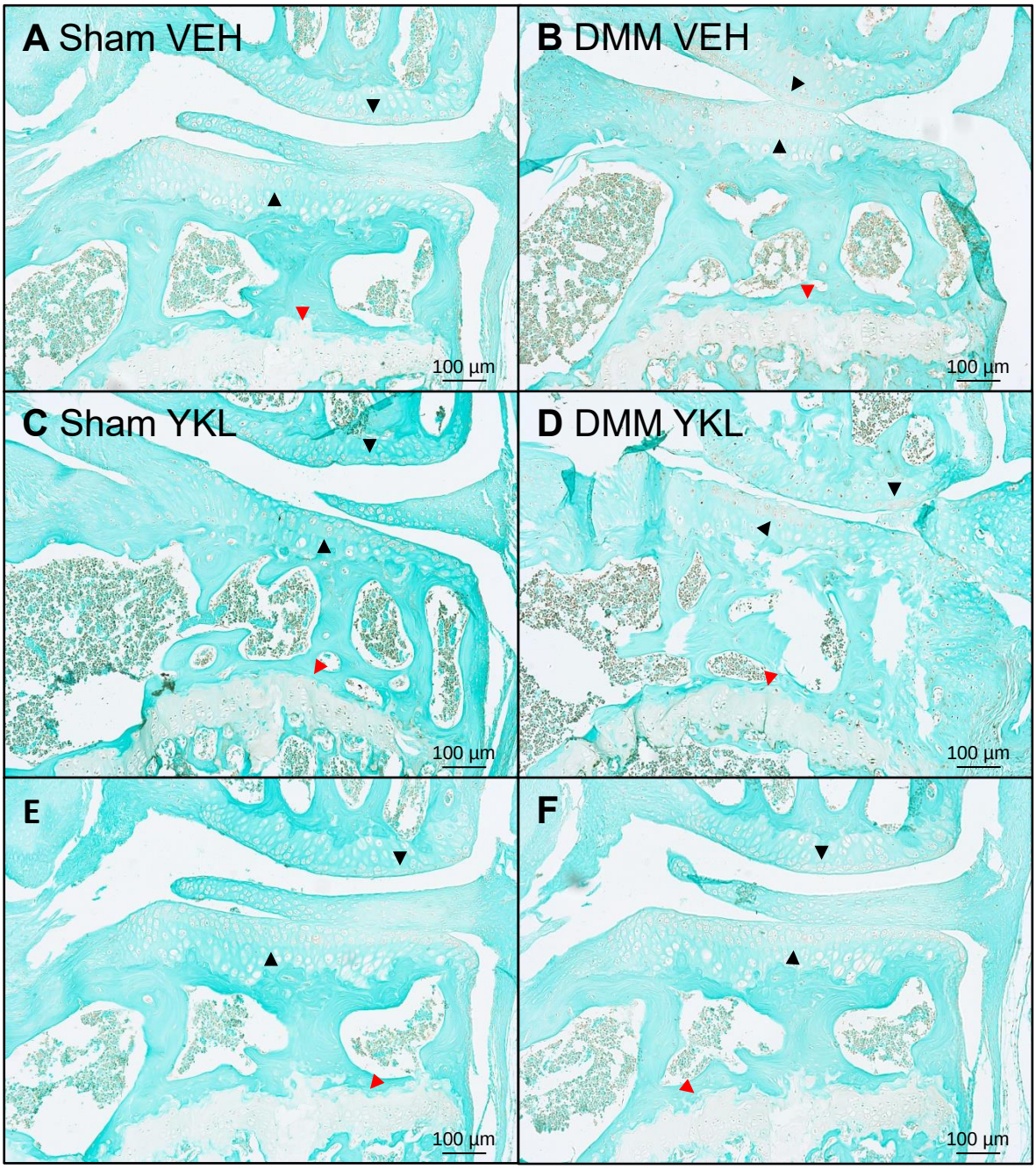

Figure 12: MMP13 staining of murine right knees with sham/DMM treated with VEH/YKL-05-099: Representative Images of treatment groups **A)** Sham VEH, **B)** DMM VEH, **C)** Sham YKL-05-099, **D)** DMM YKL-05-099. **E)** Control section incubated with anti-MMP13 antibody and without a secondary antibody **F)** Control section incubated without anti-MMP13 antibody but with a secondary antibody. Black arrows indicate tide mark, red arrows the growth plate. Positive staining was observed for the most of the cells in the non-calcified region of articular cartilage and bone marrow cells in all treatment groups **(A-D)** and controls **(E & F)**.

3.3 *In Situ* hybridization for *Prg4*

Prg4 is important for the lubrication of the knee joint and is primarily expressed in the superficial layer of articular cartilage. To evaluate the effects of YKL-05-099 treatment on chondrocytes in osteoarthritic mice, in situ hybridization was used to visualize Prg4 expression.

Paraffin-embedded murine knee sections from each group (Sham VEH, Sham YKL, DMM VEH, DMM YKL, n = 7/group) were used to assess *Prg4* expression with RNAscope® 2.5 HD Detection Reagent – Brown. Sections were counterstained with 50% hematoxylin. Treatment groups were compared among each other to elucidate differences in YKL-05-099 treatment in comparison to VEH treatment. Only medial sites of the knee were used for assessment.

Figure 13 shows representative images of murine knee sections from different treatment groups (**A)** Sham VEH, **B)** DMM VEH, **C)** Sham YKL and **D)** DMM YKL) with *Prg4 in situ* hybridization. The tissue appears light lilac, cell nuclei blue and *Prg4* expressing cells brown with brown-black dots. *Prg4* expressing cells are limited to the non-calcified region of articular cartilage (indicated by black arrows), menisci and the synovial region of the joint for all groups (**Figure 13 E**). No positive staining was detected for bone, bone marrow cells or chondrocytes of the growth plate or in the calcified region of articular cartilage. Reduced *Prg4* expression of articular chondrocytes can be seen in both DMM VEH and DMM YKL mice **(Figure 13 B & D)** while articular chondrocytes of the non-calcified region of Sham VEH and Sham YKL mice have uniform *Prg4* expression **(Figure 13 A & C)**. Chondrocytes near cartilage erosions do not express *Prg4* (**Figure 13 B**). This finding correlates with reduced proteoglycan positive staining in articular cartilage near erosions seen with Safranin O staining.

Prg4 expression of articular chondrocytes in the non-calcified region was assessed by measuring the total area of positive signal seen in **Figure 14 A**. Mice with sham surgery do not show a difference in positive staining when comparing VEH treatment and YKL treatment. DMM reduces Prg4-positive staining in comparison to sham surgery. Mice with DMM surgery have an increased positive signal area when treated with YKL-05-099 in comparison to VEH treatment. However, the increased positive signal area seen in the DMM YKL group did not correlate with the percentage of Prg4 positive cells in the non-calcified region of the articular cartilage (**Figure 14 B**). YKL-05-099 treatment does not show an increased number of *Prg4* expressing cells in comparison to VEH treatment in mice with sham or DMM surgery.

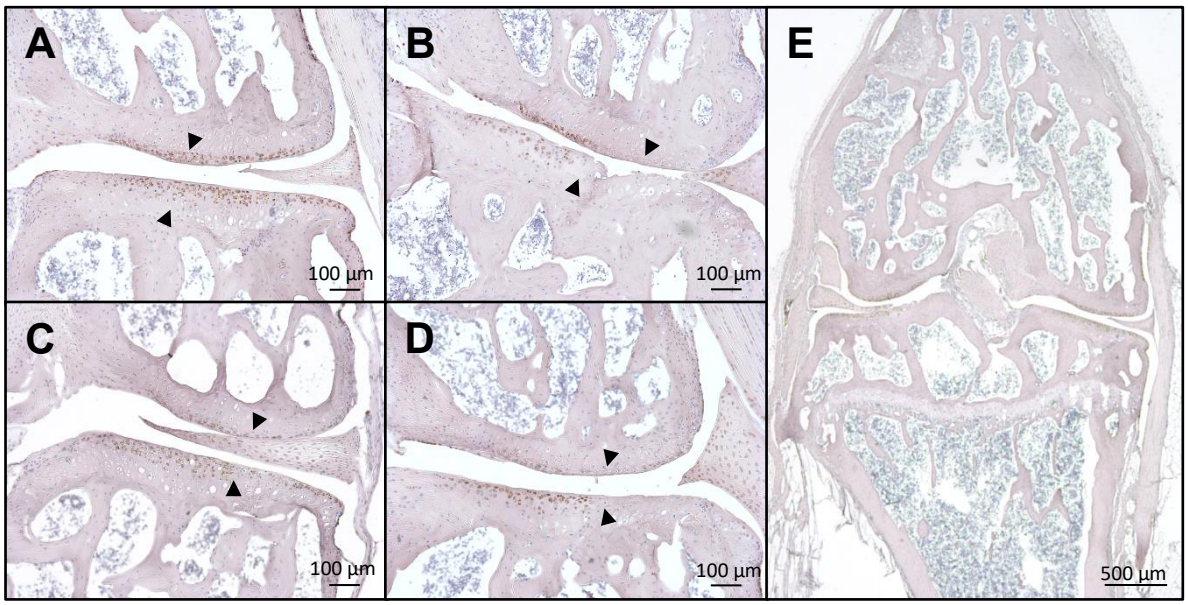

Figure 13: *Prg4 in situ* hybridizations of murine knee sections. Representation of *Prg4* expression in knee joints of mice with **A)** Sham surgery and VEH treatment, **B)** DMM surgery and VEH treatment, **C)** Sham surgery and YKL-05-099 treatment, **D)** DMM surgery and YKL-05-099 treatment. **E)** *Prg4* is expressed in chondrocytes of the non-calcified region of articular cartilage, menisci and the synovial region of the joint in all groups. *Prg4* is not expressed near cartilage erosions.

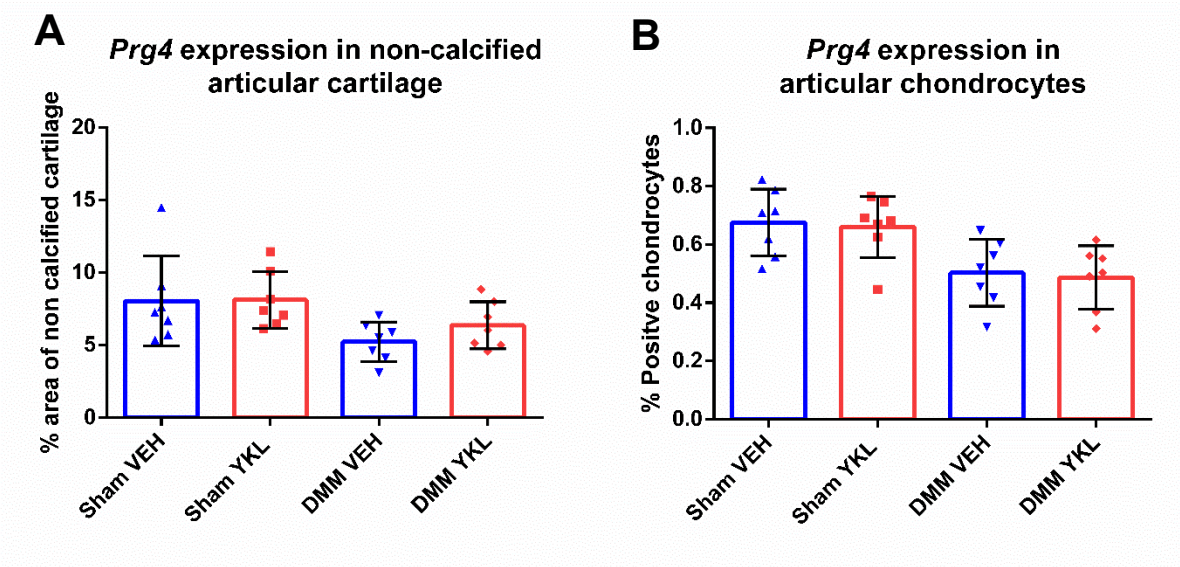

Figure 14: Prg4 expression in the non-calcified region of articular cartilage and articular chondrocytes. A) A slightly increased positive signaling area was seen in mice with DMM surgery and YKL-05-099 treatment in comparison to mice with DMM surgery and VEH treatment but was not seen in mice with sham surgery. **B)** The number of *Prg4*-positive cells in the non-calcified region of articular cartilage did not change with YKL-05-099 treatment but DMM surgery in comparison to Sham surgery.

Paraffin-embedded mouse brain tissue was used to confirm positive staining of *Prg4* (n = 2). Brain (**Figure 15** A – C) and knee (**Figure 15** D – F) sections were stained either with RNAscope® Negative Probe **Figure 15 A & D**, RNAscope® Positive Probe **Figure 15 B & E** or RNAscope® Prg4 Probe **Figure 15 C & F**. No brown signal was detected for sections sections incubated with RNAscope® Negative Probe. Brain sections incubated with RNAscope® Positive Probe show multiple brown dots per cell in comparison to knee sections where only a few dots per cell are visible. *Prg4* was only detected in murine knee sections and not in brain tissue.

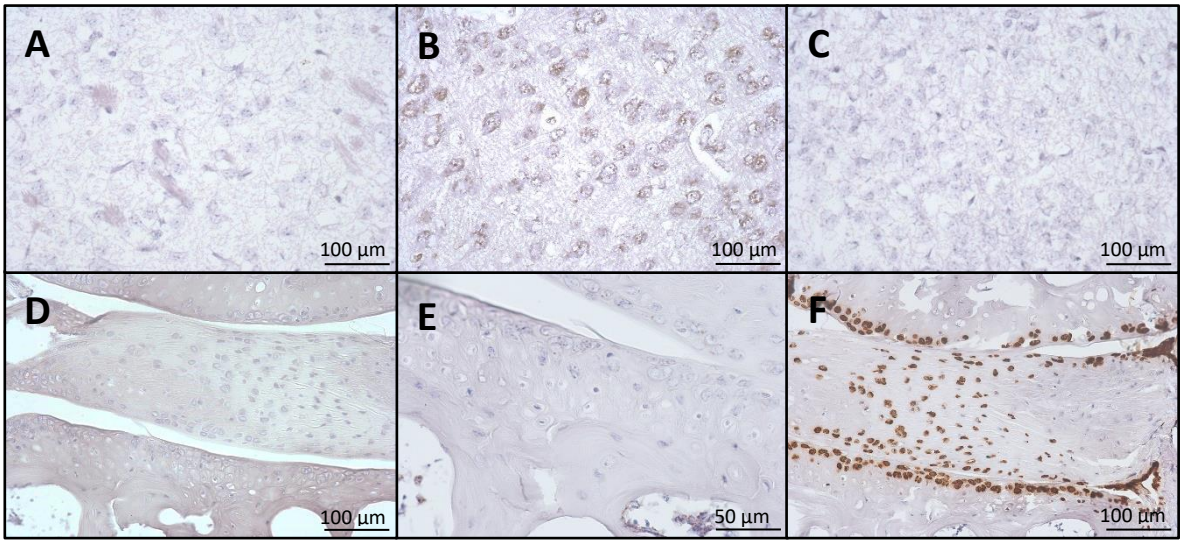

Figure 15: *Prg4 in situ* hybridizations of murine brain tissue. Mouse brain tissue (**A – C**) and mouse knee sections (**D – F**) were incubated with RNAscope® Negative Control Probe **A & D** showing no positive signal. **B)** Brain tissue incubated with RNAscope® Positive Control shows multiple positive signals per cell while **E)** knee sections only have a few positive epitopes. No positive staining was detected in brain tissue incubated with RNAscope® Prg4 Probe **C** in comparison to knee sections **F**.

3.4 *In situ* hybridization for *MMP13*

In situ hybridization was also used to assess *MMP13* expression in murine knee joints (Sham VEH, Sham YKL, DMM VEH, DMM YKL, n = 2/group) to confirm initial results with immunohistochemistry. RNAscope® 2.5 HD Detection Reagent – Brown was used for detection of *MMP13* expressing cells which appear brown-black. Sections were counterstained with 50% hematoxylin. Treatment groups were compared among each other to elucidate differences in YKL-05-099 treatment in comparison to VEH treatment. Only medial sites of the knee were used for assessment.

Figure 16 shows representative images of each treatment group (**A)** Sham VEH, **B)** DMM VEH, **C)** Sham YKL, **D)** DMM YKL, **E)** low magnification of whole knee section). Despite increased incubation time with Amplification diluents to increase the positive signal of the *MMP13* Probe, no positive signal was detected in the articular cartilage of all groups. No detectable *MMP13* was expressed near cartilage erosions seen in **Figure 16 B**. Positive

signal of *MMP13* was visible for all groups near the growth plate, the primary and the secondary ossification center and the periosteum.

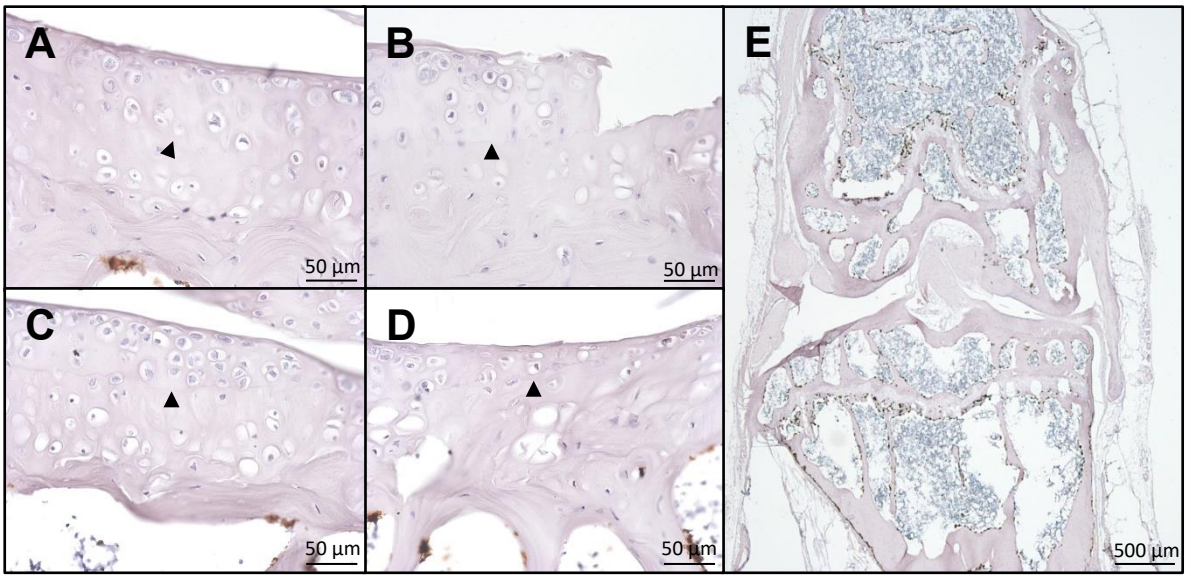

Figure 16: MMP13 *in situ* hybridization of murine knee sections. Representation of *MMP13* expression in knee joints of mice with **A)** Sham surgery and VEH treatment, **B)** DMM surgery and VEH treatment, **C)** Sham surgery and YKL-05-099 treatment, **D)** DMM surgery and YKL-05-099 treatment. *MMP13* expression could not be identified in the entire articular cartilage but near the growth plate, the primary and secondary ossification center and the periosteum. Black arrows indicate the tide mark.

To confirm *MMP13* positive staining and specificity, mouse brain tissue and mouse knee sections were incubated either with a control probe or MMP13 probe. Incubation with RNAscope® Negative Probe showed no positive staining in mouse brain (**Figure 17 A**) and mouse knee sections (**Figure 17 D**). Incubation with RNAscope® Positive Probe resulted in positive staining represented as multiple brown dots per cell in mouse brain (**Figure 17 B**) and fewer but stronger brown staining in multiple cells of the growth plate and bone marrow in mouse knee sections (**Figure 17 E**). Mouse brain had no positive staining after RNAscope® MMP13 Probe incubation (**Figure 17 C**) while mouse knee sections had a high positive signal beneath the growth plate and epiphysis with no positive staining of bone marrow cells (**Figure 17 F**)

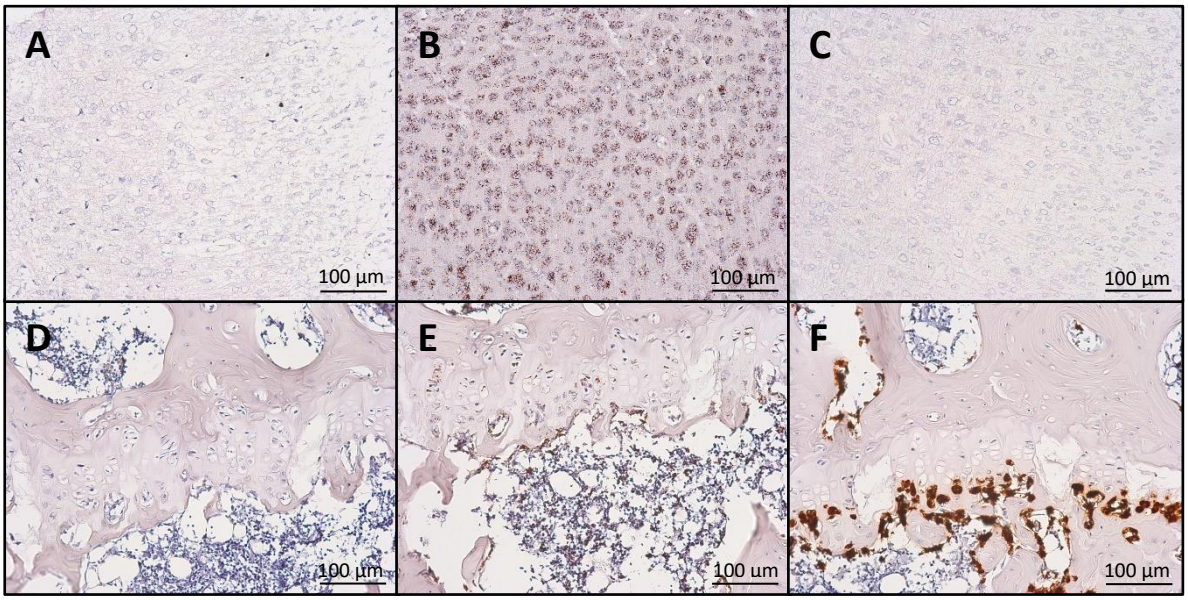

Figure 17: MMP13 probe and control probe in situ hybridization of mouse brain and mouse knee sections. Mouse brain **A**, **B**, **C** and mouse knee sections **D**, **E**, **F**, were incubated with RNAscope® Negative Probe **A**, **D**, RNAscope® Positive Probe **B**, **E** or RNAscope® MMP13 Probe **C**, **F**. A positive signal of MMP13 was only obtained for mouse knee sections.

3.5 Mouse serum CTX-II levels

Surgery-induced OA caused erosions of articular cartilage (see **Figure 8**). The measurement of CTX-II in the blood serum of 56 mice which underwent Sham/DMM surgery and treated with VEH/YKL-05-099 was used to prove enzymatic cartilage degradation by MMP13. Internal standards of the Serum Pre-Clinical CartiLaps® (CTX-II) ELISA kit were used to create a calibration curve (see **Figure 18 B**) with a correlation of R^2= 0.9969. Absorbance values of blood serum samples and the internal control sample were used to calculate the concentration of CTX-II levels. No CTX-II was detected for all samples (see **Figure 18 A**). The internal control provided by Serum Pre-Clinical CartiLaps® (CTX-II) ELISA kit was measured with a concentration of 78.4 pg/ml and complied with the expectations of the reported quality control value of 76.4 pg/ml.

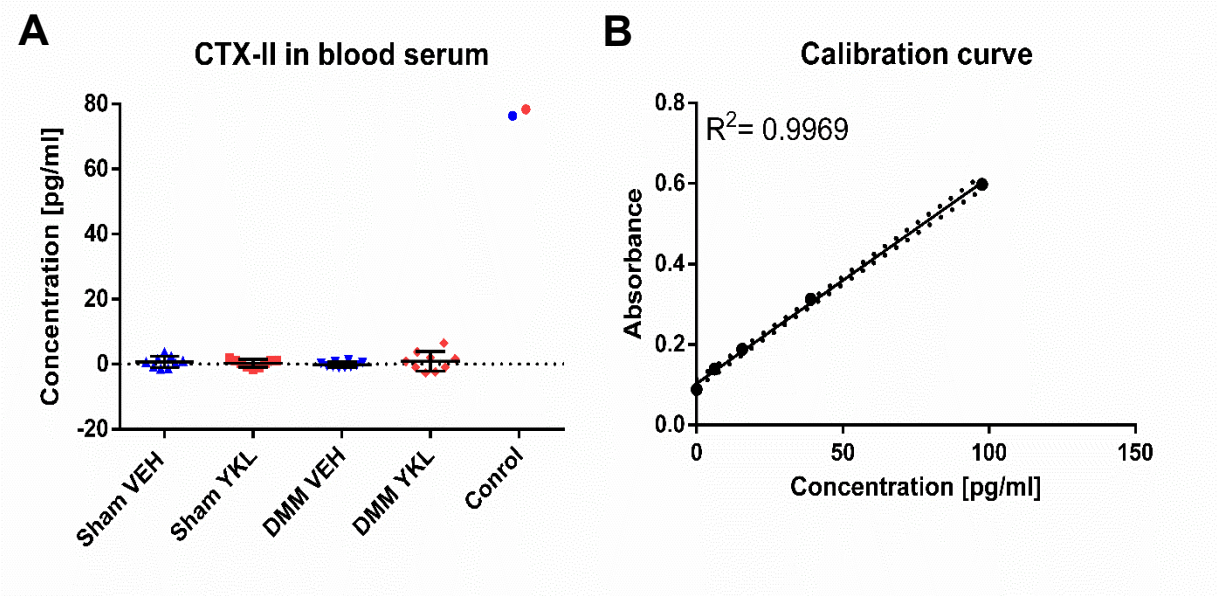

Figure 18: Serum Pre-Clinical CartiLaps® (CTX-II) ELISA kit results. A) No difference in CTX-II blood serum levels was detected between treatment groups (n= 14/group). Measurement of internal CTX-II control and calibration curve (R^2 = 0.9969) **B)** meets expectations.

3.6 Western blot

Protein phosphorylation plays an important role in the activation and translocation of key regulators of chondrocyte hypertrophy and the expression of articular cartilage matrix proteins. Immunoblotting of SIK3, CRTC2, HDAC4, HDAC5 and PKA was used to visualize changes of protein phosphorylation in primary murine sternal chondrocytes (**Figure 19 A**) and NIH3T3 (**Figure 19 B**) cells. Cells were treated with DMEM (10% FBS, 1% anti-anti, 25 µg/ml ascorbic acid) as control, PTH 200 nM for 5 min, 20 min or 60 min, Forskolin 5 µg/ml for 60 min and YKL-05-099 10 µM for 60 min to investigate treatment dependent protein expression and phosphorylation.

Phosphorylation of SIK3 at T469 is not detectable in cells with control, 5 min PTH and with YKL-05-099 treatment in both, primary chondrocytes and NIH3T3 cells. While longer treatment with PTH increases phosphorylation in primary chondrocytes, NIH3T3 cells are unaffected most likely due to lack of Pth1r expression by these cells. Forskolin treatment induces phosphorylation of SIK3 T469 in both cell types.

CRTC2 phosphorylation at S275 is higher in control primary chondrocytes then PTH-, Forskolin-, or YKL-05-099-treated cells. Longer treatment duration of PTH increases phosphorylation of CRCT2 but is lower in comparison to control cells. In NIH3T3 cells phosphorylation of CRCT2 is equal between control cells and PTH treated cells. Longer exposure time to PTH does not influence CRTC2 phosphorylation in NIH3T3 cells. Treatment with Forskolin or YKL-05-099 reduces phosphorylation of CRTC2 at S275 in NIH3T3 cells.

Detection of phosphorylated HDAC4 at S246, S259 or S155 for primary chondrocytes is not clear. No bands are visible for control cells and cells treated with PTH for 5 min and 20 min. Treatment with PTH for 60min, Forskolin or YKL-05-099 might show positive results while background staining is increasing. Total levels of HDAC 5 is consistent among treatment groups of chondrocytes. NIH3T3 cells show clear phosphorylation of HDAC4 with all treatments. However, phosphorylation is decreased when treated with Forskolin or YKL-05-099 while total levels of HDAC5 remain the same.

Immunoblotting with pPKA substrate detects peptides and proteins containing a phospho-Ser/Thr residue with arginine at the -3 and -2 positions. When comparing phosphorylation of primary chondrocytes with different treatments, control cells show reduced phosphorylation in comparison to PTH and Forskolin treatment. Furthermore, increased duration of PTH treatment seems to increase phosphorylation for some PKA substrates. Remarkably, YKL-05-099 reduces phosphorylation in comparison to all other treatments. No changes of PKA substrate phosphorylation can be detected in NIH3T3 cells treated with either PTH or YKL-05-099 and control cells. However, Forskolin treatment of NIH3T3 cells increases phosphorylation in comparison to other treatments.

β-Tubulin was used as a loading control for primary chondrocytes and NIH3T3 cells. In both cases equal amounts of proteins were loaded to the SDS-PAGE gel.

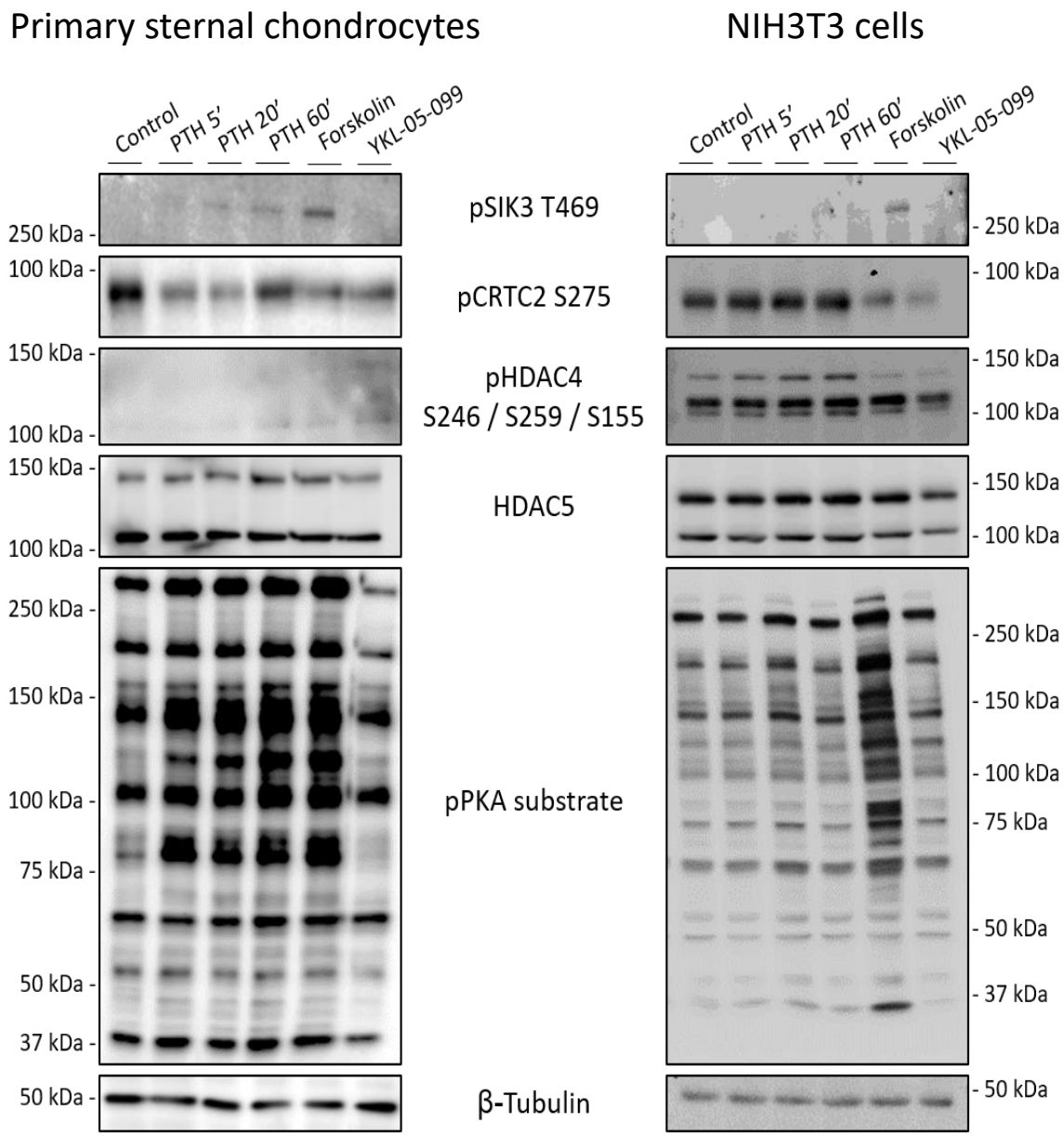

Figure 19: Immunoblot of murine primary sternal chondrocytes and NIH3T3 cells. Treatment with Forskolin shows increased phosphorylation of pSIK3 T469 in comparison to control and YKL-05-099 treatment in primary chondrocytes and NIH3T3 cells. Treatment with PTH, Forskolin and YKL-05-099 shows decreased phosphorylation of pCRTC2 S275 in comparison to controls in primary chondrocytes. Reduced levels of pCRCT2 S275 are only seen in Forskolin, and YKL-05-099 treated NIH3T3 cells. pHDAC4 S246/S259/S155 was reduced in Forskolin, and YKL-05-099 treated NIH3T3 cells, but no clear results were obtained for primary chondrocytes while total levels of HDAC5 remained the same. Phosphorylation of pPKA substrates is increased in PTH treated primary chondrocytes, increased in both cell types when treated with Forskolin and reduced in primary chondrocytes when treated with YKL-05-099. β-Tubulin was used as a loading control and was equal among treatment groups in both cell types.

3.7 Real-time PCR

qPCR was used to further investigate the molecular mechanism of PTH/PTHrP related signaling regarding mRNA expression of *Prg4* and hypertrophic associated genes such as *MMP13* and *Col10a1.* Primary murine sternal chondrocytes were treated either with DMEM (10% FBS + 1% anti/anti) as control, 200 nM PTH, 1 µM YKL-05-099, 10 µM YKL-05-099 or 5 µg/ml Forskolin for 4 h in triplicates to identify changes in RNA expression (n = 3). Expression of *Prg4*, *MMP13* and *Col10a1* was normalized to housekeeping gene *β-actin*. Differences among treatment groups are described with relative mRNA expression.

Figure 20 shows the relative mRNA expression of *Prg4* with two different Primer sets. *Prg4* expression is increased in all 4 treatment groups. While treatment with PTH 200 nM, YKL-05-099 and 5 µg/µl Forskolin are slightly elevated and comparable among each other, treatment with 10 µM YKL-05-099 is significantly increased in comparison to controls. Relative mRNA expression using *Prg4* Primer set 2 indicates a trend towards higher *Prg4* expression when treated with 10 µM YKL-05-099 while other treatments show unchanged RNA expression levels. In conclusion, YKL-05-099 treatment increases *Prg4* expression of primary murine sternal chondrocytes.

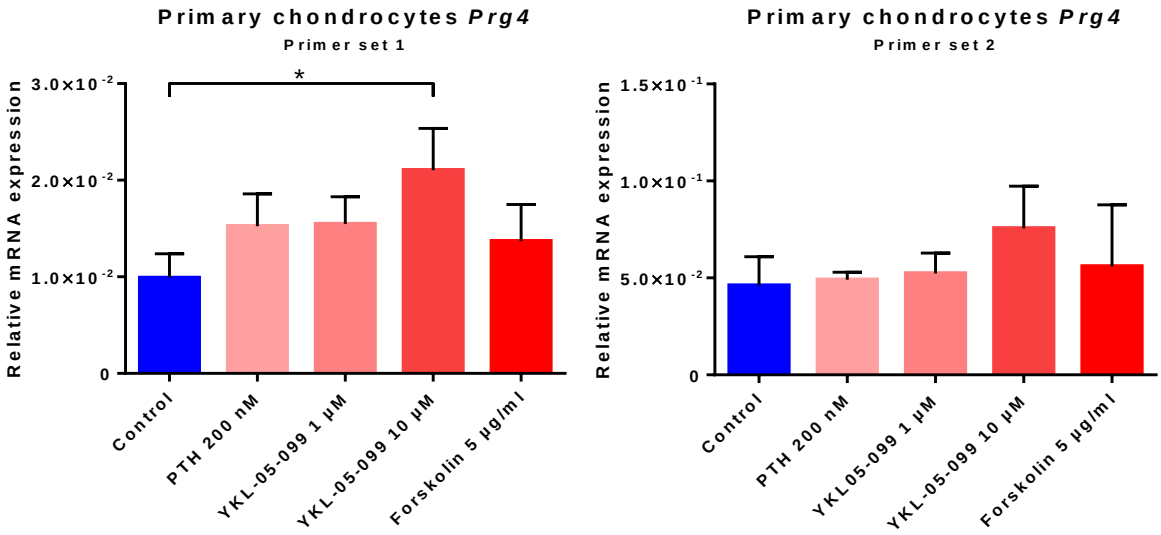

Figure 20: Relative *Prg4* expression in primary murine sternal chondrocytes. Relative *Prg4* expression is increased in primary chondrocytes treated with 10 µM YKL-05-099 and show statistically significance when using primer set 1. Treatment with 200 nM PTH, 1 µM YKL-05-099 and 5 µg/ml Forskolin show a trend in increased *Prg4* expression with primer set 1 but could not be confirmed with primer set 2 (n = 3/group).

MMP13 expression was investigated using two different primer sets, seen in **Figure 21** (n = 3). Treatment with 1 µM YKL-05-099 and 5 µg/ml Forskolin show similar gene expression levels in comparison to controls in both primer sets. Treatment with 200 nM PTH results in slightly decreased *MMP13* shown with primer set 1 while gene expression is slightly

increased with primer set 2. However, the variance between replicate treatments of 200 nM PTH for primer set 1 is high in comparison to other treatments. Treatment with 10 µM YKL-05-099 showed a significant decrease in relative *MMP13* expression with both primer sets.

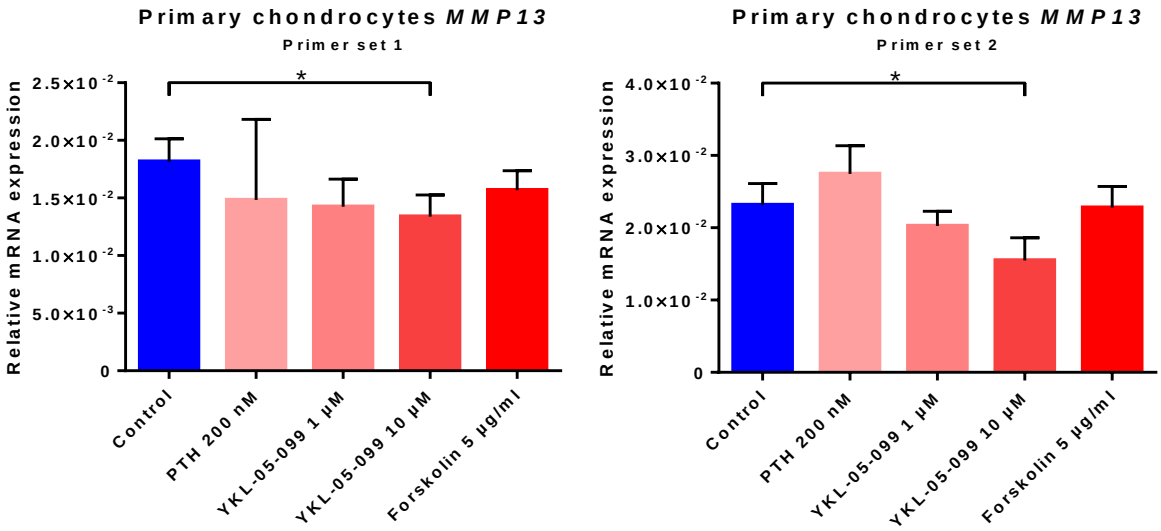

Figure 21: Relative *MMP13* expression in primary murine sternal chondrocytes. Relative gene expression of *MMP13* was significantly reduced in primary murine chondrocytes when treated with 10 µM YKL-05-099 (n = 3). Treatment effects of 200 nM PTH are not clear due to high variance between replicates and treatment with 1 µM YKL-05-099 and 5 µg/ml Forskolin do not indicate clear differences in mRNA expression.

Relative gene expression of *Col10a1* was used as the third marker to identify treatment effects on primary murine sternal chondrocytes using one primer set seen in **Figure 22** (n = 3). Treatment with 10 µM YKL-05-099 cause elevated expression of *Col10a1* while other treatments cause no obvious change in relative gene expression when comparing to the control.

To confirm these initial results, prolonged treatment with YKL-05-099 was performed. Primary murine sternal chondrocytes were treated for 1.5 h, 3 h, 6 h and 18 h with either DMEM (with 10% FBS and 1% anti/anti) as control or 5µM YKL-05-099 in triplicates.

Figure 23 shows time depended *Prg4* expression of primary murine sternal chondrocytes treated with 5 µM YKL-05-099. Primer set 1 indicates a significant increase in relative *Prg4* expression after 1,5 h, 3h and 18 h. While *Prg4* levels at 1,5 h, 3 h and 6 h are similar to each other, *Prg4* levels at 18 h incubation is dramatically increased. Primer set 2 shows a time-dependent increase of *Prg4* expression with statistically significant differences to control samples after 3h and 18 h of YKL-05-099 treatment. *Prg4* expression of all control samples remained constant throughout the whole experiment when using both primer sets.

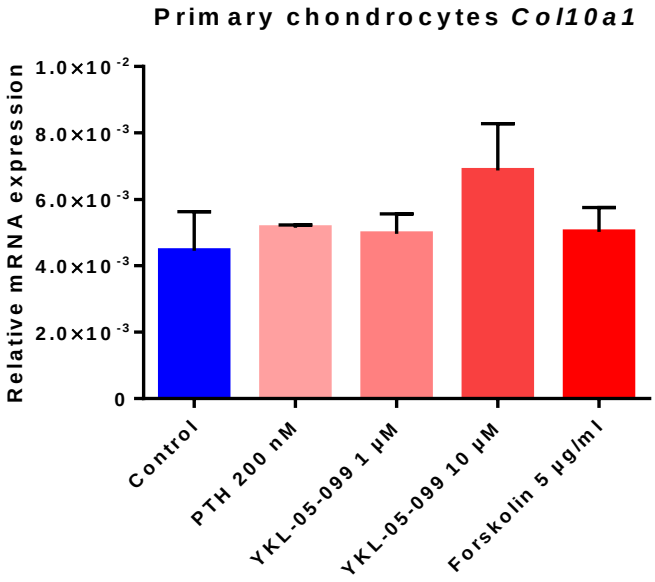

Figure 22: Relative *Col10a1* expression of primary murine sternal chondrocytes. Relative *Col10a1* expression was elevated when treated with 10 µM YKL-05-099 but did not show statistical significance (n = 3). Other treatments do not indicate a clear trend in altered mRNA expression.

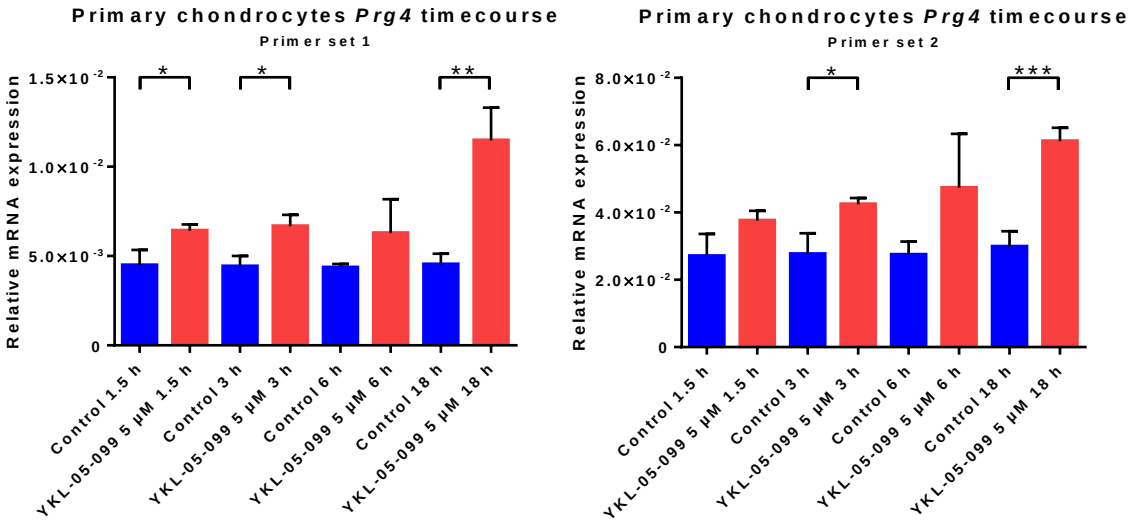

Figure 23: Time-dependent *Prg4* expression of primary murine sternal chondrocytes treated with 5 µM YKL-05-099. Relative *Prg*4 expression was significantly increased in chondrocytes treated with 5 µM YKL-05-099 in a time-dependent manner (n = 3). Control cells had similar Prg4 expression level throughout the time course with both primer sets while Prg4 expression gradually increased with longer 5 µM YKL-05-099 treatment.

Figure 24 shows relative *MMP13* expression of primary murine sternal chondrocytes treated with 5 µM YKL-05-099 over different periods (n = 3). Both primer sets show a clear trend in

decreased *MMP13* expression depending on treatment duration of YKL-05-099. Significant decreases could be observed after 1.5 h and 18 h treatments for both primer-sets and after 6 h for primer set 1. Control samples show a negative trend of relative *MMP13* samples over an incubation time of 6 h. Interestingly, relative mRNA expression of *MMP13* in control samples are increased after 18 h incubation in comparison to 6 h incubation. All control cells had reduced MMP13 expression over time when comparing to 1.5 h control cells but higher mRNA expression in comparison to their respective treatment group.

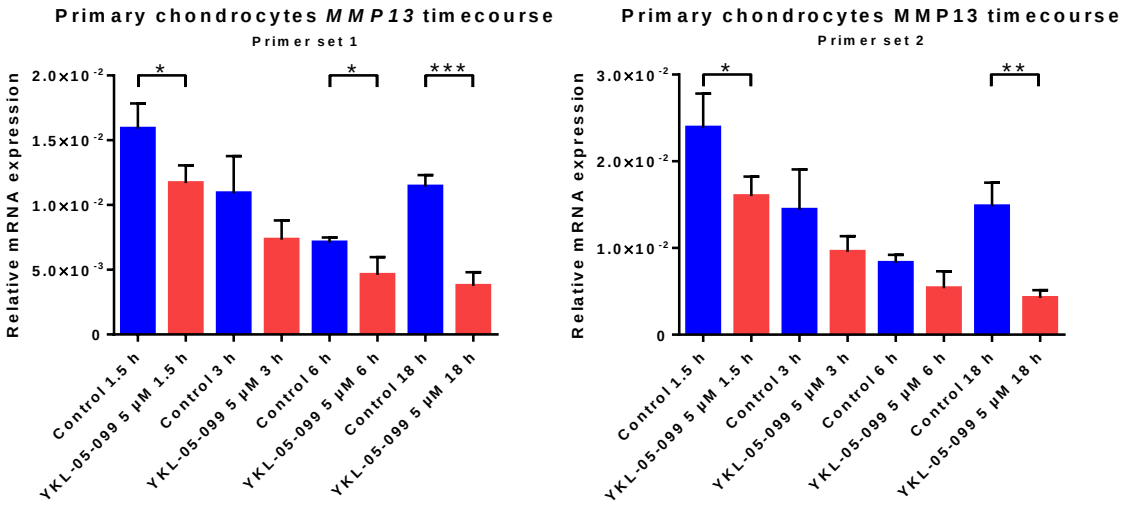

Figure 24: Time-dependent *MMP13* expression in primary murine sternal chondrocytes treated with YKL-05-099. Relative *MMP13* expression was significantly reduced in primary chondrocytes treated with 5 µM YKL-05-099 in a time-dependent manner (n = 3). All control cells had reduced *MMP13* expression over time when comparing to 1.5 h control cells but higher mRNA expression in comparison to their respective treatment group.

Expression of *Col10a1* in primary murine sternal Chondrocytes (n = 3) can be seen in **Figure 25**. YKL-05-099 treated cells have gradually increased *Col10a1* expression with longer incubation times. Treatments over 6 h and 18 h showed statistically significant increases in *Col10a1* expression when treated with YKL-05-099 in comparison to respective controls. However, relative *Col10a1* expression in all treatment groups is 30-times lower in comparison to the time dependent expression of *Prg4* and *MMP13* when treated with 5 µM YKL-05-099.

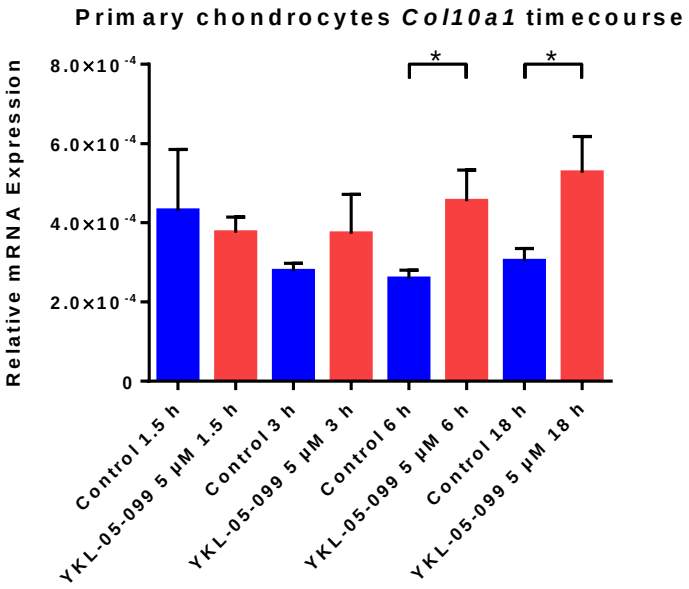

Figure 25: Time-dependent *Col10a1* expression in primary murine sternal chondrocytes treated with YKL-05-099. Relative *Col10a1* expression was significantly increased in primary chondrocytes treated with 5 µM YKL-05-099 after 6 h and 18 h incubation time. However, the *Col10a1* expression for all treatment groups is 30-times lower in comparison to other investigated genes. (n = 3).

To confirm the immaturity of primary chondrocytes and the absences of fibroblasts, alcian blue staining was performed. Primary chondrocytes slowly outgrew from the center to the edge of the culture dish and appear in a round/polygonal shape. Differentiated chondrocytes form cell clusters an appear elongated or swollen. Approximately 70% of the cell population stained positive for alcian blue, identifying immaturity of primary chondrocytes in culture (see **Figure 26**)

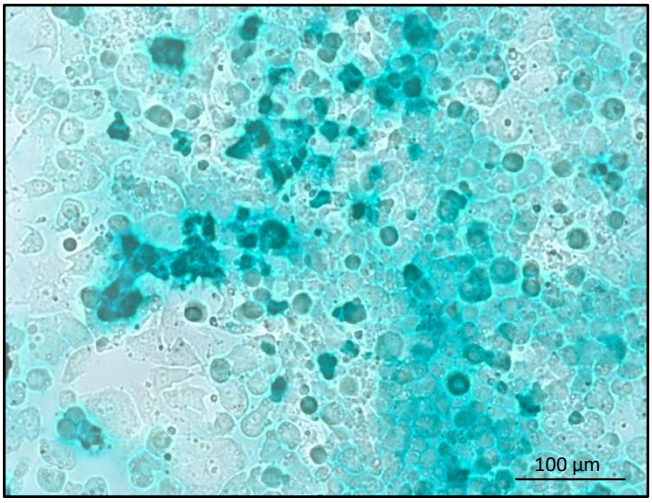

Figure 26: Alcian blue staining of primary murine sternal chondrocytes. Positive alcian blue staining of ~70% primary chondrocytes, conforming immaturity of the cell population.

Murine clonal limb bud cells were used to confirm the effects of 5 µM YKL-05-099 treatment seen in primary murine sternal chondrocytes. Murine clonal limb bud cell mRNA was isolated at day-0 and day-10 of differentiation to assess *Prg4*, *MMP13* and *Col10a1* expression.

Figure 27 shows relative mRNA expression of *Prg4* in murine clonal limb bud cells with two different primer sets in triplicates. Statistically significant reduction of *Prg4* expression was seen in day-0 mouse limb bud cells treated with 5 µM YKL-05-099 for 18 h. Shorter incubation times do not indicate a clear response to YKL-05-099 treatment. In contrast, day-10 mouse limb bud cells have slightly increased *Prg4* expression but was also reduced after 18 h of treatment. Relative *Prg4* expression was increased after 10 days of differentiation in comparison to undifferentiated cells. However, relative mRNA expression of day-0 and day-10 mouse limb bud cells is 18-times lower in comparison to time dependent *Prg4* expression primary sternal chondrocytes treated with 5 µM YKL-05-099.

Day 0 mouse limb bud cells show decreased *MMP13* expression when treated with YKL-05-099 for 1.5 h and 3 h (**Figure 28**). Treatment over 6 h do not show a difference in *MMP13* expression compared to its corresponding control while cells treated over 18 h have increased *MMP13* expression. Mouse limb bud cells differentiated for 10 days show a similar expression pattern when subjected to 5 µM YKL-05-099. Statistically significant decreased *MMP13* expression was seen after 1.5 h and 3h treatment and was decreased after 6 h treatment. RNA levels were increased after 18 h. Additionally, mouse limb bud cells differentiated for 10 days had higher *MMP13* RNA expression levels in comparison to undifferentiated mouse limb bud cells.

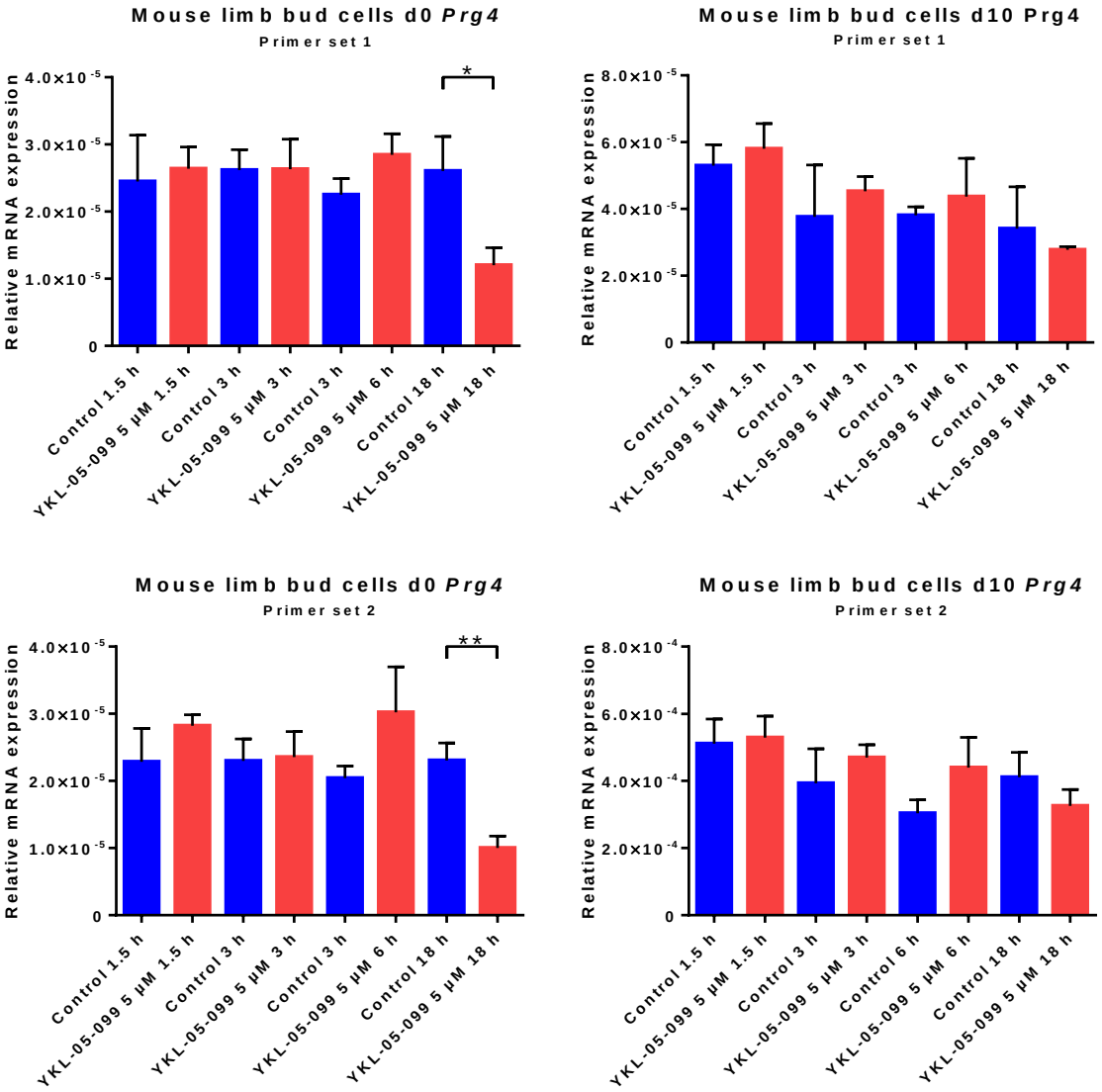

Figure 27: Relative *Prg4* expression of un-/differentiated murine clonal limb bud cells. Cells respond to 5 µM YKL-05-099 treatment with slightly increased *Prg4* expression during early treatment and with reduced *Prg4* expression after 6 h. Relative mRNA levels are 18-times lower in clonal limb bud cells in comparison to primary sternal chondrocytes (n=3).

Both, undifferentiated mouse limb bud cells and mouse limb bud cells differentiated for 10 days show a statistically significant reduction in *Col10a1* expression after 18 h treatment with YKL-05-099 **Figure 29**. Shorter treatment durations don't result in a similar reduction of *Col10a1* expression. Mouse limb bud cells differentiated for 10 days show statistically significant reduction after 1.5 h but slightly increased expression after 3 h and 6 h of 5 µM YKL-05-099 treatment. Relative RNA levels are increased by 6-folds in mouse limb bud cells differentiated for 10 days in comparison to undifferentiated cells and 30 times higher in comparison to primary murine sternal chondrocytes treated with 5 µM YKL-05-099.

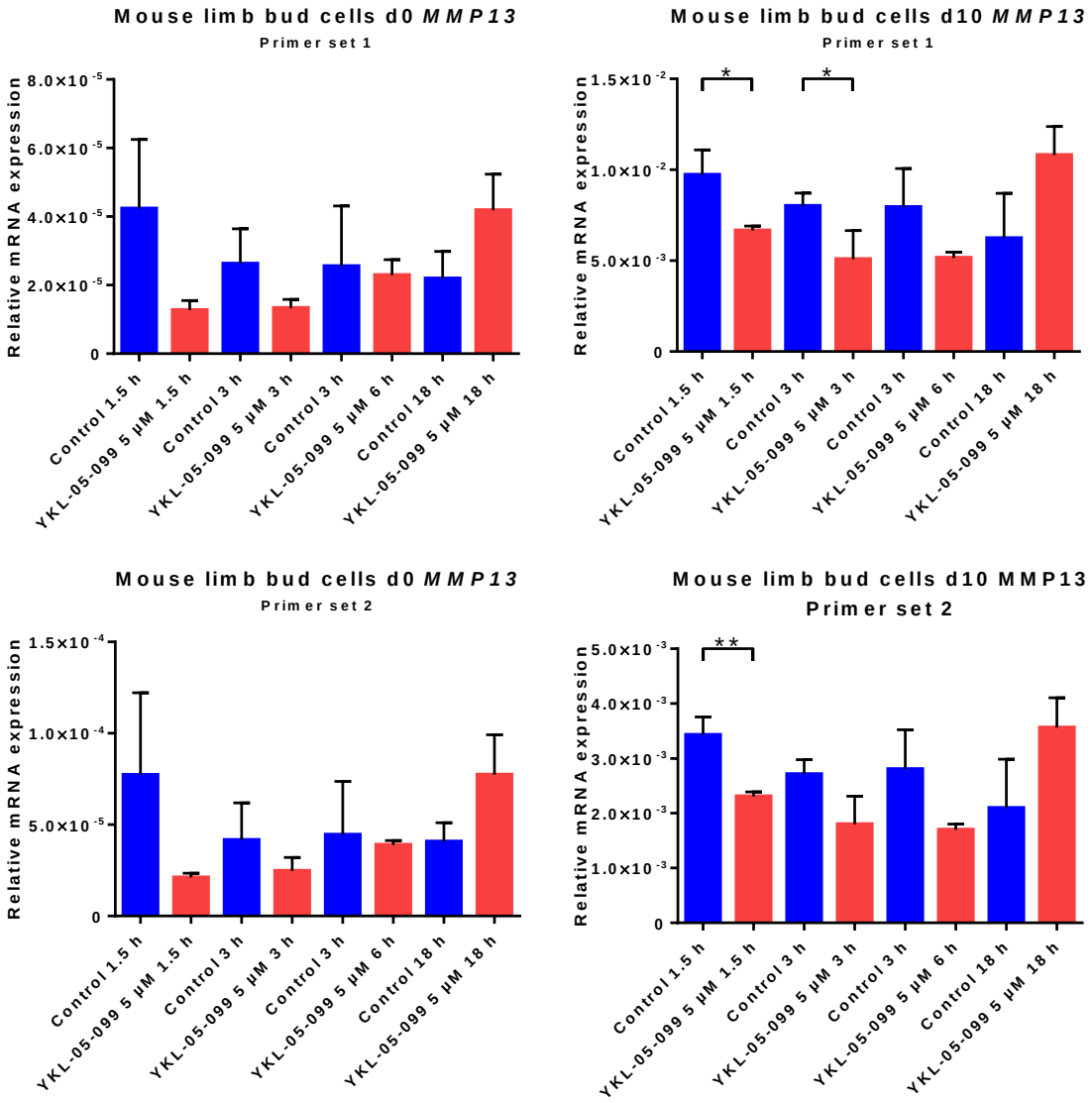

Figure 28: Relative *MMP13* expression of un-/differentiated murine clonal limb bud cells treated with YKL-05-099. Decreased *MMP13* expression levels can be seen in murine clonal limb bud cells subjected to 5 µM YKL-05-099 treatment for 1.5 h and 3 h. Day 10 differentiated cells showed also decreased *MMP13* levels after 6 h while undifferentiated cells were unaffected by the treatment. *MMP13* levels increased after 18 h 5 µM YKL-0-099 treatment in day-0 and day-10 mouse limb bud cells and day 10 cells showed higher total *MMP13* expression in comparison to undifferentiated cells.

.

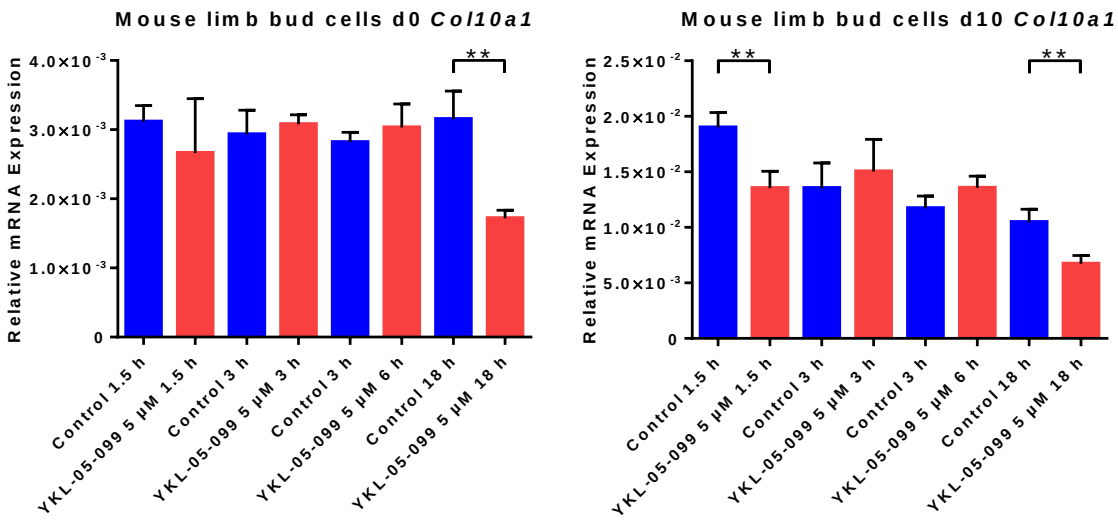

Figure 29: Relative *Col10a1* expression in un-/differentiated mouse limb bud cells treated with 5 µM YKL-05-099. A statistically significant reduction in relative *Col10a1* expression could be observed for both day 0 and day 10 mouse limb bud cells with 5 µM YKL-05-099 treatment over 18 h. D-10 mouse limb bud cells also show statistical significant reduction after 1.5 h treatment but slightly elevated levels of *Col10a1* after 3 h and 6 h treatment. Relative *Col10a1* expression levels are slightly higher in d10 mouse limb bud cells in comparison to d0 cells.

Alcian blue staining was used to identify proteoglycan expression and confirm the differentiation of clonal mouse limb bud cells into chondrocytes (see **Figure 30**). Undifferentiated cells show no clear indication of proteoglycan expression. First signs of proteoglycan expression can be seen after 2 days in culture with differentiation media. Differentiated limb bud cells appeared in clusters with moderate positive staining at day 6 and later. Mouse limb bud cells showed strong positive blue signal after 9 days in culture. Mouse limb bud cells were used for qPCR in an undifferentiated state and after 10 days of differentiation with approximately 60% proteoglycan expressing cells.

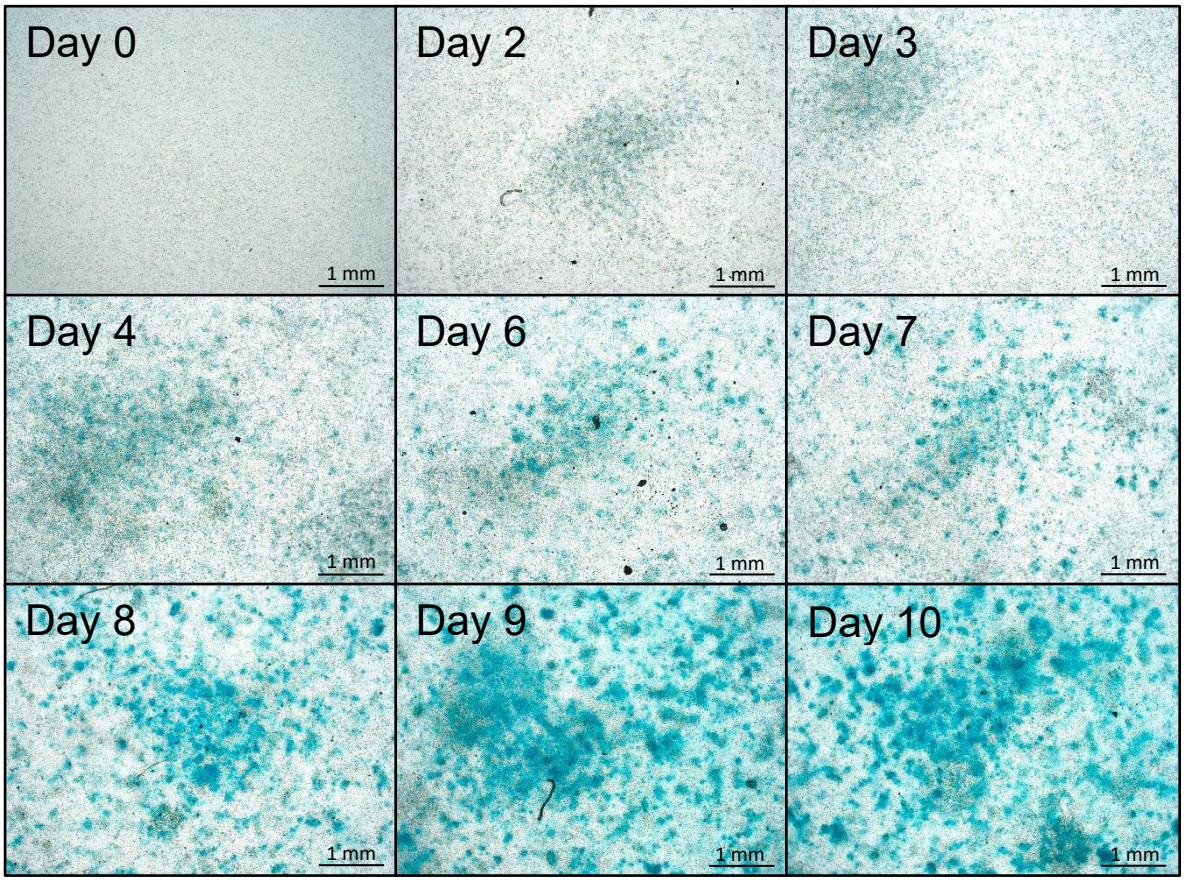

Figure 30: Alcian blue staining of differentiating clonal mouse limb bud cells. Cells were seeded at 70,000 cells/ml and supplemented with differentiation media after one day (day 0). Cells showed slightly positive staining at day 2. Cell clusters of proteoglycan-expressing cells were formed at day 6 and later. Strong positive proteoglycan staining was detected at day 9 and 10 indicating successful differentiation into chondrocytes.

4. Discussion

Pathophysiological characterization of OA in humans is usually done by radiographic methods to assess joint space width [133], [134] or histological scoring systems [135], [136]. The recommended semi-quantitative OARSI scoring system by Glasson *et al*. was used to measure DMM-induced OA in mice [172]. This scoring system is specific to mice due to the differences in the composition of articular cartilage in comparison to human. The calcified region of the articular cartilage in mice is as thick or even thicker than the non-calcified region [174]. Cartilage zones are hardly distinguishable, and pathological cartilage degradation tends to be an all-or non-phenomenon [172]. The OARSI scoring system is a subjective method that needs training and experience to be executed properly.

Serial coronary sections of the whole knee joint were performed and stained with Safranin O to visualize proteoglycans of the articular cartilage. 25% of the sections per knee were used to score the severity of OA for the whole mouse (see **Figure 8 A**). This means that regions with local erosions of the articular cartilage may have been missed which may have

resulted in a lower rating of OA severity per mouse. However, scores were given based on continuity of articular cartilage damage. Severe erosions of articular cartilage affect bigger areas of the knee joint and can be seen on consecutive sections. Even though OARSI scoring rates severity of OA based on cartilage degradation, it does not rate the state of the whole knee joint. Other scoring systems for mice also include other aspects like bone remodeling, osteophyte formation and synovial changes [172], but were not subject of this study. The primary focus of this project is to elucidate the articular chondrocyte metabolism in OA and corresponding cartilage degradation when treated with YKL-05-099 in comparison to controls.

Grub's test for outliers identified one outlier in the DMM YKL group (OARSI score = 4). This mouse was not excluded from the assessment due to the subjective nature of the OARSI scoring system and the low number of mice per group. Nevertheless, a clear trend of improved cartilage integrity is seen in mice treated with YKL-05-099.

Measuring the area of positive proteoglycan staining was used as an alternative rating system for OA severity (**Figure 9**). This method could not reveal any difference between mice treated with VEH or YKL. Mice which underwent DMM surgery show erosions of up to 50% of the non-calcified region of the articular cartilage (OARSI scoring = 4). Loss of proteoglycans without cartilage erosions or fibrillation (OARSI score = 0.5) may affect the same area as eroded articular cartilage. However, no correlation between OARSI scoring and proteoglycan area was given. Higher OARSI scores do not imply an increased loss of proteoglycans. Nevertheless, measurement of the proteoglycan area can indicate OA progression if performed in intervals as seen in the study of Lorenz *et al.* [175]. Mice with DMM induced OA showed increased loss of proteoglycans over a time course of 8 weeks in comparison to non-operated mice [175].

Surgical induction of OA is limited to a specific region of the body. DMM surgery is considered as a mild to moderate induction of OA in mice in comparison to anterior cruciate ligament transection (ACLT) [176]. Glasson *et al.* showed a significant increase in cartilage erosion in comparison to sham-operated and non-operated mice after 4 and 8 weeks of OA induction [176]. However, cartilage erosion exceeded 80% of the articular cartilage width in some mice, which could not be seen in this study or the study of Lorenz *et al.* [175], [176]. Furthermore, sham surgery and non-operated mice in the study of Glasson *et al.* had fibrillations and erosions of the superficial layer of the articular cartilage, which was also observed in this study, but not in the study of Lorenz *et al.* [175], [176]. Even though DMM surgery is an easy and reproducible technique [176], outcomes may vary with the experience of the surgeon. Another possible factor of variations in the severity of surgical induced OA is movement and behavior of mice after surgery. Kim *et al.* showed in a DMM induced OA mouse model increased cartilage erosions in mice subjected to daily exercise in comparison to mice without exercise. Mice held in a confined cage with restricted movement showed fewer cartilage erosions in comparison to mice held in a normal cage [177]. The mice in this study were held in a normal cage and mouse movement was not tracked. This may have led to variations of OARSI scores among groups (seen **Figure 8 A**). Kim *et al.* have not reported

increased cartilage degradation in sham-operated mice due to movement. However, mice with sham surgery did not show any erosions or fibrillation of the articular cartilage in comparison to this study [177].

Immunohistochemistry with Col X was performed to assess the molecular changes in articular cartilage of mice when treated with YKL-05-099 in comparison to VEH treatment (**Figure 11**). A reduction in Col X was seen for mice treated with YKL-05-099 without statistically significance. Staining with anti-collagen X antibody (Abcam #ab58632) caused very high background staining (seen in cells of the synovial compartments, bone and bone marrow **Figure 11**). This is most likely due to the cross-reactivity of the antibody with type II collagen and fibronectin, a glycoprotein necessary for cell adhesion, migration, growth and differentiation which is found in connective tissue matrices [178]. The expression of type II collagen [3] along with the expression of fibronectin [179] explains excessive positive staining and unexpected high positive staining in articular chondrocytes of mice with sham surgery. Furthermore, Col X positive staining was also seen for chondrocytes in the growth plate (not shown). This suggests that chondrocytes may express Col X throughout their maturation in low levels.

Positive staining of murine knee sections with anti-MMP-13 antibody (Abcam #ab84594) could not be considered as valid due to high background staining (**Figure 12**). MMP13 signal could not be increased with increased antibody concentration, increased incubation time or different antigen retrieval agents. Expected MMP13 positive staining was seen near the primary epiphysis below the growth plate [3], [4] but not in articular cartilage of surgery-induced OA mice [139]. However, no differences between treatment groups were observed. Only a few other studies used the anti-MMP-13 antibody (Abcam #ab84594) for protein analysis [180], [181] or immunohistochemistry [182], [183], but did not include images of MMP13 immunohistochemistry.

In situ hybridization was used to identify *MMP13* expression of chondrocytes in the articular cartilage (**Figure 16**). Despite the induction of OA with visible articular cartilage erosions, no *MMP13* expression could be detected in articular cartilage. Increased exposure to pepsin, signal enhancing solutions RNAsope® AMP 5 and RNAsope® AMP 6 or DAB increased the positive signal for *MMP13* expression near the growth plate, primary and secondary ossification center and the periosteum but not in articular cartilage. These results align with the results obtained from the immunohistochemical staining of murine knee sections with anti-MMP13 antibody (**Figure 12**). However, other studies have shown MMP13 positive chondrocytes in the superficial layer and the non-calcified region of articular cartilage in DMM-induced OA mouse models [184]–[186]. Interestingly, chondrocytes of the growth plate did not show *MMP13* expression unless they matured into a late hypertrophic state seen at the end of the growth plate (**Figure 17 F**). This suggests, that early hypertrophic chondrocytes might not express detectable amounts of *Prg4.*

To further asses the effects of YKL-05-099 treatment, murine knee sections were incubated with RNAscope® Prg4 Probe (**Figure 13**). We observed a very high signal of *Prg4* expressing chondrocytes in the non-calcified region of the articular cartilage and menisci for

all groups. *Prg4* expression was not seen in chondrocytes of the growth plate despite positive proteoglycan staining with Safranin O and complies with the literature [21], [81], [88]. Furthermore, decreased *Prg4* expression of chondrocytes overlapped with proteoglycan loss or cartilage degradation in distinct regions of the non-calcified layer of articular cartilage. This suggests a link between reduced joint lubrication and cartilage erosion. A dilution of RNAscope® Prg4 Probe in combination with omitting RNAscope® AMP 5 and RNAscope® AMP 6 resulted in decreased positive signal without false negative results. However, the semi-quantitative analysis of *Prg4* expression by counting positive epitopes per cell was not possible due to the abundant number of positive epitopes per cell. Image J was used to assess the total area of positive staining in the non-calcified region of the articular cartilage **Figure 14 A**. This method showed a slightly increased positive area for mice with DMM surgery and YKL-05-099 treatment in comparison to mice with DMM surgery and VEH treatment. This result was not confirmed by the number of *Prg4*-positive cells in comparison to *Prg4*-negative cells **Figure 14 B**. This is most-likely due to the fact, that the brightness of the image plays a major role when assessing gray values of the image. Other methods for the assessment like the modal gray value or average gray value were not appropriate to confirm treatment effects with YKL-05-099.

Serum Pre-Clinical CartiLaps® (CTX-II) ELISA kit was used to evaluate the amount of degraded type II collagen by *MMP13* in the blood serum of mice (**Figure 18**). Even though the internal calibration standards and the internal positive control was measured accurately, CTX II levels were not detectable in all groups (detection limit of the assay c = 3.7 pg/ml). *MMP13* expression was seen with *in situ* hybridization of murine knee sections (**Figure 16**) but did not result in expected CTX-II concentrations of 24 pg/ml for 8-week-old normal mice and 11.3 pg/ml for 10-week-old normal mice according to Serum Pre-Clinical CartiLaps® CTX-II Elisa kit. In this study, 23-week-old mice were used, which might explain reduced levels of CTX-II. No comparable study with similar aged mice was found. However, the clear induction of DMM-induced OA with erosions of the articular cartilage suggests increased levels of CTX-II. Other studies found increased levels of CTX-II in OA animal models [187], [188], [189] or OA patients [138], [141] in comparison to controls. Induction of OA in larger animals than mice [188] or systemically induced OA in mice [187], [189], may also increase MMP13-dependent cartilage degradation in comparison to locally induced OA in mice.

cAMP-dependent phosphorylation of proteins was investigated with PTH (incubated over 5 min, 20 min, and 60 min), Forskolin (60 min) and YKL-05-099 (60 min) treatment in murine primary sternal chondrocytes in comparison to Murine embryonic fibroblasts NIH3T3 (**Figure 19**). Previous studies have shown PTH/PTHrP mediated inhibition of chondrocyte hypertrophy by dephosphorylation of HDAC4 [39], [45] and cAMP-dependent activation of CRTC2 via PTH/PTHrP to promote *Prg4* expression [82]. Wein *et al.* showed PTH dependent activation of class II HDACs and CRTCs via SIKs in osteocytes [101]. Our findings support the hypothesis that the same regulatory mechanism can be found in chondrocytes. Primary chondrocytes treated with PTH showed decreased phosphorylation of pCRTC2 S275 and pHDAC4 S246/S259/S155 with unchanged levels of HDAC5 in

comparison to untreated primary chondrocytes. Furthermore, treatment of primary chondrocytes with PTH showed increased phosphorylation of pSIK3 T469 and pPKA substrates, which confirms cAMP-dependent phosphorylation of SIKs. PTH mediated signaling could be confirmed using Forskolin, a GPCR-independent activator of cAMP. Phosphorylation of pSIK T469 in primary chondrocytes was not increased when treated with YKL-05-099. However, phosphorylation levels of pCRTC2 S275, pHDAC4 S246/S259/S155 with unchanged levels of total HDAC5, and pPKA were decreased, confirming direct inhibition of SIKs [116] and SIKs as a downstream mediator of PTH dependent signaling. In contrast, NIH3T3 cells do not respond to PTH signaling (as they lack Pth1r expression) but do respond as expected to Forskolin and YKL-05-099.

Relative *Prg4* expression was elevated when treated with PTH, Forskolin or YKL-05-099 (**Figure 20**) and showed significant promotion when treated over a longer period with YKL-05-099 (**Figure 23**). These findings confirm PTH/PTHrP mediated expression of *Prg4* [82], and support the hypothesis of SIK dependent dephosphorylation of CRTC2 in chondrocytes (also seen in **Figure 19**). However, direct induction of *Prg4* with PTH in primary chondrocytes was lower in comparison to fluid flow shear stress-induced *Prg4* expression in epiphysial chondrocytes [82]. Mechanically influenced *Prg4* expression was also seen in articular cartilage and sternal cartilage of mice subjected to extended microgravity during 30 days of Spaceflight [190] suggesting that mechanical stimuli have a greater impact on *Prg4* expression than PTH/PTHrP related signaling.

To verify the results of relative mRNA expression of primary chondrocytes subjected to 5 µM YKL-05-099, mouse limb bud cells cultivated in differentiation media were exposed to YKL-05-099 in the same time dependent manner. This means that mouse limb bud cells were exposed to substances that induce chondrogenesis and delay chondrogenic hypertrophy at the same time. *Prg4* expression in mouse limb bud cells was slightly increased when treated with 5 µM YKL-05-099 for 1.5 h, 3 h and 6 but decreased after 18 h (see **Figure 27**). However, relative mRNA expression was 18-fold lower in mouse limb bud cells in comparison to primary chondrocytes. This is most like due to the nature of mouse limb bud cells as they resemble chondrocytes of the growth plate which do not express *Prg4* primarily in comparison to articular or sternal chondrocytes [173], [190].

The relative expression of *MMP13* in primary chondrocytes was decreased significantly when treated with 10 µM YKL-05-099 for 4 hours (**Figure 21**) or 5 µM YKL-05-099 at various time points (**Figure 24**). This finding might correlate with the reduced expression of *MMP13* in murine knee joints of mice with systemic YKL-05-099 treatment (**Figure 12**, **Figure 16**) but does not explain reduced *MMP13* expression in mice with DMM-induced OA and VEH treatment. However, treatment with PTH or Forskolin could not verify the reduced expression of *MMP13* (**Figure 21**).

Relative *MMP13* expression was also decreased in mouse limb bud cells after 1.5 h, 3 h and 6 h of treatment with 5 µM YKL-05-099 as seen in mouse primary sternal chondrocytes (see **Figure 28**). In comparison to primary chondrocytes, mouse limb bud cells had increased *MMP13* expression when treated with YKL-05-099 for 18 h. This might indicate loss of

function of YKL-05-099 over time as stability was only shown for up to 2 hours in mouse liver [116], but does not explain increased *MMP13* expression in comparison to its respective control. Furthermore, relative *MMP13* expression was increased in mouse limb bud cells cultivated for 10 days with differentiation media indicating differentiation into chondrocytes and maturation, which was confirmed with alcian blue staining (see **Figure 30**) [3].

The relative *Col10a1* expression in primary chondrocytes was slightly upregulated when treated with PTH, YKL-05-099 or Forskolin for 4 h (**Figure 22**). Upregulation was also seen in samples treated with 5 µM YKL-05-099 for 6 h and 18 h (**Figure 23**). However, *Col10a1* expression of YKL-05-099 treated samples did not exceed the expression levels of 1.5 h control samples. *Col10a1* expression was 30-times lower in comparison to clonal mouse limb bud cells differentiated for 10 days which indicates immaturity of chondrocytes [3], [4].

Mouse clonal limb bud cells had statistically significant reduction in *Col10a1* expression when undifferentiated and after 10 days of differentiation after 5 µM YKL-05-099 treatment over 18 h (see **Figure 29**). Additionally, day 10 mouse limb bud cells had statistically significant reduction in *Col10a1* expression after a 1.5 h treatment. These results do not correlate with primary murine sternal chondrocytes. Primary chondrocytes were used in an immature state with low *Col10a1* expression [3] which made a response to YKL-05-099 probably less effective.

Primary chondrocytes were seeded in a low cell density due to the lack of available cells. Primary murine chondrocytes never grew to confluency due to slow proliferation and the risk of differentiation into fibroblasts or overgrowing fibroblasts [191]. The balance between a good population of primary murine sternal chondrocytes in culture and their state of maturation and differentiation was challenging. However, primary chondrocytes used for protein analysis and gene expression were immature and did not differentiate due to too long cultivation (**Figure 26**).

Mouse clonal limb bud cells were plated at a high density to obtain confluency quickly. Furthermore, clonal limb bud cells proliferate very quickly in comparison to primary chondrocytes. Positive proteoglycan staining of mouse limb bud cells indicates differentiation into chondrocytes but must not correlate with *Prg4* expression (**Figure 30** and **Figure 27**). Mouse limb bud cells resemble chondrocytes of the growth plate which are not prone to express *Prg4* in comparison to sternal chondrocytes or chondrocytes found in articular cartilage [3], [82], [190].

Taken together, SIKs control HDAC4 and CRTC2 phosphorylation in primary murine sternal chondrocytes. Blocking SIK activity with PTH, Forskolin or pan-SIK inhibitor YKL-05-099 in primary sternal chondrocytes increases *Prg4* expression. Treatment with YKL-05-099 also decreases *MMP13* expression in primary chondrocytes. These results could be confirmed with mouse clonal limb bud cells. Additionally, reduced *Col10a1* expression was observed in mouse limb bud cells which had a 30-fold higher mRNA expression in comparison to primary sternal chondrocytes. The molecular influence of YKL-05-099 on chondrocytes may contribute to decreased articular cartilage degradation seen in the DMM-induced OA mouse model. However, systemic treatment of YKL-05-099 did no show a statistically significant

promotion in cartilage integrity. MMP13 immunohistochemistry and *in situ* hybridization revealed that Chondrocytes do not express *MMP13* in detectable levels in articular cartilage but in the growth plate when matured into a late hypertrophic state. This suggests that articular chondrocytes never reached a late hypertrophic state to start *MMP13* expression with or without induction of OA via DMM surgery. Articular chondrocytes did not respond to YKL-05-099 treatment despite the evident upregulation of *Prg4* expression seen in mouse limb bud cells and primary chondrocytes. However, the presence of YKL-05-099 in the synovial region was not confirmed in this study. The systemic treatment of YKL-05-099 in mice remains unclear and provides the opportunity for another study with local treatment. Additional immunohistochemistry of direct targets of SIK's such as HDAC4 and CRTC2 or the assessment of local *MMP13* expression in the growth plate may reveal more dramatic effects in the *in vivo* mouse model which haven't been seen in this study. Furthermore, the creation of conditional knockouts of SIK's in chondrocytes or mice could be used to confirm treatment effects and molecular changes with YKL-05-099 treatment. The presented results provide enough evidence to continue the investigations on YKL-05-099 as disease-modifying treatment option in OA and elucidating the full potential of this pan-SIK inhibitor in future studies.

Bibliography

[1] B. K. Hall and T. Miyake, “The membranous skeleton: the role of cell condensations in vertebrate skeletogenesis.,” *Anat. Embryol. (Berl).*, vol. 186, no. 2, pp. 107–24, Jul. 1992.

[2] D. M. Ornitz and P. J. Marie, “FGF signaling pathways in endochondral and intramembranous bone development and human genetic disease,” *Genes Dev.*, vol. 16, no. 12, pp. 1446–1465, 2002.

[3] E. Kozhemyakina, A. B. Lassar, and E. Zelzer, “A pathway to bone: signaling molecules and transcription factors involved in chondrocyte development and maturation,” *Development*, vol. 142, no. 5, pp. 817–831, 2015.

[4] Henry M. Kronenberg, “Developmental regulation of the growth plate,” *Nature*, vol. 423, no. 6937, pp. 332–336, 2003.

[5] R. R. Behringer, B. de Crombrugghe, W. Bi, J. M. Deng, and Z. Zhang, “Sox9 is required for cartilage formation.,” *Nat. Genet.*, vol. 22, no. 1, pp. 85–89, 1999.

[6] A. H., C. M.-C., M. J.F., S. A., and D. C. B., “The transcription factor Sox9 has essential roles in successive steps of the chondrocyte differentiation pathway and is required for expression of Sox5 and Sox6,” *Genes Dev.*, vol. 16, no. 21, pp. 2813–2828, 2002.

[7] K. L. Cooper, S. Oh, Y. Sung, R. R. Dasari, M. W. Kirschner, and C. J. Tabin, “Multiple phases of chondrocyte enlargement underlie differences in skeletal proportions,” *Nature*, vol. 495, no. 7441, pp. 375–378, Mar. 2013.

[8] C. Maes *et al.*, “Osteoblast precursors, but not mature osteoblasts, move into developing and fractured bones along with invading blood vessels,” *Dev. Cell*, vol. 19, no. 2, pp. 329–344, 2010.

[9] L. Yang, K. Y. Tsang, H. C. Tang, D. Chan, and K. S. E. Cheah, “Hypertrophic chondrocytes can become osteoblasts and osteocytes in endochondral bone formation,” *World Rev. Nutr. Diet.*, vol. 114, no. 33, p. 13, 2016.

[10] J. A. Rudnicki and A. M. C. Brown, “Inhibition of Chondrogenesis byWntGene Expressionin Vivoandin Vitro,” *Dev. Biol.*, vol. 185, no. 1, pp. 104–118, May 1997.

[11] C. Hartmann and C. J. Tabin, “Dual roles of Wnt signaling during chondrogenesis in the chicken limb.,” *Development*, vol. 127, no. 14, pp. 3141–59, 2000.

[12] X. Sun, F. V Mariani, and G. R. Martin, “Functions of FGF signalling from the apical ectodermal ridge in limb development,” *Nature*, vol. 418, no. 6897, pp. 501–508, Aug. 2002.

[13] A. T. Dudley, M. A. Ros, and C. J. Tabin, “A re-examination of proximodistal patterning during vertebrate limb development,” *Nature*, vol. 418, no. 6897, pp. 539–544, 2002.

[14] D. ten Berge, S. A. Brugmann, J. A. Helms, and R. Nusse, “Wnt and FGF signals interact to coordinate growth with cell fate specification during limb development,” *Development*, vol. 135, no. 19, pp. 3247–3257, 2008.

[15] N. Kato and H. Aoyama, “Dermomyotomal origin of the ribs as revealed by extirpation and transplantation experiments in chick and quail embryos,” *Development*, vol. 125, no. 17, pp. 3437–3443, 1998.

[16] C. Chiang *et al.*, “Cyclopia and defective axial patterning in mice lacking Sonic hedgehog gene function,” *Nature*, vol. 383, no. 6599, pp. 407–413, Oct. 1996.

[17] A. H. Monsoro-Burq, “Sclerotome development and morphogenesis: When experimental embryology meets genetics,” *Int. J. Dev. Biol.*, vol. 49, no. 2-3 SPEC. ISS., pp. 301–308, 2005.

[18] L. C. Murtaugh, J. H. Chyung, and A. B. Lassar, “Sonic hedgehog promotes somitic chondrogenesis by altering the cellular response to BMP signaling,” *Genes Dev.*, vol. 13, no. 2, pp. 225–237, 1999.

[19] L. C. Murtaugh, L. Zeng, J. H. Chyung, and A. B. Lassar, “The Chick Transcriptional Repressor Nkx3.2 Acts Downstream of Shh to Promote BMP-Dependent Axial Chondrogenesis,” *Dev. Cell*, vol. 1, no. 3, pp. 411–422, 2001.

[20] L. Zeng, L. C. Murtaugh, M. E. Sato, and A. B. Lassar, “Shh establishes an Nkx3.2/Sox9 autoregulatory loop that is maintained by BMP signals to induce somitic chondrogenesis,” *Genes Dev.*, vol. 16, pp. 1990–2005, 2005.

[21] E. Koyama *et al.*, “A distinct cohort of progenitor cells participates in synovial joint and articular cartilage formation during mouse limb skeletogenesis,” *Dev. Biol.*, vol. 316, no. 1, pp. 62–73, Apr. 2008.

[22] B. S. Yoon, D. A. Ovchinnikov, I. Yoshii, Y. Mishina, R. R. Behringer, and K. M. Lyons, “Bmpr1a and Bmpr1b have overlapping functions and are essential for chondrogenesis in vivo,” *Proc. Natl. Acad. Sci.*, vol. 102, no. 14, pp. 5062–5067, 2005.

[23] B. de Crombrugghe, V. Lefebvre, and K. Nakashima, “Regulatory mechanisms in the pathways of cartilage and bone formation.,” *Curr. Opin. Cell Biol.*, vol. 13, no. 6, pp. 721–7, Dec. 2001.

[24] W. Huang, X. Zhou, V. Lefebvre, and B. de Crombrugghe, “Phosphorylation of SOX9 by Cyclic AMP-Dependent Protein Kinase A Enhances SOX9’s Ability To Transactivate a Col2a1 Chondrocyte-Specific Enhancer,” *Mol. Cell. Biol.*, vol. 20, no. 20, pp. 7838–7838, 2000.

[25] R. Yasuhara *et al.*, “Wnt/β-Catenin and retinoic acid receptor signaling pathways interact to regulate chondrocyte function and matrix turnover,” *J. Biol. Chem.*, vol. 285, no. 1, pp. 317–327, 2010.

[26] A. D. Weston, R. A. S. Chandraratna, J. Torchia, and T. M. Underhill, “Requirement for RAR-mediated gene repression in skeletal progenitor differentiation,” *J. Cell Biol.*, vol. 158, no. 1, pp. 39–51, 2002.

[27] P. Smits *et al.*, “The transcription factors L-Sox5 and Sox6 are essential for cartilage formation.,” *Dev. Cell*, vol. 1, pp. 277–90, 2001.

[28] V. Lefebvre, W. Huang, V. R. Harley, P. N. Goodfellow, and B. de Crombrugghe, “SOX9 is a potent activator of the chondrocyte-specific enhancer of the pro alpha1(II) collagen gene.,” *Mol. Cell. Biol.*, vol. 17, no. 4, pp. 2336–2346, 1997.

[29] H. Akiyama, “Interactions between Sox9 and -catenin control chondrocyte differentiation,” *Genes Dev.*, vol. 18, no. 9, pp. 1072–1087, Apr. 2004.

[30] P. Dy *et al.*, “Sox9 Directs Hypertrophic Maturation and Blocks Osteoblast Differentiation of Growth Plate Chondrocytes,” *Dev. Cell*, vol. 22, no. 3, pp. 597–609, 2012.

[31] T. Hattori *et al.*, “SOX9 is a major negative regulator of cartilage vascularization, bone marrow formation and endochondral ossification,” *Development*, vol. 137, no. 6, pp. 901–911, 2010.

[32] S. Takeda, J. P. Bonnamy, M. J. Owen, P. Ducy, and G. Karsenty, “Continuous expression of Cbfa1 in nonhypertrophic chondrocytes uncovers its ability to induce hypertrophic chondrocyte differentiation and partially rescues Cbfa1-deficient mice,” *Genes Dev.*, vol. 15, no. 4, pp. 467–481, 2001.

[33] M. H. Drissi *et al.*, “Runx2/Cbfa1 stimulation by retinoic acid is potentiated by BMP2 signaling through interaction with Smad1 on the collagen X promoter in chondrocytes,” *J. Cell. Biochem.*, vol. 90, no. 6, pp. 1287–1298, Dec. 2003.

[34] N. Selvamurugan, M. R. Pulumati, D. R. Tyson, and N. C. Partridge, “Parathyroid hormone regulation of the rat collagenase-3 promoter by protein kinase A-dependent transactivation of core binding factor α1,” *J. Biol. Chem.*, vol. 275, no. 7, pp. 5037–5042, 2000.

[35] M. A. Arnold *et al.*, “MEF2C Transcription Factor Controls Chondrocyte Hypertrophy and Bone Development,” *Dev. Cell*, vol. 12, no. 3, pp. 377–389, 2007.

[36] C. M. Grozinger and S. L. Schreiber, “Regulation of histone deacetylase 4 and 5 and transcriptional activity by 14-3- 3-dependent cellular localization,” *Proc. Natl. Acad. Sci.*, vol. 97, no. 14, pp. 7835–7840, 2000.

[37] H. Fu, R. R. Subramanian, and S. C. Masters, “14-3-3 proteins: structure, function, and regulation.,” *Annu. Rev. Pharmacol. Toxicol.*, vol. 40, pp. 617–47, 2000.

[38] R. B. Vega *et al.*, “Histone deacetylase 4 controls chondrocyte hypertrophy during skeletogenesis,” *Cell*, vol. 119, no. 4, pp. 555–566, 2004.

[39] E. Kozhemyakina, T. Cohen, T.-P. Yao, and A. B. Lassar, “Parathyroid Hormone-Related Peptide Represses Chondrocyte Hypertrophy through a Protein Phosphatase 2A/Histone Deacetylase 4/MEF2 Pathway,” *Mol. Cell. Biol.*, vol. 29, no. 21, pp. 5751–5762, 2009.

[40] T. A. McKinsey, C. L. Zhang, and E. N. Olson, “Activation of the myocyte enhancer factor-2 transcription factor by calcium/calmodulin-dependent protein kinase-stimulated binding of 14-3-3 to histone deacetylase 5,” *Proc. Natl. Acad. Sci.*, vol. 97, no. 26, pp. 14400–14405, 2000.

[41] K. Lee *et al.*, “Parathyroid hormone-related peptide delays terminal differentiation of chondrocytes during endochondral bone development.,” *Endocrinology*, vol. 137, no. 11, pp. 5109–18, Nov. 1996.

[42] B. Lanske *et al.*, “PTH/PTHrP receptor in early development and Indian hedgehog-regulated bone growth.,” *Science*, vol. 273, no. 5275, pp. 663–6, Aug. 1996.

[43] E. C. Weir, W. M. Philbrick, M. Amling, L. A. Neff, R. Baron, and A. E. Broadus, “Targeted overexpression of parathyroid hormone-related peptide in chondrocytes causes chondrodysplasia and delayed endochondral bone formation,” *Proc. Natl. Acad. Sci. U. S. A.*, vol. 93, no. 19, pp. 10240–10245, 1996.

[44] J. Guo, U. Il Chung, H. Kondo, F. R. Bringhurst, and H. M. Kronenberg, “The PTH/PTHrP receptor can delay chondrocyte hypertrophy in vivo without activating phospholipase C,” *Dev. Cell*, vol. 3, no. 2, pp. 183–194, 2002.

[45] D. Correa *et al.*, “Zfp521 is a target gene and key effector of parathyroid hormone-related peptide signaling in growth plate chondrocytes,” *Dev. Cell*, vol. 19, no. 4, pp. 533–546, 2010.

[46] A. Vortkamp, K. Lee, B. Lanske, G. V. Segre, H. M. Kronenberg, and C. J. Tabin, “Regulation of Rate of Cartilage Differentiation by Indian Hedgehog and PTH-Related Protein,” *Science (80-.).*, vol. 273, no. 5275, pp. 613–622, Aug. 1996.

[47] B. St-Jacques, M. Hammerschmidt, and A. P. McMahon, “Indian hedgehog signaling regulates proliferation and differentiation of chondrocytes and is essential for bone formation,” *Genes Dev.*, vol. 13, no. 16, pp. 2072–2086, 1999.

[48] S. J. Karp, E. Schipani, B. St-Jacques, J. Hunzelman, H. Kronenberg, and A. P. McMahon, “Indian hedgehog coordinates endochondral bone growth and morphogenesis via parathyroid hormone related-protein-dependent and -independent pathways.,” *Development*, vol. 127, no. 3, pp. 543–8, 2000.

[49] T. Kobayashi *et al.*, “Indian hedgehog stimulates periarticular chondrocyte differentiation to regulate growth plate length independently of PTHrP,” *J. Clin. Invest.*, vol. 115, no. 7, pp. 1734–1742, 2005.

[50] C. H. Evans, S. C. Ghivizzani, and P. D. Robbins, “Gene Delivery to Joints by Intra-Articular Injection,” *Hum. Gene Ther.*, vol. 29, no. 1, pp. 2–14, 2017.

[51] F. Flandry and G. Hommel, “Normal anatomy and biomechanics of the knee,” *Sports Med. Arthrosc.*, vol. 19, no. 2, pp. 82–92, 2011.

[52] N. Holder, “An experimental investigation into the early development of the chick elbow joint.,” *J. Embryol. Exp. Morphol.*, vol. 39, pp. 115–27, 1977.

[53] J. E. Salva and A. E. Merrill, “Signaling networks in joint development,” *Dev. Dyn.*, vol. 246, no. 4, pp. 262–274, 2017.

[54] R. S. Decker, E. Koyama, and M. Pacifici, “Genesis and morphogenesis of limb synovial joints and articular cartilage,” *Matrix Biol.*, vol. 39, pp. 5–10, 2014.

[55] M. M. Ito and M. Y. Kida, “Morphological and biochemical re-evaluation of the process of cavitation in the rat knee joint: Cellular and cell strata alterations in the interzone,” *J. Anat.*, vol. 197, no. 4, pp. 659–679, 2000.

[56] G. Hyde, R. P. Boot-Handford, and G. A. Wallis, “Col2a1 lineage tracing reveals that the meniscus of the knee joint has a complex cellular origin,” *J. Anat.*, vol. 213, no. 5, pp. 531–538, 2008.

[57] T. Soeda, J. M. Deng, B. de Crombrugghe, R. R. Behringer, T. Nakamura, and H. Akiyama, “Sox9-expressing precursors are the cellular origin of the cruciate ligament of the knee joint and the limb tendons,” *genesis*, vol. 48, no. 11, pp. 635–644, Nov. 2010.

[58] X. Guo, “Wnt/ -catenin signaling is sufficient and necessary for synovial joint formation,” *Genes Dev.*, vol. 18, no. 19, pp. 2404–2417, Sep. 2004.

[59] D. Später, T. P. Hill, M. Gruber, and C. Hartmann, “Role of canonical Wnt-signalling in joint formation,” *Eur. Cells Mater.*, vol. 12, pp. 71–80, 2006.

[60] C. Hartmann and C. J. Tabin, “Wnt-14 plays a pivotal role in inducing synovial joint formation in the developing appendicular skeleton,” *Cell*, vol. 104, no. 3, pp. 341–351, 2001.

[61] E. E. Storm and D. M. Kingsley, “Joint patterning defects caused by single and double mutations in members of the bone morphogenetic protein (BMP) family.,” *Development*, vol. 122, no. 12, pp. 3969–79, 1996.

[62] R. B. Rountree *et al.*, “BMP receptor signaling is required for postnatal maintenance of articular cartilage,” *PLoS Biol.*, vol. 2, no. 11, 2004.

[63] E. KOYAMA *et al.*, “Synovial Joint Formation during Mouse Limb Skeletogenesis: Roles of Indian Hedgehog Signaling,” *Ann. N. Y. Acad. Sci.*, vol. 1116, no. 1, pp. 100–112, Nov. 2007.

[64] S. V Sambasivarao, “A distinct cohort of progenitor cells participates in synovial joint and articular cartilage formation during mouse limb skeletogenesis,” vol. 18, no. 9, pp. 1199–1216, 2013.

[65] N. M. Wolfman *et al.*, “Ectopic induction of tendon and ligament in rats by growth and differentiation factors 5, 6, and 7, members of the TGF-β gene family,” *J. Clin. Invest.*, vol. 100, no. 2, pp. 321–330, 1997.

[66] S. H. Settle, R. B. Rountree, A. Sinha, A. Thacker, K. Higgins, and D. M. Kingsley, “Multiple joint and skeletal patterning defects caused by single and double mutations in the mouse Gdf6 and Gdf5 genes,” *Dev. Biol.*, vol. 254, no. 1, pp. 116–130, 2003.

[67] E. E. Storm and D. M. Kingsley, “GDF5 coordinates bone and joint formation during digit development,” *Dev. Biol.*, vol. 209, no. 1, pp. 11–27, 1999.

[68] P. H. Francis-West *et al.*, “Mechanisms of GDF-5 action during skeletal development.,” *Development*, vol. 126, no. 6, pp. 1305–15, 1999.

[69] N. Tsumaki *et al.*, “Bone morphogenetic protein signals are required for cartilage formation and differently regulate joint development during skeletogenesis,” *J. Bone Miner. Res.*, vol. 17, no. 5, pp. 898–906, 2002.

[70] F. Jenner *et al.*, “Differential Gene Expression of the Intermediate and Outer Interzone Layers of Developing Articular Cartilage in Murine Embryos,” *Stem Cells Dev.*, vol. 23, no. 16, pp. 1883–1898, 2014.

[71] D. B. Drachman and L. Sokoloff, “The role of movement in embryonic joint development,” *Dev. Biol.*, vol. 14, no. 3, pp. 401–420, Dec. 1966.

[72] D. Mitrovic, “Development of the articular cavity in paralyzed chick embryos and in chick embryo limb buds cultured on chorioallantoic membranes.,” *Acta Anat. (Basel).*, vol. 113, no. 4, pp. 313–24, 1982.

[73] A. C. Osborne, K. J. Lamb, J. C. Lewthwaite, G. P. Dowthwaite, and A. A. Pitsillides, “Short-term rigid and flaccid paralyses diminish growth of embryonic chick limbs and abrogate joint cavity formation but differentially preserve pre-cavitated joints,” *J. Musculoskelet. Neuronal Interact.*, vol. 2, no. 5, pp. 448–456, 2002.

[74] K. J. Lamb, J. C. Lewthwaite, E. R. Bastow, and A. A. Pitsillides, “Defining boundaries during joint cavity formation: going out on a limb.,” *Int. J. Exp. Pathol.*, vol. 84, no. 2, pp. 55–67, Apr. 2003.

[75] G. P. Dowthwaite, J. C. W. Edwards, and A. A. Pitsillides, “An Essential Role for the Interaction Between Hyaluronan and Hyaluronan Binding Proteins During Joint Development,” *J. Histochem. Cytochem.*, vol. 46, no. 5, pp. 641–651, May 1998.

[76] E. R. Bastow *et al.*, “Selective activation of the MEK-ERK pathway is regulated by mechanical stimuli in forming joints and promotes pericellular matrix formation,” *J. Biol. Chem.*, vol. 280, no. 12, pp. 11749–11758, 2005.

[77] J. C. Lewthwaite, E. R. Bastow, K. J. Lamb, J. Blenis, C. P. D. Wheeler-Jones, and A. A. Pitsillides, “A specific mechanomodulatory role for p38 MAPK in embryonic joint articular surface cell MEK-ERK pathway regulation,” *J. Biol. Chem.*, vol. 281, no. 16, pp. 11011–11018, 2006.

[78] H. Mankin, “Localization of Tritated Thymidine in Articular Cartilage of Rabbits: III Mature Articular Cartilage,” *J. Bone Jt. Surg.*, vol. 45, no. 3, pp. 529–540, 1963.

[79] H. Mankin, “Localization of Tritiated Thymidine in Articuar Cartilage of Rabbits: II Repair in Immature Cartilage,” *J. Bone Jt. Surg.*, vol. 44, no. 4, pp. 688–698, 1962.

[80] C. W. Archer, H. Morrison, and A. A. Pitsillides, “Cellular aspects of the development of diarthrodial joints and articular cartilage,” *J. Anat.*, vol. 184, no. 3, pp. 447–456, 1994.

[81] S. Ikegawa, M. Sano, Y. Koshizuka, and Y. Nakamura, “Isolation, characterization and mapping of the mouse and human PRG4 (proteoglycan 4) genes,” *Cytogenet. Genome Res.*, vol. 90, no. 3–4, pp. 291–297, 2000.

[82] H. Ogawa, E. Kozhemyakina, H. H. Hung, A. J. Grodzinsky, and A. B. Lassar, “Mechanical motion promotes expression of Prg4 in articular cartilage via multiple CREB-dependent, fluid flow shear stress-induced signaling pathways,” *Genes Dev.*, vol. 28, no. 2, pp. 127–139, 2014.

[83] S. R. Lamandé *et al.*, “Mutations in TRPV4 cause an inherited arthropathy of hands and feet.,” *Nat. Genet.*, vol. 43, no. 11, pp. 1142–6, Oct. 2011.

[84] C. J. O’Conor, H. A. Leddy, H. C. Benefield, W. B. Liedtke, and F. Guilak, “TRPV4-mediated mechanotransduction regulates the metabolic response of chondrocytes to dynamic loading,” *Proc. Natl. Acad. Sci.*, vol. 111, no. 4, pp. 1316–1321, 2014.

[85] W. Lee *et al.*, “Synergy between Piezo1 and Piezo2 channels confers high-strain mechanosensitivity to articular cartilage,” *Proc. Natl. Acad. Sci.*, vol. 111, no. 47, pp. E5114–E5122, 2014.

[86] A. D. Pearle, R. F. Warren, and S. A. Rodeo, “Basic science of articular cartilage and osteoarthritis,” *Clin. Sports Med.*, vol. 24, no. 1, pp. 1–12, 2005.

[87] M. Mow, VC; Proctor, CS; Kelly, “Biomechanics of the articular cartilage,” *Basic Biomech. muscoskeletal Syst.*, pp. 31–57, 1989.

[88] M. Wong, P. Wuethrich, P. Eggli, and E. Hunziker, “Zone-specific cell biosynthetic activity in mature bovine articular cartilage: A new method using confocal microscopic stereology and quantitative autoradiography,” *J. Orthop. Res.*, vol. 14, no. 3, pp. 424–432, May 1996.

[89] B. L. Schumacher, C. E. Hughes, K. E. Kuettner, B. Caterson, and M. B. Aydelotte, “Immunodetection and partial cDNA sequence of the proteoglycan, superficial zone protein, synthesized by cells lining synovial joints,” *J. Orthop. Res.*, vol. 17, no. 1, pp. 110–120, Jan. 1999.

[90] B. L. Schumacher, J. A. Block, T. M. Schmid, M. B. Aydelotte, and K. E. Kuettner, “A Novel Proteoglycan Synthesized and Secreted by Chondrocytes of the Superficial Zone of Articular Cartilage,” *Arch. Biochem. Biophys.*, vol. 311, no. 1, pp. 144–152, May 1994.

[91] A. Mankin, HJ; Mow, VC; Buckwalter, JA; Iannotti, JP; Ratcliffe, “Articular cartilage structure, composition, and function,” *Orthop. basic Sci. Biol. Biomech. muscoskeletal Syst.*, pp. 444–470, 1999.

[92] T. Macirowski, “Cartilage Stresses in the Human Hip Joint,” *J. Biomech. Eng.*, vol. 116, no. 1, p. 10, Feb. 1994.

[93] G. A. Ateshian and H. Wang, “Rolling resistance of articular cartilage due to interstitial fluid flow,” *Proc. Inst. Mech. Eng. Part H J. Eng. Med.*, vol. 211, no. 5, pp. 419–424, May 1997.

[94] A. MAROUDAS, “Balance between swelling pressure and collagen tension in normal and degenerate cartilage,” *Nature*, vol. 260, no. 5554, pp. 808–809, Apr. 1976.

[95] M. A. Soltz and G. A. Ateshian, “Interstitial Fluid Pressurization During Confined Compression Cyclical Loading of Articular Cartilage,” *Ann. Biomed. Eng.*, vol. 28, no. 2, pp. 150–159, Feb. 2000.

[96] M. A. Soltz and G. A. Ateshian, “Experimental verification and theoretical prediction of cartilage interstitial fluid pressurization at an impermeable contact interface in confined compression.,” *J. Biomech.*, vol. 31, no. 10, pp. 927–34, Oct. 1998.

[97] H. Jüppner *et al.*, “A G Protein-Linked Receptor for Parathyroid Hormone and Parathyroid Hormone-Related Peptide Jr ., Henry M . Kronenberg and Gino V . Segre Published by : American Association for the Advancement of Science Stable URL : https://www.jstor.org/stable/2879719,” *Science (80-.).*, vol. 254, no. 5034, pp. 1024–6, 1991.

[98] K.-D. Schlüter, “PTH and PTHrP: Similar Structures but Different Functions,” *Physiology*, vol. 14, no. 6, pp. 243–249, 2017.

[99] M. Lee and N. C. Partridge, “Parathyroid hormone signaling in bone and kidney,” *Curr. Opin. Nephrol. Hypertens.*, vol. 18, no. 4, pp. 298–302, Jul. 2009.

[100] N. S. Datta and A. B. Abou-Samra, “PTH and PTHrP signaling in osteoblasts.,” *Cell. Signal.*, vol. 21, no. 8, pp. 1245–54, Aug. 2009.

[101] M. N. Wein *et al.*, “SIKs control osteocyte responses to parathyroid hormone,” *Nat. Commun.*, vol. 7, pp. 1–17, 2016.

[102] Z. N. Wang, H. Takemori, S. K. Halder, Y. Nonaka, and M. Okamoto, “Cloning of a novel kinase (SIK) of the SNF1/AMPK family from high salt diet-treated rat adrenal,” *FEBS Lett.*, vol. 453, no. 1–2, pp. 135–139, 1999.

[103] M. Okamoto, H. Takemori, and Y. Katoh, “Salt-inducible kinase in steroidogenesis and adipogenesis,” *Trends Endocrinol. Metab.*, vol. 15, no. 1, pp. 21–26, 2004.

[104] M. N. Wein, M. Foretz, D. E. Fisher, R. J. Xavier, and H. M. Kronenberg, “Salt-Inducible Kinases: Physiology, Regulation by cAMP, and Therapeutic Potential,” *Trends Endocrinol. Metab.*, vol. 29, no. 10, pp. 723–735, 2018.

[105] M. Haberland, R. L. Montgomery, and E. N. Olson, “The many roles of histone deacetylases in development and physiology: Implications for disease and therapy,” *Nat. Rev. Genet.*, vol. 10, no. 1, pp. 32–42, 2009.

[106] J. Y. Altarejos and M. Montminy, “CREB and the CRTC co-activators: Sensors for hormonal and metabolic signals,” *Nat. Rev. Mol. Cell Biol.*, vol. 12, no. 3, pp. 141–151, 2011.

[107] T. Sonntag, J. M. Vaughan, and M. Montminy, “14-3-3 proteins mediate inhibitory effects of cAMP on salt-inducible kinases (SIKs).,” *FEBS J.*, vol. 285, no. 3, pp. 467–480, 2018.

[108] S. Nishimori *et al.*, “Salt-inducible kinases dictate parathyroid hormone receptor action in bone development and remodeling.,” *J. Clin. Invest.*, Aug. 2019.

[109] I. Pateraki *et al.*, “ Manoyl Oxide (13R), the Biosynthetic Precursor of Forskolin, Is Synthesized in Specialized Root Cork Cells in Coleus forskohlii ,” *Plant Physiol.*, vol. 164, no. 3, pp. 1222–1236, 2014.

[110] I. Pateraki *et al.*, “Total biosynthesis of the cyclic AMP booster forskolin from Coleus forskohlii,” *Elife*, vol. 6, pp. 1–28, 2017.

[111] K. B. Seamon, W. Padgett, and J. W. Daly, “Forskolin: Unique diterpne activator of adenylate cyclase in membranes and in intact cells,” vol. 78, no. 6, pp. 3363–3367, 1981.

[112] V. Wagh, P. Patil, S. Surana, and K. Wagh, “Forskolin: Upcoming antiglaucoma molecule,” *J. Postgrad. Med.*, vol. 58, no. 3, p. 199, 2012.

[113] Y. Toya, C. Schwencke, and Y. Ishikawa, “Forskolin Derivatives with Increased Selectivity for Cardiac Adenylyl Cyclase,” *J. Mol. Cell. Cardiol.*, vol. 30, no. 1, pp. 97–108, Jan. 1998.

[114] M. Kikura, K. Morita, and S. Sato, “Pharmacokinetics and a simulation model of colforsin daropate, new forskolin derivative inotropic vasodilator, in patients undergoing coronary artery bypass grafting.,” *Pharmacol. Res.*, vol. 49, no. 3, pp. 275–81, Mar. 2004.

[115] M. Godard, B. Johnson, S. Richmond, and B. Olson, “Body Composition And Hormonal Adaptations Associated With Forskolin Consumption In Overweight And Obese Males.,” *Med. Sci. Sport. Exerc.*, vol. 37, no. Supplement, p. S39, 2005.

[116] T. B. Sundberg *et al.*, “Development of Chemical Probes for Investigation of Salt-Inducible Kinase Function in Vivo,” *ACS Chem. Biol.*, vol. 11, no. 8, pp. 2105–2111, 2016.

[117] WHO Scientific Group on the Burden of Musculoskeletal Conditions at the Start of the New Millennium, “The burden of musculoskeletal conditions at the start of the new millennium.,” *World Health Organ. Tech. Rep. Ser.*, vol. 919, pp. i–x, 1–218, back cover, 2003.

[118] D. Pereira, E. Ramos, and J. Branco, “Osteoarthritis,” *Acta Med. Port.*, vol. 28, no. 1, pp. 99–106, 2015.

[119] J. M. Hootman and C. G. Helmick, “Projections of US prevalence of arthritis and associated activity limitations,” *Arthritis Rheum.*, vol. 54, no. 1, pp. 226–229, 2006.

[120] I. R. Reid, “Short-term and long-term effects of osteoporosis therapies,” *Nat. Rev. Endocrinol.*, vol. 11, no. 7, pp. 418–428, 2015.

[121] M. J. Lespasio, N. S. Piuzzi, M. E. Husni, G. F. Muschler, A. Guarino, and M. A. Mont, “Knee Osteoarthritis: A Primer.,” *Perm. J.*, vol. 21, pp. 16–183, 2017.

[122] Y. Zhang and J. M. Jordan, “Epidemiology of Osteoarthritis,” *Rheum. Dis. Clin. North Am.*, vol. 34, no. 3, pp. 515–529, Aug. 2008.

[123] V. K. Srikanth, J. L. Fryer, G. Zhai, T. M. Winzenberg, D. Hosmer, and G. Jones, “A meta-analysis of sex differences prevalence, incidence and severity of osteoarthritis.,” *Osteoarthr. Cartil.*, vol. 13, no. 9, pp. 769–81, Sep. 2005.

[124] H. J. Mankin, “The response of articular cartilage to mechanical injury.,” *J. Bone Joint Surg. Am.*, vol. 64, no. 3, pp. 460–6, Mar. 1982.

[125] J. A. Buckwalter and H. J. Mankin, “Articular cartilage: degeneration and osteoarthritis, repair, regeneration, and transplantation.,” *Instr. Course Lect.*, vol. 47, pp. 487–504, 1998.

[126] S. Akizuki, V. C. Mow, F. Muller, J. C. Pita, and D. S. Howell, “Tensile properties of human knee joint cartilage. II. Correlations between weight bearing and tissue pathology and the kinetics of swelling,” *J. Orthop. Res.*, vol. 5, no. 2, pp. 173–186, 1987.

[127] W. M. Lai, J. S. Hou, and V. C. Mow, “A Triphasic Theory for the Swelling and Deformation Behaviors of Articular Cartilage,” *J. Biomech. Eng.*, vol. 113, no. 3, p. 245, 1991.

[128] T. Lyyra, I. Kiviranta, U. Väätäinen, H. J. Helminen, and J. S. Jurvelin, “In vivo characterization of indentation stiffness of articular cartilage in the normal human knee.,” *J. Biomed. Mater. Res.*, vol. 48, no. 4, pp. 482–7, 1999.

[129] T. Franz, E. M. Hasler, R. Hagg, C. Weiler, R. P. Jakob, and P. Mainil-Varlet, “In situ compressive stiffness, biochemical composition, and structural integrity of articular cartilage of the human knee joint,” *Osteoarthr. Cartil.*, vol. 9, no. 6, pp. 582–592, Aug. 2001.

[130] J. H.-C. Wang, F. Jia, T. W. Gilbert, and S. L.-Y. Woo, “Cell orientation determines the alignment of cell-produced collagenous matrix.,” *J. Biomech.*, vol. 36, no. 1, pp. 97–102, Jan. 2003.

[131] Z. M. *et al.*, “Induced superficial chondrocyte death reduces catabolic cartilage damage in murine posttraumatic osteoarthritis,” *J. Clin. Invest.*, vol. 126, no. 8, pp. 2893–2902, 2016.

[132] Y. Yahara *et al.*, “Pterosin B prevents chondrocyte hypertrophy and osteoarthritis in mice by inhibiting Sik3,” *Nat. Commun.*, vol. 7, pp. 1–12, 2016.

[133] A. J. Fosang, H. Stanton, C. B. Little, and L. M. Atley, “Neoepitopes as biomarkers of cartilage catabolism.,” *Inflamm. Res.*, vol. 52, no. 7, pp. 277–82, Jun. 2003.

[134] P. Ravaud *et al.*, “Variability in knee radiographing: Implication for definition of radiological progression in medial knee osteoarthritis,” *Ann. Rheum. Dis.*, vol. 57, no. 10, pp. 624–629, 1998.

[135] H. J. Mankin, “Biochemical and metabolic aspects of osteoarthritis.,” *Orthop. Clin. North Am.*, vol. 2, no. 1, pp. 19–31, Mar. 1971.

[136] W. Waldstein, G. Perino, S. L. Gilbert, S. A. Maher, R. Windhager, and F. Boettner, “OARSI osteoarthritis cartilage histopathology assessment system: A biomechanical evaluation in the human knee,” *J. Orthop. Res.*, vol. 34, no. 1, pp. 135–140, 2016.

[137] R. E. Miller, R. J. Miller, and A.-M. Malfait, “Osteoarthritis joint pain: The cytokine connection,” *Cytokine*, vol. 70, no. 2, pp. 185–193, Dec. 2014.

[138] N. Charni-Ben Tabassi, S. Desmarais, A. C. Bay-Jensen, J. M. Delaissé, M. D. Percival, and P. Garnero, “The type II collagen fragments Helix-II and CTX-II reveal different enzymatic pathways of human cartilage collagen degradation,” *Osteoarthr. Cartil.*, vol. 16, no. 10, pp. 1183–1191, 2008.

[139] M. W. Lark *et al.*, “Aggrecan degradation in human cartilage: Evidence for both matrix metalloproteinase and aggrecanase activity in normal, osteoarthritic, and rheumatoid joints,” *J. Clin. Invest.*, vol. 100, no. 1, pp. 93–106, 1997.

[140] P. M. Lin, C. T. C. Chen, and P. A. Torzilli, “Increased stromelysin-1 (MMP-3), proteoglycan degradation (3B3- and 7D4) and collagen damage in cyclically load-injured articular cartilage,” *Osteoarthr. Cartil.*, vol. 12, no. 6, pp. 485–496, 2004.

[141] P. Garnero *et al.*, “Uncoupling of type II collagen synthesis and degradation predicts progression of joint damage in patients with knee osteoarthritis,” *Arthritis Rheum.*, vol. 46, no. 10, pp. 2613–2624, 2002.

[142] M. Reijman *et al.*, “A new marker for osteoarthritis: Cross-sectional and longitudinal approach,” *Arthritis Rheum.*, vol. 50, no. 8, pp. 2471–2478, 2004.

[143] N. Charni, F. Juillet, and P. Garnero, “Urinary type II collagen helical peptide (HELIX-II) as a new biochemical marker of cartilage degradation in patients with osteoarthritis and rheumatoid arthritis,” *Arthritis Rheum.*, vol. 52, no. 4, pp. 1081–1090, 2005.

[144] R. W. Farndale, D. J. Buttle, and A. J. Barrett, “Improved quantitation and discrimination of sulphated glycosaminoglycans by use of dimethylmethylene blue.,” *Biochim. Biophys. Acta*, vol. 883, no. 2, pp. 173–7, Sep. 1986.

[145] P. J. Roughley and J. S. Mort, “The role of aggrecan in normal and osteoarthritic cartilage,” *J. Exp. Orthop.*, vol. 1, no. 1, pp. 1–11, 2014.

[146] B. C. Sondergaard *et al.*, “Relative contribution of matrix metalloprotease and cysteine protease activities to cytokine-stimulated articular cartilage degradation,” *Osteoarthr. Cartil.*, vol. 14, no. 8, pp. 738–748, 2006.

[147] B. Porée *et al.*, “Interleukin-6 (IL-6) and/or soluble IL-6 receptor down-regulation of human type II collagen gene expression in articular chondrocytes requires a decrease of Sp1·Sp3 ratio and of the binding activity of both factors to the COL2A1 promoter,” *J. Biol. Chem.*, vol. 283, no. 8, pp. 4850–4865, 2008.

[148] G. Livshits *et al.*, “Interleukin-6 is a significant predictor of radiographic knee osteoarthritis: The Chingford Study,” *Arthritis Rheum.*, vol. 60, no. 7, pp. 2037–2045, 2009.

[149] T. Mabey and S. Honsawek, “Cytokines as biochemical markers for knee osteoarthritis,” *World J. Orthop.*, vol. 6, no. 1, pp. 95–105, 2015.

[150] L. DIng *et al.*, “IL-37 is associated with osteoarthritis disease activity and suppresses proinflammatory cytokines production in synovial cells,” *Sci. Rep.*, vol. 7, no. 1, pp. 1–8, 2017.

[151] K. B. Marcu, M. Otero, E. Olivotto, R. M. Borzi, and M. B. Goldring, “NF-kappaB signaling: multiple angles to target OA.,” *Curr. Drug Targets*, vol. 11, no. 5, pp. 599–613, 2010.

[152] M. Shakibaei, G. Schulze-Tanzil, T. John, and A. Mobasheri, “Curcumin protects human chondrocytes from IL-l1beta-induced inhibition of collagen type II and beta1-integrin expression and activation of caspase-3: an immunomorphological study.,” *Ann. Anat.*, vol. 187, no. 5–6, pp. 487–97, Nov. 2005.

[153] P. Wojdasiewicz, Ł. A. Poniatowski, and D. Szukiewicz, “The role of inflammatory and anti-inflammatory cytokines in the pathogenesis of osteoarthritis,” *Mediators Inflamm.*, vol. 2014, 2014.

[154] J. Saklatvala, “Tumour necrosis factor alpha stimulates resorption and inhibits synthesis of proteoglycan in cartilage.,” *Nature*, vol. 322, no. 6079, pp. 547–9.

[155] O. Micheau and J. Tschopp, “Induction of TNF receptor I-mediated apoptosis via two sequential signaling complexes.,” *Cell*, vol. 114, no. 2, pp. 181–90, Jul. 2003.

[156] A. Anandacoomarasamy and L. March, “Current evidence for osteoarthritis treatments,” *Ther. Adv. Musculoskelet. Dis.*, vol. 2, no. 1, pp. 17–28, 2010.

[157] W. Zhang *et al.*, “OARSI recommendations for the management of hip and knee osteoarthritis, Part II: OARSI evidence-based, expert consensus guidelines,” *Osteoarthr. Cartil.*, vol. 16, no. 2, pp. 137–162, 2008.

[158] D. T. Felson, Y. Zhang, J. M. Anthony, A. Naimark, and J. J. Anderson, “Weight loss reduces the risk for symptomatic knee osteoarthritis in women. The Framingham Study.,” *Ann. Intern. Med.*, vol. 116, no. 7, pp. 535–9, Apr. 1992.

[159] D. J. Hart, D. V Doyle, and T. D. Spector, “Incidence and risk factors for radiographic knee osteoarthritis in middle-aged women: the Chingford Study.,” *Arthritis Rheum.*, vol. 42, no. 1, pp. 17–24, Jan. 1999.

[160] R. Christensen, A. Astrup, and H. Bliddal, “Weight loss: The treatment of choice for knee osteoarthritis? A randomized trial,” *Osteoarthr. Cartil.*, vol. 13, no. 1, pp. 20–27, 2005.

[161] S. P. Messier *et al.*, “Exercise and Dietary Weight Loss in Overweight and Obese Older Adults with Knee Osteoarthritis: The Arthritis, Diet, and Activity Promotion Trial,” *Arthritis Rheum.*, vol. 50, no. 5, pp. 1501–1510, 2004.

[162] B. Bannwarth, “Acetaminophen or NSAIDs for the treatment of osteoarthritis.,” *Best Pract. Res. Clin. Rheumatol.*, vol. 20, no. 1, pp. 117–29, Feb. 2006.

[163] P. McGettigan and D. Henry, “Cardiovascular risk and inhibition of cyclooxygenase: a systematic review of the observational studies of selective and nonselective inhibitors of cyclooxygenase 2.,” *JAMA*, vol. 296, no. 13, pp. 1633–44, Oct. 2006.

[164] E. Qvistgaard, R. Christensen, S. Torp-Pedersen, and H. Bliddal, “Intra-articular treatment of hip osteoarthritis: A randomized trial of hyaluronic acid, corticosteroid, and isotonic saline,” *Osteoarthr. Cartil.*, vol. 14, no. 2, pp. 163–170, 2006.

[165] N. Bellamy, J. Campbell, V. Robinson, T. Gee, R. Bourne, and G. Wells, “Intraarticular corticosteroid for treatment of osteoarthritis of the knee.,” *Cochrane database Syst. Rev.*, no. 2, p. CD005328, Apr. 2006.

[166] N. Bellamy, J. Campbell, V. Robinson, T. Gee, R. Bourne, and G. Wells, “Viscosupplementation for the treatment of osteoarthritis of the knee.,” *Cochrane database Syst. Rev.*, no. 2, p. CD005321, Apr. 2006.

[167] K. Pavelka *et al.*, “Diacerein: Benefits, Risks and Place in the Management of Osteoarthritis. An Opinion-Based Report from the ESCEO,” *Drugs and Aging*, vol. 33, no. 2, pp. 75–85, 2016.

[168] S. E.R., H. M.J., M. R.A., A. H., R. R.N., and Z. M.J., “Teriparatide as a chondro-regenerative therapy for injury-induced knee osteoarthritis,” *Osteoarthr. Cartil.*, vol. 19, no. 101, p. S227, 2011.

[169] O. Ethgen, O. Bruyère, F. Richy, C. Dardennes, and J.-Y. Reginster, “Health-related quality of life in total hip and total knee arthroplasty. A qualitative and systematic review of the literature.,” *J. Bone Joint Surg. Am.*, vol. 86, no. 5, pp. 963–74, May 2004.

[170] S. S. Leopold, “Minimally invasive total knee arthroplasty for osteoarthritis.,” *N. Engl. J. Med.*, vol. 360, no. 17, pp. 1749–58, Apr. 2009.

[171] J. S. Wayne, C. L. Mcdowell, and M. C. Willis, “Long-term survival of regenerated cartilage on a large joint surface,” vol. 38, no. 2, pp. 191–200, 2001.

[172] S. S. Glasson, M. G. Chambers, W. B. Van Den Berg, and C. B. Little, “The OARSI histopathology initiative e recommendations for histological assessments of osteoarthritis in the mouse,” *Osteoarthr. Cartil.*, vol. 18, pp. S17–S23, 2010.

[173] V. Rosen, J. Nove, J. J. Song, R. S. Thies, K. Cox, and J. M. Wozney, “Responsiveness of clonal limb bud cell lines to bone morphogenetic protein 2 reveals a sequential relationship between cartilage and bone cell phenotypes.,” *J. Bone Miner. Res.*, vol. 9, no. 11, pp. 1759–68, Nov. 1994.

[174] W. H. Simon, “Scale effects in animal joints. I. Articular cartilage thickness and compressive stress.,” *Arthritis Rheum.*, vol. 13, no. 3, pp. 244–56.

[175] J. Lorenz *et al.*, “Melanocortin 1 receptor-signaling deficiency results in an articular cartilage phenotype and accelerates pathogenesis of surgically induced murine osteoarthritis,” *PLoS One*, vol. 9, no. 9, 2014.

[176] S. S. Glasson, T. J. Blanchet, and E. A. Morris, “The surgical destabilization of the medial meniscus (DMM) model of osteoarthritis in the 129/SvEv mouse,” *Osteoarthr. Cartil.*, vol. 15, no. 9, pp. 1061–1069, 2007.

[177] B. J. Kim *et al.*, “Establishment of a reliable and reproducible murine osteoarthritis model,” *Osteoarthr. Cartil.*, vol. 21, no. 12, pp. 2013–2020, 2013.

[178] V. L. Kolachala *et al.*, “Epithelial-derived Fibronectin Expression, Signaling, and Function in Intestinal Inflammation,” *J. Biol. Chem.*, vol. 282, no. 45, pp. 32965–32973, Nov. 2007.

[179] S. A. Flowers *et al.*, “Lubricin binds cartilage proteins, cartilage oligomeric matrix protein, fibronectin and collagen II at the cartilage surface,” *Sci. Rep.*, vol. 7, no. 1, pp. 1–11, 2017.

[180] A. V Stone *et al.*, “Osteoarthritic changes in vervet monkey knees correlate with meniscus degradation and increased matrix metalloproteinase and cytokine secretion.,” *Osteoarthr. Cartil.*, vol. 23, no. 10, pp. 1780–9, Oct. 2015.

[181] A. V Stone, R. F. Loeser, K. S. Vanderman, D. L. Long, S. C. Clark, and C. M. Ferguson, “Pro-inflammatory stimulation of meniscus cells increases production of matrix metalloproteinases and additional catabolic factors involved in osteoarthritis pathogenesis.,” *Osteoarthr. Cartil.*, vol. 22, no. 2, pp. 264–74, Feb. 2014.

[182] J. Liu *et al.*, “Homemade-device-induced negative pressure promotes wound healing more efficiently than VSD-induced positive pressure by regulating inflammation, proliferation and remodeling.,” *Int. J. Mol. Med.*, vol. 39, no. 4, pp. 879–888, Apr. 2017.

[183] H. Tabeian *et al.*, “IL-1β Damages Fibrocartilage and Upregulates MMP-13 Expression in Fibrochondrocytes in the Condyle of the Temporomandibular Joint.,” *Int. J. Mol. Sci.*, vol. 20, no. 9, May 2019.

[184] S. E. Usmani, V. Ulici, M. A. Pest, T. L. Hill, I. D. Welch, and F. Beier, “Context-specific protection of TGFα null mice from osteoarthritis,” *Sci. Rep.*, vol. 6, no. March, pp. 1–11, 2016.

[185] L. Liao *et al.*, “Deletion of Runx2 in Articular Chondrocytes Decelerates the Progression of DMM-Induced Osteoarthritis in Adult Mice,” *Sci. Rep.*, vol. 7, no. 1, pp. 1–12, 2017.

[186] P. er Wang *et al.*, “Bushenhuoxue formula attenuates cartilage degeneration in an osteoarthritic mouse model through TGF-β/MMP13 signaling,” *J. Transl. Med.*, vol. 16, no. 1, pp. 1–12, 2018.

[187] T. Watari, K. Naito, K. Sakamoto, H. Kurosawa, I. Nagaoka, and K. Kaneko, “Evaluation of the effect of oxidative stress on articular cartilage in spontaneously osteoarthritic STR/OrtCrlj mice by measuring the biomarkers for oxidative stress and type II collagen degradation/synthesis,” *Exp. Ther. Med.*, vol. 2, no. 2, pp. 245–250, 2011.

[188] B. Bai and Y. Li, “Combined detection of serum CTX-II and COMP concentrations in osteoarthritis model rabbits: An effective technique for early diagnosis and estimation of disease severity,” *J. Orthop. Surg. Res.*, vol. 11, no. 1, pp. 1–7, 2016.

[189] S. Oestergaard *et al.*, “Evaluation of cartilage and bone degradation in a murine collagen antibody-induced arthritis model,” *Scand. J. Immunol.*, vol. 67, no. 3, pp. 304–312, 2008.

[190] J. Fitzgerald, J. Endicott, U. Hansen, and C. Janowitz, “Articular cartilage and sternal fibrocartilage respond differently to extended microgravity,” *npj Microgravity*, vol. 5, no. 1, pp. 1–5, 2019.

[191] M. Gosset, F. Berenbaum, S. Thirion, and C. Jacques, “Primary culture and phenotyping of murine chondrocytes,” *Nat. Protoc.*, vol. 3, no. 8, pp. 1253–1260, 2008.

List of Figures

Figure 1: Endochondral bone formation. 7
Figure 2: Regional expression of genes in chondrocytes......10
Figure 3: Anatomy of the human knee joint.. 11
Figure 4: Zonal arrangement of articular cartilage. 14
Figure 5: Changes in the osteoarthritic knee joint. 17
Figure 6: PTH/PTHrP dependent signaling pathway in chondrocytes. 22
Figure 7: Histomorphometric comparison of representative right knee joints from sham / DMM operated mice with VEH / YKL-05-099 treatment......34
Figure 8: OARSI scores assessment murine right knee joints from sham / DMM operated mice with VEH / YKL-05-099 treatment. 35
Figure 9: Proteoglycan loss of non-calcified articular cartilage.. 36
Figure 10: Ratio of Col X positive stained chondrocytes in articular cartilage. 37
Figure 11: Type X collagen staining of murine right knees with sham/DMM surgery treated with VEH/YKL-05-099.. 38
Figure 12: MMP13 staining of murine right knees with sham/DMM treated with VEH/YKL-05-099.. 40
Figure 13: *Prg4 in situ* hybridizations of murine knee sections. 42
Figure 14: Prg4 expression in the non-calcified region of articular cartilage and articular chondrocytes......42
Figure 15: *Prg4 in situ* hybridizations of murine brain tissue.. 43
Figure 16: MMP13 *in situ* hybridization of murine knee sections.. 44
Figure 17: MMP13 probe and control probe in situ hybridization of mouse brain and mouse knee sections.. 45
Figure 18: Serum Pre-Clinical CartiLaps® (CTX-II) ELISA kit results. 46
Figure 19: Immunoblot of murine primary sternal chondrocytes and NIH3T3 cells...48
Figure 20: Relative *Prg4* expression in primary murine sternal chondrocytes.. 49
Figure 21: Relative *MMP13* expression in primary murine sternal chondrocytes.. 50
Figure 22: Relative *Col10a1* expression of primary murine sternal chondrocytes......51
Figure 23: Time-dependent *Prg4* expression of primary murine sternal chondrocytes treated with 5 µM YKL-05-099......51
Figure 24: Time-dependent *MMP13* expression in primary murine sternal chondrocytes treated with YKL-05-099......52
Figure 25: Time-dependent *Col10a1* expression in primary murine sternal chondrocytes treated with YKL-05-099. 53
Figure 26: Alcian blue staining of primary murine sternal chondrocytes.. 53
Figure 27: Relative *Prg4* expression of un-/differentiated murine clonal limb bud cells.. 55

Figure 28: Relative *MMP13* expression of un-/differentiated murine clonal limb bud cells treated with YKL-05-099......56
Figure 29: Relative *Col10a1* expression in un-/differentiated mouse limb bud cells treated with 5 µM YKL-05-099......57
Figure 30: Alcian blue staining of differentiating clonal mouse limb bud cells......58

List of Tables

Table 1: Recommended semi-quantitative OARSI scoring system for all four quadrants in mice. 25
Table 2: Primer sequences for real time PCR 31
Table 3: Real time PCR program.....31

List of Abbreviations

AMPK	AMP-activated protein kinase
ATP	Adenosine triphosphate
BMP	Bone morphogenic protein
Bmpr1b	BMP receptor 1b
cAMP	Cyclic Adenosine mono phosphate
COX-2	Cyclooxygenase 2
CRCT	CREB-regulated transcription coactivator
CRE	cAMP-responsive Element
CREB	CRE-binding Protein
CTX-II	C-telopeptide of type II collagen
dH_2O	Distilled Water
DMM	Destabilization of the medial meniscus
EtOH	Ethanol
FDA	Food and Drug Administration
FGF	Fibroblast growth factor
GDF	Growth and differentiation factor
HDAC	Histone deacetylase
IHH	Indian hedge hog
IL	Interleukin
LFC	Lateral femoral condyle
LTP	Lateral Tibial Plateau
Mef	Myocyte enhancer factor
MFC	Medial femoral condyle
MMP	Metalloproteinase
MTP	Medial Tibial Plateau
NSAID	Non-steroidal anti-inflammatory drugs
OA	Osteoarthritis
OARSI	OA research society international
PG	Proteoglycan
PKA	Protein kinase A
PRG4	Proteoglycan 4
PTH	Parathryoid Hormone
PTH1r	PTH receptor 1
PTHrP	PTH related peptide
RA	Retinoic acid
Runx	Runt-related transcription factor
SIK	Salt-inducible kinase
SppI	Secreted Phosphoprotein I

TNF	Tumour necrosis factor
TRPV4	Transient receptor potential cation channel subfamily V member 4
VEH	VVehicle
VGEFA	Vascular Endothelial Growth Factor A
WOMAC	Western Ontario and McMaster Universities Osteoarthritis Index